Doctoral Thesis

Synthesis, Properties of Graphene Oxide, Graphene Oxide Quantum Dots, and Its Composite: A Cesium Detector for Environmental Monitoring

(酸化グラフェン、酸化グラフェン量子ドット、その複合体の合成と性質：環境モニタリングのためのセシウム検出器)

BANGUN SATRIO NUGROHO
D192886

(Submitted to the Hiroshima University, in fulfilment of the requirements for the degree of Doctor of Philoshopy)

DEPARTMENT OF CHEMISTRY
GRADUATE SCHOOL OF SCIENCE
HIROSHIMA UNIVERSITY
2022

Keywords

Graphene oxide, Graphene oxide quantum dots, Oxidation debris, Dawson-type Polyoxometalate, Nanocomposite, Cesium, Radionuclides, Cesium green molecule, Reflux method, Modified Hummer`s method, C/O ratio, sp^2/sp^3 carbon domain, Photoluminescence, Detection system, Fukushima Daiichi Nuclear Power Plant Accident, Synthesis, Adsorption performance.

Abstract

The Fukushima Daiichi Nuclear Power Plant (FDNPP) accident that occurred in March, 2011, caused a substantial amount of radioactive materials released to the environment. Among the radioactive materials released to the environment, radiocesium (^{134}Cs and ^{137}Cs) beside radioiodine (^{131}I) is the most major released volatile radionuclide having a direct impact on land contamination. The radioactivity can be measured using radiation measurement techniques. In the present PhD thesis, I tried to capture radiocesium and also tried to form a cesium detection system. Background and objective of research are given in detail in Chapter 1.

Chapter 2 shows the Exploration of the Cs Trapping Phenomenon by Combining Graphene Oxide with α-$K_6P_2W_{18}O_{62}$ as Nanocomposite. Graphene oxide (GO) surface has an interesting interaction using a polar -COO(H) and non-polar (-CH3) group in order to adsorb different kinds of cations (charge, size, complexing capability) by a proposed ion-bridging mechanism. In addition, Polyoxometalates (POMs) provide an excellent, robust, and discrete material, which has reversible multi-electron redox properties. Some researchers have employed POMs as a potential Cs adsorption material by using a cation exchange mechanism. Considering the tremendous properties of GO and α-$K_6P_2W_{18}O_{62}$, it is highly desirable to synthesize a new nanocomposite with Cs adsorption ability using the GO and POMs. In this chapter, two types of GO samples were employed. One is GO, which has a large amount of carbon (C), and the other is GO, which has a large amount of oxygen (O). They have a variant sp^2/sp^3 structure. These GOs can be produced by controlling the oxidation degree, which depends on several factors such as the reaction condition, oxidizing agent, and graphite source. It has been known that the GO structure is not precisely determined because of a variety of local arrangements of functional groups. Each GO sample was incorporated with α-$K_6P_2W_{18}O_{62}$. I investigated the interaction of Cs^+ with the nanocomposite by characterizing the surface structure of the

composite material and also by considering the adsorption capacity of the nanocomposite for radioactive Cs. Each property in each material is expected to synergistically strengthen the adsorption capacity of the nanocomposite. A high Cs adsorption capacity was clearly achieved by using the nanocomposite.

Chapter 3 shows the improvement of Cs detection performance and formation of CsCl and Cs nanoparticles by tuning graphene oxide quantum dot-based nanocomposite. In recent years, graphene oxide (GO) and graphene oxide quantum dots (GOQDs) are widely studied in several applications such as metal adsorbent (Cs^{+}, Eu^{3+}, Sr^{2+}) , and designed as fluorescence probes by considering their quantum confinement and the edge effect. In addition, the GO and GOQDs have almost similar properties because they have various oxygen functional groups. The functional group can act as a binding point to synthesize a new nanocomposite to improve their properties. Another important thing is that the photoluminescence (PL) of GOQDs was independent of pH. It means that the emission wavelength does not shift in different pH condition (only change in the PL intensity). Further investigation also revealed that the PL of GO has shown a reversible response to ionic strength and pH. The previous work confirmed that the different number of layers of GO (single and a few layers) showed different optical responses in various organic solvent. More currently, Yao *et al.* have employed graphene quantum dot-based fluorescence sensing as a dual detector of copper ion (Cu^{2+}) and tiopronin (MPG). They proposed a novel fluorescence turn OFF for the Cu^{2+} detection and turn ON for the tiopronin (MPG) detection. Therefore, to facilitate the development of a Cs detection system, it is highly desirable to create a new nanocomposite using functionalized graphene oxide quantum dots (GOQDs) with cesium green molecule. In Chapter 3, I produced a new nanocomposite that has the ability to recognize Cs in water with different pH conditions (acidic and basic condition) by considering the turn ON/OFF response.

Chapter 4 shows the general conclusions. The present findings have provided the fundamental understanding of specific characteristic and structural diversity of GO and its nanocomposite. In particular, the C/O ratio and the GO acidity (influenced by the oxidation debris particle) of the GO sample have significantly influenced the adsorption capacity, the sensitivity and the accuracy of the detection system of the GO-based nanocomposite. It can be used as an entry point to design the structure and the function system for a new advanced nanocomposite. And, the present study offers a bridge between GO and other potential materials. Also, this work may open an application in environmental protection with more deep investigation.

List of Publications

1. **Potentiality of graphene oxide and polyoxometalate as radionuclide adsorbent to restore the environment after Fukushima disaster: A mini review.**
   Bangun Satrio Nugroho, Muh. Nur Khoiru Wihadi, Fabian Grote, Siegfried Eigler, Satoru Nakashima.
   Indones. J. Chem., 2021, 21 (3), 776-786.
   DOI: 10.22146/ijc.60493

2. **Exploration of Cs trapping phenomenon by combining graphene oxide with $K_6P_2O_{18}W_{62}$ as Nanocomposite.**
   Bangun Satrio Nugroho, Akane kato, Chie Kowa, Tomoya Nakashima, Atsushi Wada, Muh. Nur Khoiru Wihadi, Satoru Nakashima.
   Materials, 2021, 14, 5577.
   DOI: 10.3390/ma14195577

3. **Improvement of Cs detection performance and formation of CsCl and Cs nanoparticles by tuning graphene oxide quantum dot-based nanocomposite**
   Bangun Satrio Nugroho and Satoru Nakashima.
   RSC advances, 2022.
   DOI: 10.1039/d2ra02091b

Acknowledgement

It is with a deep sense of gratitude I would like to greatly thank Prof. Satoru Nakashima as a supervisor for the encouragement, assistance, personal guidance, remarkable advice and suggestions enabling me to proceed with my study from zero until the finish. Five years Ph.D program was so challenging. Your valuable knowledge and your attitude have thought me a lot for research work and provided an excellent basis for life. Under your guidance, I feel like become a new person.

Most importantly, I also would like to greatly thank (dedicated this work) my beautiful family for your love, kindness, and your duas. My dear Lia Kumala Dewi (my wife) who struggled a lot from zero until now, my love Ghaisani Dhuha Sakanti (my daughter), my love Athawakil Muhammad Cahayanu (my son), my beloved parents, mbah kung, mbah uti, yangkung (alm.), yangti, my sister (Radiati moviana, Mighfar khamida), pakde boy (mas Wiwid), mba Corry, you all are amazing. May every tear that has ever fallen from your eyes on my behalf become a river for you in paradise.

I would like to acknowledge the financial support of Phoenix Leader Education Program (for the scholarship), Chemistry department, Hiroshima University. I also acknowledge the OSIMO Foundation (for the scholarship) and YAMAMOTO company (being a good working place for part time job) for the support within 5-years Ph.D program.

A word of thanks should be expressed to my colleagues (chemistry members and LP members), Triyono Basuki, Habibur Rahman, Heri Wijayanto for helping out in every single challenged during my study and being my remarkable family.

I also indebted to Dr. Makoto Maeda (Natural Science Centre for Basic Research and Development, Hiroshima University) for the technical support and discussion during the TEM measurement all the time.

I would also like to thank Dr. Takaaki Taniguchi, Dr. Leanddas Nurdiwijayanto as a mentor and for the discussion. This work was performed in part by National Institute for Materials Science internship program (NIMS, Tsukuba, Japan).

I would also like to thank my collaborator Dr. Muh. Nur. Khoiru Wihadi, Prof. Siegfried Eigler, Fabian Grote, Akane kato, Chie Kowa, Tomoya Nakashima, Atsushi Wada for their contributions to the publication.

I also would like to thank Dr. Tuswadi, (alm.) Prof. Trijaka, Prof. Jabri, Pak Akbar Dharma Wahana, who are strongly supported continuing this 5-years Ph.D. program. Finally, my special appreciation and gratitude goes to Pak Aryo, Bude Donna and family for your kind help, all the fun we shared, and being remarkable neighborhood.

Table of Contents

Chapter I. General Introduction

1.1 Background of study

The Fukushima Daiichi nuclear power plant (FDNPP) disaster (March 2011) affected the biotic and abiotic environment. FDNPP accident released radioactive elements that possess long half-lives (30 years for cesium (^{137}Cs)), β-decay to barium (^{137}Ba), and emit γ-radiation. It has been reported that the soil present around FDNPP and the soil in the neighboring prefectures were contaminated with approximately 100,000 MBq/km^2 and 10,000 MBq/km^2 of ^{137}Cs, respectively [1]. The soil surface area was the most contaminated [2]. It has been predicted that several radionuclides, such as cesium (^{137}Cs, ^{136}Cs, ^{134}Cs), strontium (^{90}Sr, ^{89}Sr), uranium (UO^{2+}), iodine (131I), thorium (^{90}Th), barium (^{140}Ba), lanthanum (^{140}La), and tritium (^{3}H) are present. Ananalysis by Tokyo Electric Power Company (TEPCO), an electric power company, revealed that a major part of the fuel (in unit 1 nuclear reactor) was present in its molten state [3]. The radioactive isotopes released during the Fukushima accident and predominantly responsible for the observed radioactivity were the radioactive isotopes of Sr and Cs. It has been reported that Sr exhibits a faster rate of migration compared to other elements [4]. It has been observed that Cs (^{137}Cs, ^{136}Cs, ^{134}Cs) and ^{131}I become the more radioactive elements that were released from the fuel if compared with Sr (^{90}Sr, ^{89}Sr) [5-6].

It is necessary to estimate the quantity of radionuclides and chemicals released during the accident to determine the immediate and long-term effects of radioactivity on the environment and health of organisms. Researchers have studied the mobility of radioactivity, especially the uptake of radioactive nuclides by plants [7]. The uptake of radioactive nuclides by plants can potentially lead to food contamination that can eventually lead to genome damage or cancer in human beings. Further investigation also reported that slightly high levels of radioactive cesium were detected in some rice varieties grown in areas approximately 60 km northwest of the nuclear reactor plant, a few years after the accident in Fukushima City [8]. Researchers have reported that the transfer factor (from the soil to the rice) of radioactive cesium depended on the oxidizing or reducing soil atmosphere [9]. The penetration depth (in soil) of radiocesium is influenced by soil characteristics (such as the particle size, organic carbon content, and clay contents) [10]. One of the key factors influencing the penetration depth of radiocesium in the soil is the amount of medium-sized sand particles present in the soil

[11]. Moreover, an investigation was carried out with soil samples collected from the area around the Hibara Lake (Yama gun, Fukushima prefecture), situated 100 km away from FDNPP, revealing that radionuclides (originating from the Fukushima prefecture) were present in the sediments deposited in the shallow areas of the lake. ^{134}Cs and ^{137}Cs isotopes were detected (4.5 and 5.2 Bq/kg, respectively) in the soil of these areas. The results revealed the long-distance migration of radioactive cesium. The high solubility of radiocesium in water assists soil penetration. Compared to the process of direct deposition of the nuclides (originating from the exhaust of the accident), the process of nuclide transport by rivers into lakes (and its subsequent sedimentation) is more likely to occur [12]. Shizuma et al. investigated the quality of drinking water in the Haramachi district (Minamisoma City). The authors detected dissolved ^{137}Cs in tap water and groundwater. The maximum concentration of ^{137}Cs was approximately 300 mBq/L in August 2013 and 27 mBq/L in September 2014 [13]. The degree of contamination was not solely dependent on the distance of the place under observation from the area of the nuclear accident. Other factors, such as weather conditions (such as wind direction and precipitation), also affected the degree of soil contamination [14].

These results revealed that radionuclide contamination, which can potentially impact human lives, is a severe environmental problem. The contamination had spread far and wide, away from the Fukushima nuclear power plant. Therefore, it is necessary to decontaminate the environment effectively. A few decontamination strategies, such as removing the litter layer and superficial soil layer in the forests, have already been implemented [15-16]. Decontamination has also been attempted by scraping off the topsoil and cleaning tree barks. The reverse plowing technique has also been used for the same aim [17]. Recently, researchers have attempts to synthesize high-quality adsorbent nanomaterials that can potentially remove radionuclides from the environment. Graphene oxide (GO) and polyoxometalates (POM) derivatives are the two classes of materials that have recently attracted immense intention. GO has been the focus of research as it has its application in various fields, such as biomedicine [18-19] and environmental protection [20- 22]. It has also been used to develop energy storage devices [23], polymer composites [24], and gas sensors [25]. The properties of GO can be tuned by systematically functionalizing the material. This can lead to improved performance of the materials [26]. The synthesis of materials that can function as radionuclide adsorbents, such as H-titanate nanotubes [27] and phlogopite [28], has been reported. However, not

all the reported materials are excellent adsorbents. Therefore, a potential material that can function as a highly efficient radionuclide adsorbent should be identified.

GO is a promising candidate that can be potentially used for adsorbing radionuclides. The epoxide and hydroxyl groups are the two major functional groups present on both sides of the basal plane of the GO sheets [26]. GO contains numerous structural defects. Other functional groups, such as carbonyl groups, phenol-like groups, and carboxyl groups, are present at the rims of these defects. The particle size of GO plays an important role in determining the functional group composition of the material [29-30]. Therefore, the adsorption capacity of GO is dictated by the accessible surface area. Thus, it is important to understand the structural characteristics of GO to gain insight into the adsorption process.

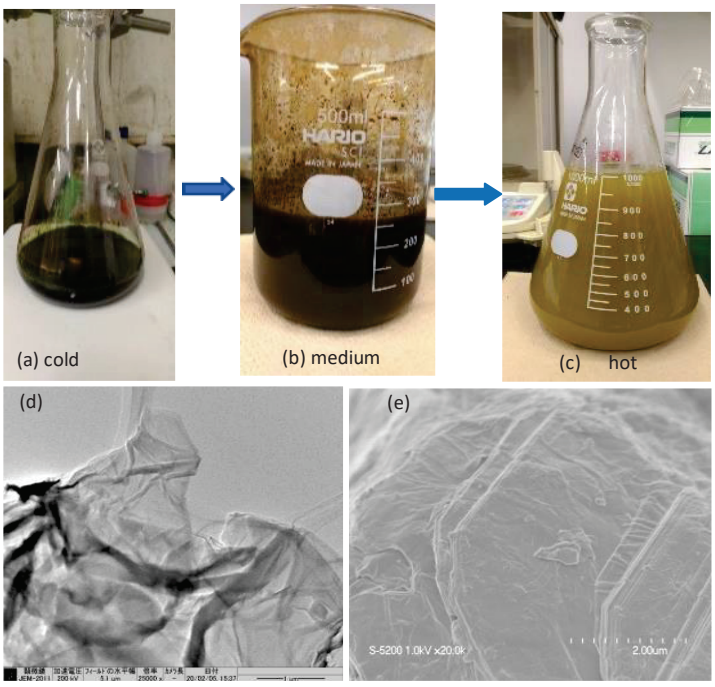

Fig. 1. Synthesis of GO using the modified Hummer's method. (a) Cold stage (Blackish green), (b) Medium stage (Brown), (c) Hot stage (Golden yellow particles of GO), (d) Transmission electron microscopy (TEM) image of GO, and (e) Scanning electron microscopy (SEM) image of GO. Image is taken from personal data based on an experimental.

Recently, researchers have followed the combined method proposed by Grote et al. and attempted the fabrication of GO. The oxo-functionalized graphene bears an almost intact hexagonal carbon lattice (unlike the conventional GO material fabricated following

Hummer's method) [31]. The fabrication method involves a three-step process (the cold, medium, and hot stages). The transition from one stage to the other is accompanied by a change in color of the reaction mixture, which indicates the successful completion of each stage (Fig. 1(a), (b), and (c)) [32]. The fabrication of a single (or a few) layers of GO can be achieved through the processes of chemical oxidation and exfoliation [33]. The transmission electron microscopy (TEM) and scanning electron microscopy (SEM) techniques were used to visualize the surface morphology of GO (Fig. 1(d) and (e)). The SEM and TEM images revealed the presence of wrinkled and overlapping GO sheets. These properties were a result of the hydrogen- bonding interactions present between the surface functional groups. The wrinkled and overlapped samples exhibit different optical and electrical properties [34]. Guerrero-Contreras and Caballero-Briones reported that the degree of GO oxidation dictates this particular characteristic, especially the surface chemistry of the sheets. These properties can be exploited by decorating GO [35].

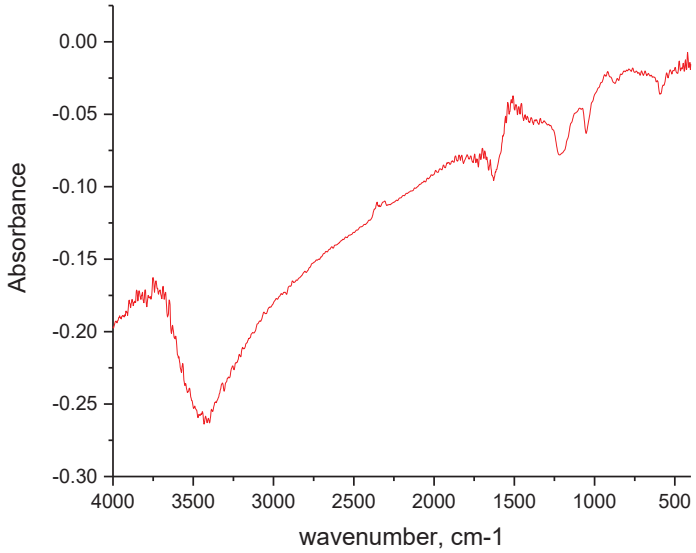

Fig. 2. FTIR spectral profile of GO. Graphic took from personal data based on an experimental study

The characteristic peaks of different functional groups were observed in the Fourier transform infrared (FTIR) spectral profiles (Fig. 2). The peaks observed at 1057, 1230, 1730, and 3424 cm^{-1} corresponded to the stretching vibrations of C–O, C–OH, C=O, and –OH groups, respectively. The peak corresponding to the unoxidized graphitic area was observed at 1618 cm^{-1} [36].

The Fukushima disaster of 2011 led researchers to focus on developing new materials capable of adsorbing radioactive elements. Experiments were conducted to investigate the effectiveness of GO as radionuclide (especially actinide) adsorbents. The results revealed that the process of coagulation contributed significantly to the adsorption process. Cation-induced coagulation leads to the quick precipitation of GO. The coagulation of GO (in the presence of cations) is affected by pH. Cations with different charges behave differently under the same pH conditions. For example, sodium (Na^+), calcium (Ca^{2+}), and lanthanide (Eu^{3+}), at the same pH, exhibited different critical coagulation concentration (CCC). The changes visible to the naked eye were observed. The interactions present in the GO sheets impart the GO layers with improved adsorption properties (compared to bentonite clays and activated carbon) [37].

Table 1. Eu(III), Sr(II), and Cs^+ sorption capacity of GO and other materials

Nanocomposite	Maximum sorption capacity (mg/g)			pH range	Ref.
	Eu (III)	Sr (II)	Cs		
PS_25GO	-	20.2	-	2.0–8.0	[43]
PS_15GO-COOH	-	11.47	-	2.0–7.0	[43]
GO nanosheet	175.44	-	-	6.0	[21]
GO nanosheet	161.29	-	-	4.5	[21]
H-titanates nanotubes short	22.8	-	-	4.2	[27]
GO	-	-	528	12	[40]
GO	-	-	465	7	[40]
Phlogopite	-	-	14.8	2	[28]
Ca-phlogopite	-	-	60.4	2	[28]
PANI@GO	-	266.3	121.7	3	[22]

As commonly used for cationic radionuclides, bentonite clays and activated carbon have different physical characteristics. Bentonite consists mostly of montmorillonite (a three-layered mineral) having octahedral and tetrahedral sheets [38]. Activated carbon is a non-porous material possessing a large specific surface area. However, functional groups are absent. Therefore, researchers have attempted to functionalize the surface of activated carbon to improve its adsorption ability [39]. Kaewmee et al. reported that the cesium sorption capacity of pristine GO was comparable to the cesium sorption capacity of Prussian blue. It was experimentally demonstrated that the maximum adsorption capacity was approximately 528 mg Cs/g of GO. The sorption ability was tuned by

adjusting the pH of the medium [40]. An interesting phenomenon was observed when the experiments were carried out under a broad range of pH. It experimentally found that the sorption capacity of a magnetic GO nanocomposite, in the pH range of 5 to 9, exceeded 90% (removal of americium (Am) and plutonium (Pu) from solution) [41]. Yang et al. successfully developed a composite consisting of Prussian blue, Fe_3O_4 nanoparticles, and GO. It was reported that GO is an efficient cesium adsorbent. The cesium sorption capacity of the PB/Fe_3O_4/GO composite (55.56 mg/g) was higher than that of the PB/Fe_3O_4 composite (46.30 mg/g). The successful removal of Cs (by H^+-exchange or ion trapping) can be attributed to the anchoring of Prussian blue and Fe_3O_4 nanoparticles on the surface of GO. However, peaks corresponding to GO were not observed in the PXRD pattern because of the low GO content of the samples [42].

Bubenikova et al. reported that the adsorption capacity of GO could be improved via the carboxylation process (PS_25GO, PS_15GO-COOH, Table 1). The results revealed that the uptake kinetics of strontium (II) was fast. A simple method was used for carboxylation. Multiple carboxylate groups were introduced on the GO surface using a solution of chloroacetic acid in water. Subsequently, a GO-polystyrene (GO-PS) nanocomposite was fabricated to develop the desired material [43].

Recently, researchers have attempted to tune the properties and control the degree of oxidation of the graphene-like materials by tailoring their oxygen content (following specific methods) [44-45]. Novacek et al. reported that a significant increase in the sorption capacity could be achieved by oxidizing GO multiple times. The multiple oxidation process is the key to achieve high oxygen content and significantly increased carboxylic acid content, leading to the significantly high sorption capacity of the material [46]. Researchers have also investigated the role of cation bridging in promoting the formation of GO complexes. The Cs cations were better transport inhibitors at higher concentrations than other monovalent cations. The surface functional groups played an important role in achieving transport inhibition. GO can form inner-sphere complexes with Cs cations [47].

Similar to GO, the POM derivatives are high-performance adsorbent nanomaterials. POMs are anionic metal oxide clusters consisting of tungsten (W), vanadium (V), molybdenum (Mo), and niobium (Nb) in their high oxidation states. POMs possess interesting properties (such as redox, acidic, photochemical, and magnetic properties) [48]. To date, many families of POMs have been reported [49-50], such as the phosphotungstate family, which is one of the most popular families of POMs. The

Keggin-type compound $[PW_{12}O_{40}]^{3-}$ is a member of the phosphotungstate family consisting of one phosphate unit surrounded by 12 tungstate units. Other members of the family include the Dawson-type compound $[P_2W_{18}O_{60}]^{6-}$ formed of two phosphate and 18 tungstate units and the Preyssler-type compound $[P_5W_{30}O_{110}Na(H_2O)]^{14-}$ consisting of five phosphates surrounded by 30 tungstates (Fig. 3). Structurally diverse POMs can find their applications in a wide range of fields. In this mini-review, we have focused on the removal of radionuclides using POM. Recently, it has been investigated if POMs exhibiting the Dawson-type structure can be used to extract thorium and actinium [51]. This work has successfully exploited the coordination chemistry of thorium and actinium and has conducted experiments under acidic conditions (using ion-exchange resins) to extract nuclides using the Dawson-type POM. The Keggin-type POM (Fig. 3) exhibits excellent Bronsted acidity and interesting redox properties. They can be potentially used for protecting the environment [52]. Reduction-induced Cs^+ uptake was achieved by the redox-active ionic crystal [α-$SiMo_{12}O_{40}$] in the presence of ascorbic acid [53]. In a strongly acidic solution, the central sodium ion of the Preyssler anion $[NaP_5W_{30}O_{110}]^{14-}$ can be replaced by Eu^{3+} [54].

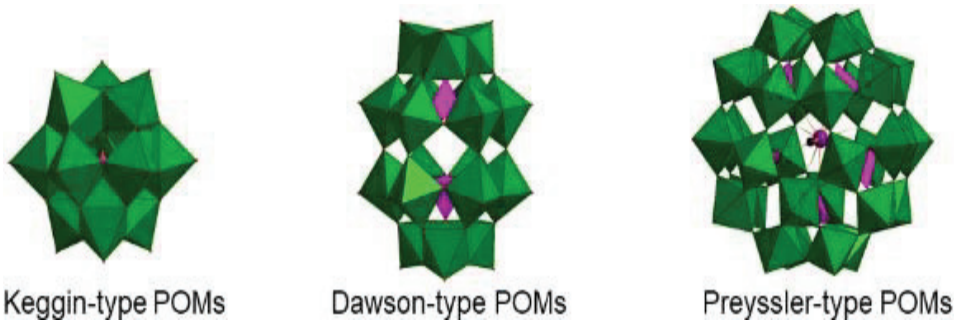

Fig. 3. Members of the Phosphotungstate family of POMs

Therefore, the synergistic effect between POMs and other molecules can assist the efficient removal of nuclides (Fig. 4) [55]. Wang et al. fabricated graphene/POM composites utilizing covalent bonding. Fabrication of the composites exploiting the concept of covalent bonding addressed the problem of POM detachment from the carriers. The report revealed that the surface area of the GO/POM composite was five times larger than that of the POM-only [56]. Lu et al. reported strong interlayer interactions could be produced by POMs (on the GO sheets) when epoxy groups are substituted by ethylenediamine groups (EN, weak reductant). Abundant hopping sites are generated that promote the rapid propagation of protons. It has been reported that the anchoring of

POM nanoparticles onto the GO layers helps to generate mobile protons and flexible routes for proton transport. Therefore, the protons can exploit the hopping sites to change their motion path and speed up the process of transportation [57]. The TEM images reveal that the individual clusters of POM appear as black spots on the surface area (when POM is anchored onto the GO layer). It can be concluded that the oxygen functional group on the graphene sheet and the corner shared metal-oxygen site of POMs in an aqueous solution, interacting with each other via electrostatic interactions [58].

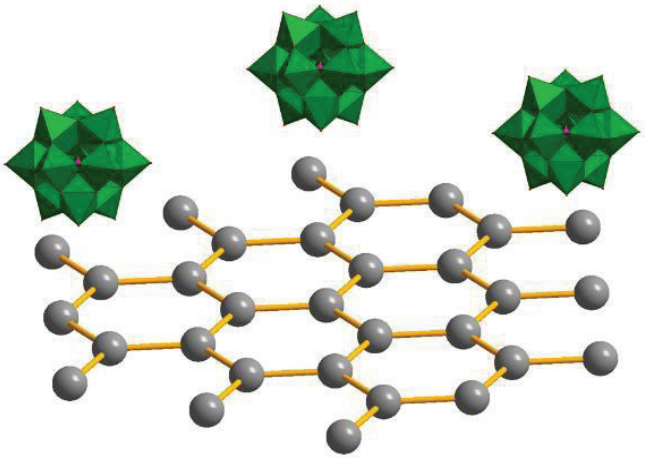

Fig. 4. Plausible interaction between Keggin-type POMs and GO

To date, many researchers have attempted to synthesize POM composites that can potentially serve as adsorbents. Herrmann et al. investigated the effects of chemisorption and physisorption of POM-ionic liquid (POM-IL) [59]. Liu et al. investigated these effects in more detail. They successfully fabricated a GO-based nanocomposite by impregnating POM on the GO layer (following the impregnation method), exhibiting an improved loading ability of GO. The fabrication process can potentially lead to the strong electrostatic attraction between the adsorbate and the absorbent [60]. Sures and Nyman carried out their experiments with $A_8[Nb_6O_{19}]\cdot nH_2O$ (A = Li, K, Rb, Cs), ($[Nb_2W_4O_{19}]^{4-}$, and $[Nb_4W_2O_{19}]^{6-}$. They concluded that Cs exhibits a strong tendency to form complexes with anionic surfaces. The formation of the complexes can also be mediated by a mediation sphere [61]. Hitose and Uchida studied compounds I and II (Wells–Dawson-type POMs, [α- $P_2M_{18}O_{62}$]) that exhibit fast adsorption kinetics (1 h to reach equilibrium). They reported that the compounds exhibited an increased cesium uptake capacity [62]. However, it is challenging to deal with radionuclides (in solution and solid surfaces). Radionuclides, such as Cs^+ that utilize their unusually high coordination number to form

complexes, exhibit abnormal behavior (ion-pairing) [61]. The radiation emitted from a radioactive material can potentially lead to the generation of another variable in adsorption materials that can potentially affect their structural stability [63]. Therefore, a better understanding of the mechanism of action of POMs is required to tune and improve the functions of POM-based materials. POM, which has different arrangements, sizes, charges, and structures, can form several types of crystalline structures [58,64]. Their unique structures make them important to stabilize ligands for redox-active high-valance metallic fragments [65]. The interaction between electrons and alkali metals (during their migration) in POM-based porous crystals can be explained by the redox ion-exchange phenomenon [66]. Thus, the unique characteristics of POMs eventually lead to improved properties of the material formed by the interaction between POM and the support materials.

Based on that, in this thesis, we fabricated two types of a new nanocomposites as radionuclides adsorbents and radionuclides detections to restore environmental conditions. In the synthesis methodology, Hummer`s method was used as oxidation method. First, graphene oxide combining with POM material (Dawson-type POM) as Cs removal. Second, graphene oxide quantum dot (GOQDs) functionalized by cesium green molecule ($C_{32}H_{33}NO_8$) as Cs detection. As a result, we found that a high Cs adsorption capacity was achieved by using the nanocomposite. In addition, the nanocomposite has ability to recognize Cs in water with different pH conditions (acidic and basic) by considering the turn ON/OFF response.

1.2. The purpose of study

This thesis has some specific objectives as follows:

- Investigate the role of the C/O ratio of graphene oxide (GO) specifically to cesium (Cs) adsorption performance after forming the composite
- Investigate the role of the oxidized zone (sp^2/sp^3 hybrid carbon cluster) before and after forming the composite as an important factor in the enhancement of adsorption capacity
- Synthesis GO-POM (polyoxometalate) nanocomposite as a Cs removal
- Investigate the optical properties of GO quantum nano dots and their composite as cesium (Cs) detection in mixed solution (Distilled water/THF)
- Synthesis graphene oxide quantum dot-based nanocomposite (combining with cesium green molecule, $C_{32}H_{33}NO_8$) as Cs detector
- Investigate the Cs cluster formation under electron beam irradiation

1.3. References

[1] Yasunari, T.J., Stohl, A., Hayano, R.S., Burkhart, J.F., Eckhardt, S., and Yasunari, T., 2011, Cesium- 137 deposition and contamination of Japanese soils due to the Fukushima nuclear accident, Proc. Natl. Acad. Sci. U.S.A., 108 (49), 19530–19534.
[2] Nakanishi, T.M., 2017, Research with radiation and radioisotopes to better understand plant physiology and agricultural consequences of radioactive contamination from the Fukushima Daiichi nuclear accident, J. Radioanal. Nucl. Chem., 311 (2), 947–971.
[3] Tokyo Electric Power Company, 2011, The evaluation status of reactor core damage at Fukushima Daiichi nuclear, power station unit 1 of 3, https://www.tepco.co.jp/en/nu/fukushima np/ images/handouts_111130_04-e.pdf.
[4] Wang, X., Chen, L., Wang, L., Fan, Q., Pan, D., Li, J., Chi, F., Xie, Y., Yu, S., Xiao, C., Luo, F., Wang, J., Wang, X., Chen, C., Wu, W., Shi, W., Wang, S., and Wang, X., 2019, Synthesis of novel nanomaterials and their application in efficient removal of radionuclides, Sci. China Chem., 62 (8), 933–967.
[5] Nishihara, K., Yamagishi, I., Yasuda, K., Ishimori, K., Tanaka, K., Kuno, T., Inada, S., and Gotoh, Y., 2015, Radionuclide release to stagnant water in the Fukushima-1 nuclear power plant 1, J. Nucl. Sci. Technol., 52 (3), 301–307.
[6] Foreman, M.R.S.J., 2015, An introduction to serious nuclear accident chemistry, Cogent Chem., 1 (1), 1049111.

[7] Uchida, S., and Tagami, K., 2007, Soil-to-plant transfer factors of fallout ^{137}Cs and native ^{133}Cs in various crops collected in Japan, J. Radioanal. Nucl. Chem., 273 (1), 205–210.
[8] Matsuda, N., and Nakashima, S., 2014, Radioactive cesium in water and soil and its adsorption to rice plant (interim report) (in Japanese), Radiat. Saf. Manage., 13 (1), 84–91.
[9] Nguyen, H.T., Tsujimoto, M., and Nakashima, S., 2019, Study on paddy soil in Fukushima using Mössbauer spectroscopy, Hyperfine Interact., 240 (1), 122.
[10] Koarashi, J., Atarashi-Andoh, M., Matsunaga, T., Sato, T., Nagao, S., and Nagai, H., 2012, Factors affecting vertical distribution of Fukushima accident- derived radiocesium in soil under different land–use conditions, Sci. Total Environ., 431, 392–401.
[11] Tsujimoto, M., Miyashita, S., Nguyen, H.T., and Nakashima, S., 2020, Monthly change in radioactivity concentration of ^{137}Cs, ^{134}Cs, and ^{40}K of paddy soil and rice plants in Fukushima Prefecture, Radiat. Saf. Manage., 19, 10–22.
[12] Basuki, T., Miyashita, S., Tsujimoto, M., and Nakashima, S., 2018, Deposition density of ^{134}Cs and ^{137}Cs and particle size distribution of soil and sediment profile in Hibara Lake area, Fukushima: An investigation of ^{134}Cs and ^{137}Cs indirect deposition into lake from surrounding area, J. Radioanal. Nucl. Chem., 316 (3), 1039–1046.
[13] Shizuma, K., Fujikawa, Y., Kurihara, M., and Sakurai, Y., 2018, Identification and temporal decrease of ^{137}Cs and ^{134}Cs in groundwater in Minami–Soma City
following the accident at the Fukushima Dai-ichi nuclear power plant, Environ. Pollut., 234, 1–8.
[14] Steinhauser, G., Brandl, A., and Johnson, T.E., 2014, Comparison of the Chernobyl and Fukushima nuclear accidents: A review of the environmental impacts, Sci. Total Environ., 470-471, 800–817.
[15] Ayabe, Y., Hijii, N., and Takenaka, C., 2017, Effects of local-scale decontamination in a secondary forest contaminated after the Fukushima nuclear power plant accident, Environ. Pollut., 228, 344–353.
[16] Koarashi, J., Atarashi-Andoh, M., Nishimura, S., and Muto, K., 2020, Effectiveness of decontamination by litter removal in Japanese forest ecosystems affected by the Fukushima nuclear accident, Sci. Rep., 10 (1), 6614.
[17] IAEA, 2015, The Fukushima Daiichi Accident: Technical Volume 5–Post-Accident Recovery, International Atomic Energy Agency, Vienna, https://www-pub.iaea.org/MTCD/Publications/PDF/ AdditionalVolumes/P1710/Pub1710-TV5-Web.pdf.
[18] del Valle, E.M.M., Galán, M.A., and Carbonell, R.G., 2009, Drug delivery technologies: The way forward in the new decade, Ind. Eng. Chem. Res., 48 (5), 2475–2486.
[19] Tabish, M.S., Hanapi, N.S.M., Ibrahim, W.N.W., Saim, N., and Yahaya, N., 2019, Alginate-graphene oxide biocomposite sorbent for rapid and selective extraction of non-

steroidal anti-inflammatory drugs using micro-solid phase extraction, Indones. J. Chem., 19 (3), 684–695.
[20] Nor, N.M., Kamil, N.H.N., Mansor, A.I., and Maarof, H.I., 2020, Adsorption analysis of fluoride removal using graphene oxide/eggshell adsorbent, Indones. J. Chem., 20 (3), 579–586.
[21] Sun, Y., Wang, Q., Chen, C., Tan, X., and Wang, X., 2012, Interaction between Eu(III) and graphene oxide nanosheets investigated by batch and extended X-ray absorption fine structure
spectroscopy and by modeling techniques, Environ. Sci. Technol., 46 (11), 6020–6027.
[22] Sun, Y., Shao, D., Chen, C., Yang, S., and Wang, X., 2013, Highly efficient enrichment of radionuclides on graphene oxide-supported polyaniline, Environ. Sci. Technol., 47 (17), 9904–9910.
[23] Ke, Q., and Wang, J., 2016, Graphene-based materials for supercapacitor electrodes – A review, J. Materiomics, 2 (1), 37–54.
[24] Fan, J., Shi, Z., Lian, M., Li, H., and Yin, J., 2013, Mechanically strong graphene oxide/sodium
alginate/polyacrylamide nanocomposite hydrogel with improved dye adsorption capacity, J. Mater. Chem. A, 1 (25), 7433–7443.
[25] Debataraja, A., Manurung, R.V., Asri, L.A.T.W., Yuliarto, B., Nugraha, N., and Sunendar, B., 2018, Synthesis and characterization of nanocomposites of tin–oxide graphene doping Pd using Polyol method, Indones. J. Chem., 18 (2), 344–348.
[26] Eigler, S., Dotzer, C., Hof, F., Bauer, W., and Hirsch, A., 2013, Sulfur species in graphene oxide, Chem. Eur. J., 19 (29), 9490–9496.
[27] Petrov, V.G., Chen, Z., Romanchuk, A.Y., Demina, V.O., Tang, Y., and Kalmykov, S.N., 2019, Sorption of Eu(III) onto nano-sized H-titanates of different structures, Appl. Sci., 9 (4), 697.
[28] Tamura, K., Kogure, T., Watanabe, Y., Nagai, C., and Yamada, H., 2014, Uptake of cesium and strontium ions by artificially altered phlogopite, Environ. Sci. Technol., 48 (10), 5808–5815.
[29] Dideikin, A.T., and Vul, A.Y., 2019, Graphene oxide and derivatives: The place in graphene family, Front. Phys., 6, 149.
[30] Szabó, T., Berkesi, O., Forgó, P., Josepovits, K., Sanakis, Y., Petridis, D., and Dékány, I., 2006, Evolution of surface functional groups in a series of progressively oxidized graphite oxides, Chem. Mater., 18 (11), 2740–2749.
[31] Grote, F., Gruber, C., Börrnert, F., Kaiser, U., and Eigler, S., 2017, Thermal disproportionation of oxo- functionalized graphene, Angew. Chem. Int. Ed., 56 (31), 9222–9225.
[32] Hummers, W.S., and Offeman, R.E., 1958, Preparation of graphitic oxide, J. Am. Chem. Soc., 80 (6), 1339.

[33] Ranjan, P., Agrawal, S., Sinha, A., Rao, T.R., Balakrishnan, J., and Thakur, A.D., 2018, A low-cost non-explosive synthesis of graphene oxide for scalable applications, Sci. Rep., 8 (1), 12007.
[34] Cote, L.J., Kim, J., Zhang, Z., Sun, C., and Huang, J., 2010, Tunable assembly of graphene oxide surfactant sheets: Wrinkles, overlaps and impacts on thin film properties, Soft Matter, 6 (24), 6096–6101.
[35] Guerrero-Contreras, J., and Caballero-Briones, F., 2015, Graphene oxide powders with different oxidation degree, prepared by synthesis variations of the Hummers method, Mater. Chem. Phys., 153, 209–220.
[36] Xu, Y., Liu, Z.W., Xu, Y.L., Zhang, Y.Y., and Wu, J.L., 2014, Preparation and characterization of
graphene/ZnS nanocomposites via a surfactant-free method, J. Exp. Nanosci., 9 (4), 415–420.
[37] Romanchuk, A.Y., Slesarev, A.S., Kalmykov, S.N., Kosynkin, D.V., and Tour, J.M., 2013, Graphene oxide for effective radionuclide removal, Phys. Chem. Chem. Phys., 15 (7), 2321–2327.
[38] Seliman, A.F., Lasheen, Y.F., Youssief, M.A.E., Abo- Aly, M.M., and Shehata, F.A., 2014, Removal of some radionuclides from contaminated solution using natural natural clay: Bentonite, J. Radioanal. Nucl. Chem., 300 (3), 969–979.
[39] Mahmoud, M.R., Sharaf El-deen, G.E., and Soliman, M.A., 2014, Surfactant-impregnated activated carbon for enhanced adsorptive removal of Ce(IV) radionuclides from aqueous solutions, Ann. Nucl. Energy, 72, 134–144.
[40] Kaewmee, P., Manyam, J., Opaprakasit, P., Le, G.T.T., Chanlek, N., and Sreearunothai, P., 2017, Effective removal of cesium by pristine graphene oxide: Performance, characterizations and mechanisms, RSC Adv., 7 (61), 38747–38756.
[41] Semcuk, S., 2018, Application of graphene oxide based nanocomposites and Šaltiškiai clay
For radionuclides removal from contaminated solutions, Dissertation, Institute of Physics of the State Research Institute for Physical Science and Technology, Vilnius University, Lithuania.
[42] Yang, H., Sun, L., Zhai, J., Li, H., Zhao, Y., and Yu, H., 2014, In situ controllable synthesis of magnetic Prussian blue/graphene oxide nanocomposites for removal of radioactive cesium in water, J. Mater. Chem. A, 2 (2), 326–332.
[43] Bubeníková, M., Ecorchard, P., Szatmáry, L., Mrózek, O., Salačová, P., and Tolasz, J., 2018, Sorption of Sr(II) onto nanocomposites of graphene oxide-polymeric matrix, J. Radioanal. Nucl. Chem., 315 (2), 263–272.
[44] Morimoto, N., Kubo, T., and Nishina, Y., 2016, Tailoring the oxygen content of graphite and reduced graphene oxide for specific applications, Sci. Rep., 6 (1), 21715.

[45] Ebajo, V.D., Santos, C.R.L., Alea, G.V., Lin, Y.A., and Chen, C.H., 2019, Regenerable acidity of graphene oxide in promoting multicomponent organic synthesis, Sci. Rep., 9 (1), 15579.
[46] Nováček, M., Jankovský, O., Luxa, J., Sedmidubský, D., Pumera, M., Fila, V., Lhotka, M., Klímová, K., Matějková, S., and Sofer, Z., 2017, Tuning of graphene oxide composition by multiple oxidations for carbon dioxide storage and capture of toxic metals, J. Mater. Chem. A, 5 (6), 2739–2748.
[47] Xia, T., Qi, Y., Liu, J., Qi, Z., Chen, W., and Wiesner, M.R., 2017, Cation-inhibited transport of graphene oxide nanomaterials in saturated porous media: The Hofmeister effects, Environ. Sci. Technol., 51 (2), 828–837.
[48] Pope, M.T., and Müller, A., 1991, Polyoxometalate chemistry: An old field with new dimensions in several disciplines, Angew. Chem. Int. Ed. Engl., 30 (1), 34–48.
[49] Nyman, M., and Burns, P.C., 2012, A comprehensive comparison of transition- metal and actinyl polyoxometalates, Chem. Soc. Rev., 41 (22), 7354– 7367.
[50] Wihadi, M.N.K., Hayashi, A., Ichihashi, K., Ota, H., Nishihara, S., Inoue, K., Tsunoji, N., Sano, T., and Sadakane, M., 2019, A sandwich complex of bismuth cation and mono-lacunary α-Keggin-type phosphotungstate: Preparation and structural characterization, Eur. J. Inorg. Chem., 2019 (3-4), 357–362.
[51] Hatcher, J.L., 2018, Fundamental chemistry related to separations and coordination of actinium-225, thorium-227, and technetium-99, Dissertation, The Graduate Center, City University of New York, US. [52] Petit, C., and Bandosz, T.J., 2009, Graphite oxide/polyoxometalate nanocomposites as adsorbents of ammonia, J. Phys. Chem. C, 113 (9), 3800–3809.
[53] Seino, S., Kawahara, R., Ogasawara, Y., Mizuno, N., and Uchida, S., 2016, Reduction-induced highly selective uptake of cesium ions by an ionic crystal based on silicododecamolybdate, Angew. Chem. Int. Ed., 55 (12), 3987–3991.
[54] Kim, K.C., Pope, M.T., Gama, G.J., and Dickman, M.H., 1999, Slow proton exchange in aqueous solution. Consequences of protonation and hydration within the central cavity of Preyssler anion derivatives, $[|M(H_2O)|\supset P_5W_{30}O_{110}]^{n-}$, J. Am. Chem. Soc., 121 (48), 11164–11170.
[55] Li, H., Pang, S., Feng, X., Müllen, K., and Bubeck, C., 2010, Polyoxometalate assisted photoreduction of graphene oxide and its nanocomposite formation, Chem. Commun., 46 (34), 6243–6245.
[56] Wang, R., Dang, L., Liu, Y., and Jiao, W., 2019, Preparation, characterization and photocatalytic activity of Dawson type phosphotungstate/graphene oxide composites, Adv. Powder Technol., 30 (7), 1400–1408.
[57] Liu, Y., Liu, S., Lai, X., Miao, J., He, D., Li, N., Luo, F., Shi, Z., and Liu, S., 2015, Polyoxometalate- modified sponge-like graphene oxide monolith with high proton-conducting performance, Adv. Funct. Mater., 25 (28), 4480–4485.

[58] Kim, Y., and Shanmugam, S., 2013, Polyoxometalate-reduced graphene oxide hybrid catalyst: Synthesis, structure, and electrochemical properties, ACS Appl. Mater. Interfaces, 5 (22), 12197–12204.
[59] Herrmann, S., De Matteis, L., de la Fuente, J.M., Mitchell, S.G., and Streb, C., 2017, Removal of multiple contaminants from water by polyoxometalate supported ionic liquid phases (POM-SILPs), Angew. Chem. Int. Ed., 56 (6), 1667– 1670.
[60] Liu, Y., Luo, F., Liu, S., Liu, S., Lai, X., Li, X., Lu, Y., Li, Y., Hu, C., Shi, Z., and Zheng, Z., 2017, Aminated graphene oxide impregnated with photocatalytic polyoxometalate for efficient adsorption of dye pollutants and its facile and complete photoregeneration, Small, 13 (4), 1603174.
[61] Sures, D.J., and Nyman, M., 2017, "Anomalous cesium ion behavior in aqueous polyoxometalate solutions" in Cesium: Properties, Production and Application, Eds. Hall, B., Nova Science Publisher, Inc., New York, 119–148.
[62] Hitose, S., and Uchida, S., 2018, Rapid uptake/release of Cs^+ in isostructural redox-active porous ionic crystals with large-molecular-size and easily reducible Dawson-type polyoxometalates as building blocks, Inorg. Chem., 57 (9), 4833–4836.
[63] Belloni, F., Kütahyali, C., Rondinella, V.V., Carbol, P., Wiss, T., and Mangione, A., 2009, Can carbon nanotubes play a role in the field of nuclear waste management?, Environ. Sci. Technol., 43 (5), 1250– 1255.
[64] Ammam, M., 2013, Polyoxometalates: Formation, structures, principal properties, main deposition, methods and application in sensing, J. Mater. Chem. A, 1 (21), 6291–6312.
[65] Miras, H.N., Yan, J., Long, D.L., and Cronin, L., 2012, Engineering polyoxometalates with emergent properties, Chem. Soc. Rev., 41 (22), 7403–7430.
[66] Kawahara, R., Uchida, S., and Mizuno, N., 2015, Redox-induced reversible uptake-release of cations in porous ionic crystals based on polyoxometalate: Cooperative migration of electrons with alkali metal ions, Chem. Mater., 27 (6), 2092–2099.

Chapter II. Exploration of Cs trapping phenomenon by combining graphene oxide (GO) with $K_6P_2O_{18}W_{62}$ as Nanocomposite

2.1. Introduction

The destruction of the reactor cores of Fukushima Daiichi Nuclear Power Plant (FDNPP) ten years ago has influenced much the environmental condition. Many researchers predicted the quantity of released material [1] and modelling of the radiation fallout immediately [2]. It is important to consider the radioactive isotopes delivered to agriculture area [3], tap water [4], and forest area [5]. The subject of considerable concern by the people is the possibility of the radiation exposure to their body. Both the external exposure and internal exposure have a possibility to show the radiological consequences to cause developing cancer [6][7]. Therefore, it is an essential task to treat and decontaminate the contaminated environment.

^{137}Cs, which has a half-life of 30 years, is one of the nuclides that have been found in the contaminated area [8]. The ^{137}Cs was originated from the Tokyo Electric Power Company (TEPCO) FDNPP accident [9]. Many studies have investigated how to handle radioactive cesium as a crucial radioisotope [10]. Chemical adsorption methods by using composite [11], clay [12] to catch the Cs are the techniques suggested in many papers. According to these methods, the adsorption mechanism emerges as an important concept (like hydroxyl-interlayered vermiculate, 3D microporous composite) and encourages the synthesis of new material. Therefore, the goal of this work is to create a new sorbent material, which has an ability to adsorb the Cs with high efficiency. As is well known, the skeleton of GO having different oxygen functional groups can be considered as a bonding point [13]. Based on that, the chemical modification opens up the idea for tailoring the graphene oxide (GO) with another compound.

Zilong Liu et al. (2019) investigated that as a novel carbonaceous material GO surface has an interesting interaction using polar –COO(H) and non-polar ($-CH_3$) group in order to adsorb different kind of cation (charge, size, complexing capability) by proposed ion bridging mechanism [14]. Another important thing is the solubility of GO in the diverse range of solvent including water due to the hydroxyl, epoxide functional group and carboxyl group attached on the surface and the sheet edge [15], [16].

On the other hand, polyoxometalates (POMs) provide an excellent, robust and discrete material, which has reversible multi-electron redox properties [17]. Some researchers have employed POMs as potential Cs adsorption material by using a cation

exchange mechanism [18]. For example, it was investigated that the interaction of Cs^+ with POMs makes it easier to enter and diffuse through the solid-state structure compared to other type of cation by considering the dehydration enthalpy and hydration radius of the cations [19]. The $K_6P_2W_{18}O_{62}$ as a Dawson-type compound has an anionic molecular framework constructed by two phosphates, 18 tungstates surrounding a central potassium. POM has a large molecular size [20], high potential to reduce [17], and it is a structurally well-defined oxide cluster anion. Furthermore, R.D. Gall et al. confirmed that POM particles could easily be adsorbed on the carbon material [22]. It is also proved by previous study that the anionic PW_{12} cluster can be adsorbed on the reduced GO and can improve the dispersibility of water on the reduced graphene sheet [21].

Considering the tremendous properties of GO and α-$K_6P_2W_{18}O_{62}$, it is highly desirable to synthesize a new nanocomposite with Cs adsorption ability using the GO and POMs [79]. In this study, two types of GO samples were employed. One is GO which has high carbon (C) element and the other is GO which has high oxygen (O) element. They have a variant sp^2/sp^3 structure. These GOs can be produced by controlling oxidation degree, which depends on several factors such as reaction condition, oxidizing agent, graphite source [23]. It has been known that the GO structure is not precisely determined because of a variety of local arrangement of functional group [24], [25]. Each GO sample was incorporated with α-$K_6P_2W_{18}O_{62}$. We investigated the interaction of Cs^+ with the nanocomposite by characterizing the surface structure of the composite material and also by considering the adsorption capacity of nanocomposite for radioactive Cs. Each property in each material is expected to synergistically strengthen the adsorption capacity of nanocomposite. High Cs adsorption capacity was clearly achieved by using nanocomposite.

2.2. Materials and Methods

2.2.1 Materials

All raw chemicals were reagent grade and were used without purification, and distilled water was used in all experiments. Graphite, $Na_2WO_4{\cdot}2H_2O$, CsCl, and methanol were purchased from Sigma Aldrich Chemistry. $NaNO_3$, H_2SO_4, HCl, H_3PO_4, and KCl were purchased from Fuji Film Wako Pure Chemical Corporation. $KMnO_4$ and H_2O_2 were purchased from Tokyo Chemical Industry.

2.2.2 Characterizations

Fourier transform infrared spectroscopy (FT-720, HORIBA, Ltd), powder X-ray diffraction measurement (Rigaku, Thermo plus, XRD-DSC II), Raman spectroscopy (Raman spectrometer HORIBA, Ltd., T64000) were conducted to characterize the functional groups, crystallinity, number of layers of GO, size of GO samples, interlayer distance and the quality of samples. Scanning electron microscope (SEM) (Ultra-high resolution field emission scanning electron microscope device (Hitachi High-Technologies Corporation, S-5200)), EDAX (Genesis XM2), Transmission electron microscopy (TEM) (Ultra-high resolution transmission electron microscope (JEOL Ltd., JEM-2010)) were performed to collect imaging data of the samples. ICP-AES (atomic emission spectroscopy) (SPS3500, SII Nanotechnology Inc.) was used to calculate the adsorption capability of the samples.

2.2.3. Synthesis of graphene oxide (GO)

All GO samples were synthesized using the modified Hummers method [26]. A pre-cooling procedure was implemented by keeping all the reagents and solvent in the refrigerator for one night before the synthesis process [27]. In order to start the synthesis process, first, a graphite 1.0 g, $NaNO_3$ 1.5 g were put into the vial. Then, a concentrated H_2SO_4 (50 ml) was added carefully. Stirred the mixture for 30 minutes at room temperature. In this step, the colour was blackish green. Put the mixture in the refrigerator for 30 minutes to keep it in the cooling condition below 10 °C. After that, going to the critical step, added $KMnO_4$ 4.0 g slowly and carefully. Stirred for about 20 minutes. Set the temperature at 35 °C under stirring for 2 h. After this reaction, the colour of the solution became brown. Diluted the mixture with 80 ml distilled water with stirring for 15 minutes. Then, continued stirring for the other 30 minutes at room temperature. Added 150 ml distilled water slowly and carefully with stirring for 15 minutes. After that, 12 ml of 30% H_2O_2 was dropped carefully to the solution. A large number of bubbles were released. The solution became golden yellow. The solid particle was filtered, washed using 5% HCl and followed by using distilled water. Dried the solid at 60 °C for 24 h. In order to distinguish each GO-sample, we termed these GO samples by index number, which have different amount of C based on elemental analysis. There are two types of GO-sample based on C/O composition (Table 1). The GO_{c70} and GO_{c72} have 70-72 wt% C element, while GO_{c39} and GO_{c40} have ~39 wt% C element.

2.2.4. Synthesis of α-$K_6P_2W_{18}O_{62}$

The α-$K_6P_2W_{18}O_{62}$ was synthesized according to the modified Nadjo Method [28]. The synthesis route started with dissolving the starting material, $Na_2WO_4 \cdot 2H_2O$ 15 g into 17.5 ml distilled water. Straightforward with vigorous stirring for 15 minutes until the cloudy solution becomes limpid. Followed by acidification process, HCl 4M (12.5 ml) was added dropwise for 45 minutes carefully. In this process, white precipitate was formed. In order to avoid agglomeration and to disperse homogenously during the acidification process, the vigorous stirring was performed. Checked the pH to be around 6-7. Then, 2M H_3PO_4 (12.5 ml) was added, checked the pH to become around 2-3. The solution was refluxed for 24 h. And this solution was cooled at room temperature for a while. Then KCl 7.5 g was added to the solution. Filtered off by paper filtration and the crude material was obtained. Dissolved it into 32.5 ml distilled water and the solution becomes limpid. The next reflux process was performed at 80 °C for 72 h. Then, it was cooled at room temperature. The last step was keeping the solution in refrigerator, and after 24 h, the well-behaved crystals of α-$K_6P_2W_{18}O_{62}$ were produced (6.5 g).

2.2.5. Synthesis of GO-POM composite

The composite sample was distinguished into eight types of composite. Each composite was produced by incorporating GO-sample (GO_{c70}, GO_{c72}, GO_{c39}, and GO_{c40}) with Dawson-type POM. The GO-POM composite was generated in two different concentration ratios (concentration ratio GO:POM, 1:8 and 4:1). The constitution is summarized in Table 3. These treatments (different concentration ratio of GO:POM) were employed in order to investigate the role of GO and Dawson-type POM in the Cs adsorption and to know the proper composition. In this synthesis process, mixed solvent was used with the ratio 1:1 (distilled water/methanol). The GO aqueous dispersion in the first concentration condition (1:8) was prepared by dispersing 1g GO into the solvent (100 ml) with sonification treatment for 5 minutes. Prepared the POM solution by dissolving 1 g α-$K_6P_2W_{18}O_{62}$ into the solvent 12.5 ml. Poured the POM solution into the GO suspension vial, added diluted HCl to adjust the pH in the range 2-3 and then forwarded to vigorous stirring process for 24 h. In the second concentration condition (4:1), prepared the GO solution by dispersing GO 0.5 g into the solvent 25 ml with sonification treatment for 5 minute. POM solution was prepared by dissolving the α-$K_6P_2W_{18}O_{62}$ 0.5 g into the solvent 100 ml. The POM solution was poured into the GO suspension, added diluted HCl to adjust the pH in the range 2-3, after that stirred for 24 h. Finally, the solid material was collected by using filter paper and dried at 90 °C for 24 h. Then, the composite

product was indexed based on the value of C element of GO (c70, c72, c39, c40 due to elemental analysis) and the concentration ratio of GO/POM (1:8 and 4:1) in order to distinguish each composite's name, as follows $[GO_{70}POM]_{18}$, $[GO_{70}POM]_{41}$, $[GO_{72}POM]_{18}$, $[GO_{72}POM]_{41}$, $[GO_{39}POM]_{18}$, $[GO_{39}POM]_{41}$, $[GO_{40}POM]_{18}$, $[GO_{40}POM]_{41}$. Contant's group reported the hydrolytic stability of Dawson-type POM depending on the acidity of the solution. That is, Dawson-type POM was stable at pH lower than 6 and when the pH increased above 6, the formation of lacunary species occurs [81]. In the case of our system, preparation and adsorption experiment were performed at pH lower than 5. Therefore, the Dawson-type POM was stable in the present solution.

2.2.6. Adsorption experiment

The cesium adsorption was conducted as below. First, each sample (POM, GO-samples, GO-POM composites) 0.08 g was dispersed into distilled water 30 ml with sonification treatment for 5 minutes. Second, 0.6 g of CsCl (3.6 mmol) was added to the solution. And then the mixture was stirred for 24 h.

The performance of Cs adsorption was analysed by using ICP optical emission spectroscopy. The solid adsorbent was separated from the solution by using paper filtration. The measurement was conducted duplicate in each sample solution. The adsorption efficiency was calculated by equation (1) and the adsorption capacity by equation (2).

$$Adsorption\ efficiency\ \left(\%\ Ads.eff.\right) = \frac{\left(C_0 - C_t\right)}{C_0} \times 100 \quad \textbf{(1)}$$

$$Adsorption\ capacity = \frac{\%\ Ads.eff. \times C_0}{W} \quad \textbf{(2)}$$

Where C_0 (mmol) is the initial concentration of Cs, and C_t (mmol) is the remained concentration of Cs in the solution after treatment. W (gr) is the dry weight of adsorbent used in the adsorption experiment.

2.3. Results and Discussion

2.3.1. Elemental analysis

Table 1. Elemental analysis of GO sample.

Sample	C%	H%	N%	O%	C/O
GO_{c70}	70.87	7.95	-	21.18	3.34
GO_{c72}	72.04	8.07	-	19.89	3.61
GO_{c39}	39.28	2.76	0.27	57.69	0.68
GO_{c40}	39.61	2.58	0.25	57.56	0.69

Table 1 shows the results of elemental analysis of GO_{c70}, GO_{c72}, GO_{c39}, and GO_{c40}. It can be seen that the GO_{c70} and GO_{c72} have 70-72 wt% C element, while GO_{c39} and GO_{c40} have ~39 wt% C element. In the synthesis process, there is one thing that might make the sample a bit different. In the treatment of $KMnO_4$, especially for GO_{c39} and GO_{c40}, putting the $KMnO_4$ was treated more carefully (one minute stop, one minute go). It was shown that the degree of oxidation was controlled by the controlled oxidation process. In particular, it can be assumed that there is a difference in structure between the two types of GO. The GO_{c70} and GO_{c72} indicating few oxygen defect in the structure have an important contrast with the GO_{c39} and GO_{c40}. However, deeper characterization is still required since the oxygen defect is not only the case. As emphasized in the previous literature, there is no evident relation between oxidation degree and ordered domain that is exhibited in Raman spectrum [13].

2.3.2. FT-IR spectra

Figures S6, S7 and S8 (see supporting information) show the FT-IR spectra of GO and Dawson-type compound. The Dawson-type POM was successfully produced by Nadjo synthesis route. The IR absorptions of the present α-$K_6P_2W_{18}O_{62}$ are similar with those of the literature [28]. All GO samples exhibit broad absorption band of O-H stretching vibration around 3400 cm^{-1}, C=C bond stretching at around 1620 cm^{-1}, C=O vibration at around 1720 cm^{-1}, C-O vibration band at around 1420 cm^{-1}, and epoxides at 1200-1250 cm^{-1}. In addition, the vibration band at around 830 cm^{-1} – 850 cm^{-1} was detected especially in GO_{c39} and GO_{c40} samples. This band might be assigned as C-Cl vibration band as reported in the other work [76]. However, the C-Cl vibration band is unexplained because in this work there is no other additional treatment that refers to the addition of Cl. Since the GO

is nonstoichiometric compound, the structure analysis is quite difficult and the variety of composition depends on the synthesis condition. It can be assumed that the remaining Cl impurity is coming from laboratory glass material. The difference in the degree of oxidation was revealed between GO_{c70}, GO_{c72}, and GO_{c39}, and GO_{c40}, i.e., epoxide signal was seen in GO_{c39}, and GO_{c40} samples.

2.3.3. Morphology of GO

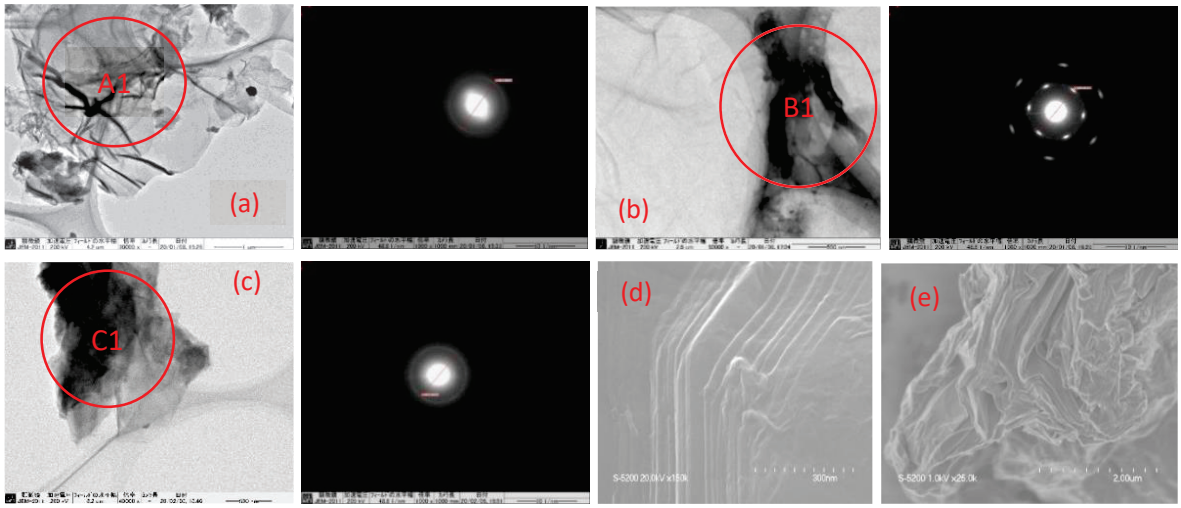

Figure 1. TEM imaging of (a) GO_{c70} (b) GO_{c72} (c) GO_{c39} and SEM imaging of (d) GO_{c39} (e) GO_{c40}, and SAED pattern from the location (A1, B1, C1) marked in pict (a, b, c), respectively.

TEM imaging and SAED diffraction are used to draw the structural model in each GO sample as shown in Fig 1. The 200 kV was applied in each sample for TEM image measurement. Under this condition, the GO samples were shown that the morphologies were lamellar, wrinkled and overlaps and found to be stable. The image indicates that the some GOs had been exfoliated. This is in agreement with the previous research that both wrinkled and overlaps are the essential feature of GO based bulk material [29]. The sharp spots in an SAED pointed out the crystalline region in GO. Especially GO_{c72} shows typical diffraction pattern representing the crystalline nature of GO sample. The present SAEDs are in agreement with the previous work that presented the amorphous region (see Figure 1(A1),(C1)) and crystalline region (see Figure 1(B1)) in GO sample [30]. Particularly, the amorphous zone is associated with the presence of the sp^2/sp^3 carbon cluster (as presented in Table 4, see section 3.7.2) in all GO samples [31]. In the other imaging using SEM measurement, it is shown in the Figure 1 (d) and (e) that the GO sample consists of several layers (see Table S14, supporting information). Previous work emphasized that the morphology and quality of multilayers of GO depend on several

factors such as the source of graphite, degree of oxidation, and reaction condition [32]. These all GO samples are aligned with a few layers of GO in the previous work [33].

2.3.4. Morphology of GO-POM composite and its EDS map

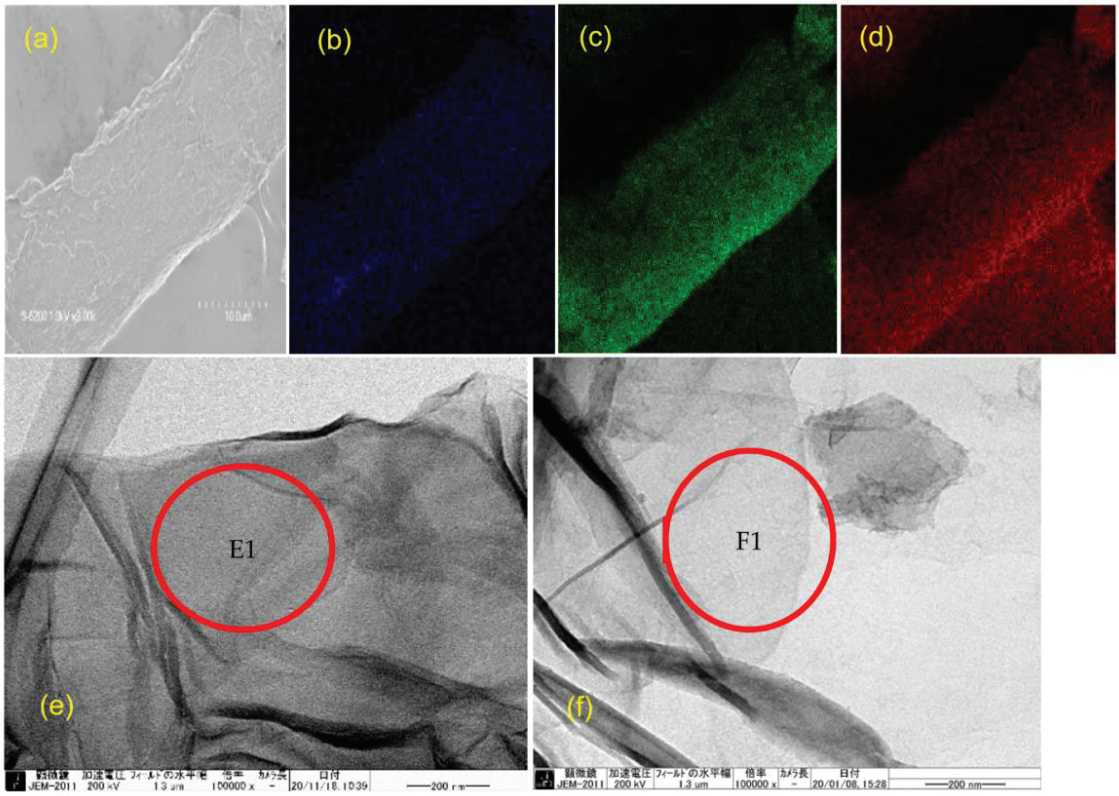

Figure 2. SEM measurement (a) $[GO_{70}POM]_{41}$, its EDS map (b) Tungsten element, (c) Oxygen element, (d) Carbon K-α X-ray element, TEM image (e) $[GO_{70}POM]_{41}$, (f) GO_{C70}, showing the formation of layer after forming composite $[GO_{70}POM]_{41}$ (E1) compared with original GO_{C70} (F1) in the same scale image (200 nm).

The SEM image of GO-POM nanocomposite and its EDS map are shown in Fig 2, S1, and S2 (see supporting information). Fig 2(a) shows the SEM of $[GO_{70}POM]_{41}$, and Fig 2(b), (c), and (d) show the W, O, C element distribution, respectively. Tungsten element is dominantly originated from the α-$K_6P_2W_{18}O_{62}$ particle, and carbon element is coming from the GO. The result suggests that the tungsten, oxygen, and carbon elements were homogeneously distributed in the GO-POM nanocomposite, showing the successful combination between GO and POM [34]. This phenomenon was also confirmed by TEM measurement. Figure 2 (e) show the homogenous POM particle in the surface area of GO after forming composite. The SEM image of $[GO_{70}POM]_{41}$ (Fig. 2(e)) is darker than that of original GO_{C70} (Fig. 2(f)). The formation of layer after forming composite $[GO_{70}POM]_{41}$

(E1) was confirmed by comparing it with original GO_{C70} (F1) in the same scale image (200 nm).

3.5. Powder X-ray diffraction pattern (PXRD)

Powder X-ray diffraction (PXRD) measurement was carried out to characterize the GO, Dawson-type POM, and GO-POM nanocomposite structures. As shown in Figure 4, S4 and S5 (see supporting information), the PXRD patterns of the GO_{c70}, GO_{c72}, GO_{c39}, and GO_{c40} show diffractions at 2θ= 11.58°, 8.66°, 8.91° and 9.13°, respectively. The d-spacing increases from 0.34 nm of graphite spacing (002) to 0.77 nm – 1.02 nm, which corresponds to the typical diffraction peak of GO nanosheet (table S14, see supporting information). The interlayer distance was calculated by the Bragg's law, as is shown below:

$$d = \lambda/2\sin(\theta) = 0.154nm/2\sin(\theta) \quad (1)$$

Where d is the distance between the layers of GO, ɵ is the diffraction angle, λ is the wavelength of the X-ray beam (λ=0.154nm).

Although the d-spacing of GO_{c70} is shorter than those of GO_{c72}, GO_{c39}, and GO_{c40}, it is suggested that oxygen-containing functional groups (epoxide, hydroxyl on the basal plane and carboxyl groups on the edge of basal plane) successfully formed in different degree of oxidation. This is the reasonable explanation to the enhancement of the interlayer spacing of GO [38].

The diffraction peaks of all samples were slightly shifted by forming the composite (Fig 4 and S5 (see supporting information)). That is, d-spacing decreased by forming the composite, except for $[GO_{70}POM]_{41}$ (Table S14, see supporting information). The result of $[GO_{70}POM]_{41}$ might agree with the previous work that might be assumed as consequence of a partial intercalation of the POM species and random arrangement of the carbon layers [39]. The results except for $[GO_{70}POM]_{41}$ result revealed that the α-$K_6P_2W_{18}O_{62}$ species are not embedded in between the GO sheets, however, it could be assumed that the POM species decorated on the surface of GO as is assumed in the Fig S3 (see supporting information). It is already known that the molecular size of the α-$K_6P_2W_{18}O_{62}$ species is large (ca. 1.03 nm x 1.5 nm) [20] than the d-spacing of each GO-sample (0.77 nm – 1.02 nm).

In addition, we could see in the Table S12 (see supporting information) the out of plane crystallite size of GO samples. The size was calculated by using the Debye Scherrer equation:

$$D\,(nm) = 0.9\lambda ß^{-1} \cdot (\cos(\theta))^{-1} \quad (2)$$

Where D is the average out of plane crystallite size (nm), λ is the wavelength of the X-ray beam, ß is FWHM (full width at half maximum), ɵ is XRD peak position.

The in-plane crystallite size of GO samples and the average number of graphene oxide layers (n) per domain were also estimated by using PXRD data. The following general formula is described in [42]:

$$L\ (nm) = 1.84\ \lambda / ß \cdot \cos(ɵ) \quad (3)$$

$$n = D/d + 1 = (0.9\lambda ß^{-1} \cdot (\cos(ɵ))^{-1}/d) + 1 \quad (4)$$

where D is the average out of plane crystallite size (nm), d is interlayer distance, λ is the wavelength of the X-ray beam, ß is FWHM (full width at half maximum), ɵ is XRD peak position, n is the number of layers of GO sample. These calculations provide crucial information regarding the average crystallite size (reflecting the enhancement or reduction of graphitic zone and the grain boundaries or lateral defect formation) and the average number of GO-layer (see Fig S14, supporting information).

2.3.6. Raman spectroscopy

The Raman spectroscopy was used to characterize the GO material and also it provides the structural information in detail to draw its quality [43]. From the spectra, we could see that the D band located at 1356 cm^{-1}, 1352 cm^{-1}, 1352 cm^{-1}, 1347 cm^{-1} for GO_{c70}, GO_{c72}, GO_{c39}, and GO_{c40}, respectively (see Fig S9 supporting information). This indicates the extensive oxidation of graphite and extended amounts of the sp^3-hybridized carbon atoms [65]. The G band located at 1586, 1581, 1590, and 1590 cm^{-1} for GO_{c70}, GO_{c72}, GO_{c39}, and GO_{c40}, respectively, is corresponding to the sp^2-hybridized carbon atoms in the hexagonal framework. The G band is inherently with 2D band (the second order Raman modes) that appears at 2700 cm^{-1}. The critical thing to fully and accurately characterize the GO sample is the consideration of the second order Raman modes [44]. The area ratio of the 2D also has a linear correlation with the hole mobility [45]. In addition, the previous work has explained the packing mechanism of multiple layers GO (bi-, tri- layers) by STEM-ADF image simulation. It showed that the disorder of graphene sheet and the roughness have been created by the random covalent attachment of oxygen on the top and bottom surfaces. It influences the lattice distortion and breaks the symmetry of the system [80]. Therefore, it can be predicted that the different C/O ratio of GO samples in our work is sufficient to influence the material structure of the GO-POM composite and the ability to adsorb the Cs.

As presented in Table S13 (see supporting information), the intensity ratio of I_D/I_G of each original material (GO_{c70}, GO_{c72}, GO_{c39}, and GO_{c40}) are 0.93, 0.91, 0.89, and 0.88, respectively. These values are correlated with the different composition of C/O ratio on each GO-sample that is already discussed in the previous section. The intensity ratio (I_D/I_G) tends to increase by forming composite (see Table 4). Therefore, we may conclude that the anchored process of POM on the GO has affected the structure of GO. In this case, also, there was an opposite trend for GO_{c70}.

2.3.7. Cs adsorption performance

2.3.7.1. Adsorption efficiency and adsorption capacity of GO and POM

Table 2. Adsorption capacity, adsorption efficiency, and adsorption condition.

Materials	Adsorption efficiency (%)	Adsorption capacity (mmol/gr)	Stirring Time	Sonification time (minute)
POM-Cs	58.3	32.8	24 h	5
GO_{c70}-Cs	58.8	33.1	24 h	5
GO_{c72}-Cs	56.8	31.9	24 h	5
GO_{c39}-Cs	61.3	34.5	24 h	5
GO_{c40}-Cs	56.3	31.7	24 h	5

The Cs adsorption capacity of GO_{c70}, GO_{c72}, GO_{c39}, and GO_{c40} and POM are summarized in Table 2. Those of GO-POM nanocomposites are presented in Table 3 (see section 3.7.2). The GO samples were classified into two types according to the elemental analysis. The GO_{c70} and GO_{c72} have 70-72 wt% C element, while GO_{c39} and GO_{c40} have ~39 wt% C element. As shown in the Table 2, the result of the present work pointed out that the Cs^+ adsorption by POM, GO_{c70}, GO_{c72}, GO_{c39}, and GO_{c40} has not much difference among the samples. The role of different C/O ratio in capturing Cs cannot be revealed. It is also already strengthened by other researchers that the C/O ratio of GO does not have systematic correlation with the value of ion exchange capacity [65].

Furthermore, in this work, the interaction between GO_{c70} and Cs cation occurred immediately less than one minute after the stirring process (see Figure S16, S17, supporting information). A brown milky coagulation was formed. The same behaviour was observed between GO_{c72} and Cs, however, there was a difference for GO_{c39}, the brown milky coagulation was formed in small quantity, and the milky coagulation was not formed for GO_{c40}. The difference might be related to the variance in C/O ratio between GO_{c70}, GO_{c72}, and GO_{c39}, GO_{c40}. Moreover, it was explained that by using surface functional

group, the GO can attract the Cs cation by forming inner-sphere complexes [48]. The metal complexing in the oxidized GO strongly encourages the aggregation behaviour and can be quantified by the critical coagulation concentrations (CCC) [69]. TEM measurement shows that there are many Cs clusters in the surface of GO_{c70} (see Fig 3c). Especially for this phenomenon, we also considered that the Cs cluster may include Al impurity (see Fig 3d). It might come from laboratory glass material as reported by other work [13]. The black spots also can be seen in the $[GO_{40}POM]_{41}$, which consists of GO_{c40}/POM. However, the black spots are not uniformly found in all surface area. It is theoretically explained that the most surface reactions eventuate only on the active site and do not happen uniformly over the surface area [71]. As proposed by other work, the edge site of graphene (carbene- and carbyne-type carbon atoms) has a significant role for adsorption on the surface of sp^2-hybridized carbon [70]. It is also confirmed by previous

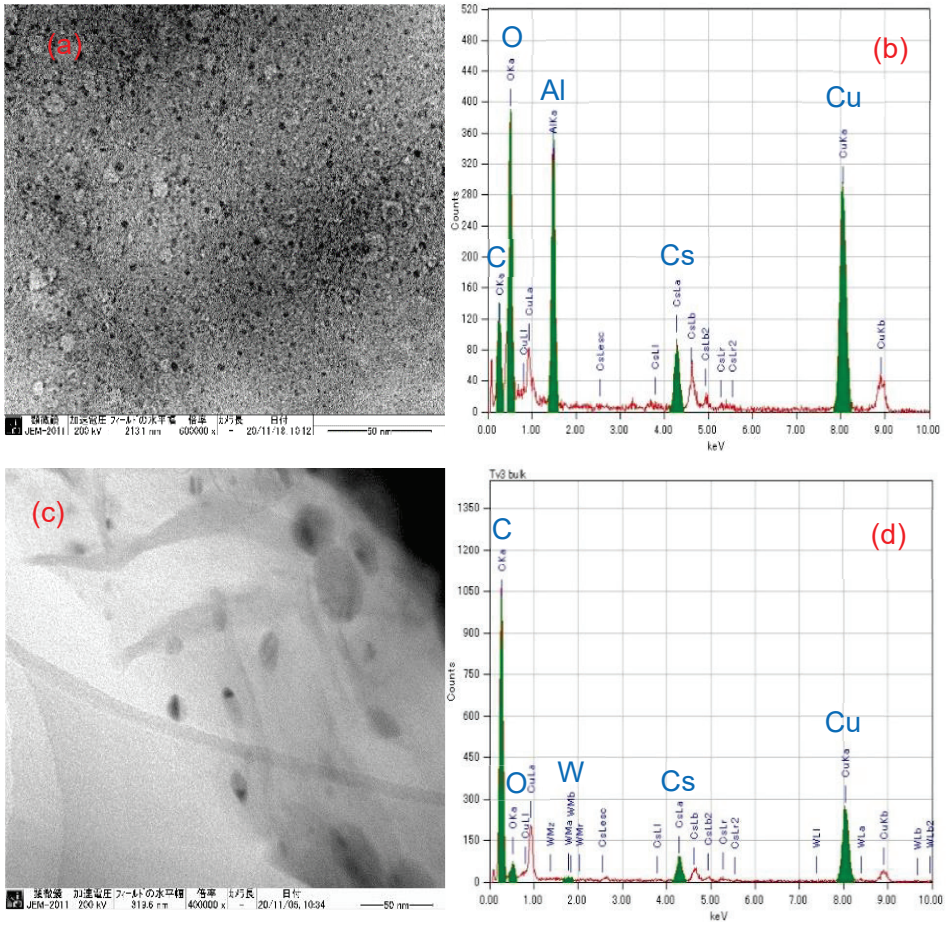

Fig 3. TEM image (a) GO_{c70} after Cs adsorption, many small Cs cluster are seen (b) Elemental analysis of fig 8a, (c) $[GO_{40}POM]_{41}$ after Cs adsorption, small black spots are identified (d) Elemental analysis of fig 8c.

study that some ions or molecules dissolved in water have a good penetration rate through the graphene nanocapillaries until the physical size of the ions or molecules exceeds the critical one [68]. A highly oxidized domain and the hydrophobic domain in GO have different role. The highly oxidized domain would be responsible for rapid water transport in the interlayer of GO, while the hydrophobic domain would serve a network of capillaries [65]. Other researcher also considered the polarizability of graphene in order to estimate the orientation of interfacial water [66]. And the interfacial water can be used to observe the surface adsorption behaviour [67]. Based on these analysis, it can be assumed that the interfacial water may support the Cs interaction with GO.

The other important evidence of Cs adsorption is also visible in PXRD measurement. The sharp and intense diffraction peaks were reduced by introducing Cs (Fig 4 and S5 (see supporting information)). The broad diffraction of GO_{c70}, GO_{c72}, GO_{c39}, and GO_{c40} showed the non-uniform surface complexation with Cs cation. PXRD and TEM show the formation of Cs cluster. This might correspond to the origin of GO acidity, which contributes to high cation exchange capacity (CEC). The GO acidity is made by oxygen functional groups and the main moieties responsible for the acidic properties are carboxyl groups [65]. Moreover, as the result by Dimiev et. al. (2012), there is one acidic site for every six to eight carbon atoms, i.e. 100 g of GO sample contains 500-800 mmol of active acidic sites [73]. The adsorption capacity of the present GOs (~3200 mmol/100 g) (Table 2) is larger than the concentration of active acidic site. This is due the formation of Cs cluster. It is also generally accepted that the basicity and the size of the molecule to be adsorbed are a significant aspect in adsorption process [40] [41]. In this work, the pH of the solution is around 5-6 when the Cs contacts the GO-POM composite or GO only. Some previous researchers have proved that the pH condition in GO samples influences the adsorption capacity. It can be explained that at pH above 3.9 (pH_{pzc}), the surface area of GO is partially negatively charged and the electrostatic attractions between cations and GO are stronger because of deprotonation reaction [63]. It is also caused by the higher availability of active site on the GO sheets [47].

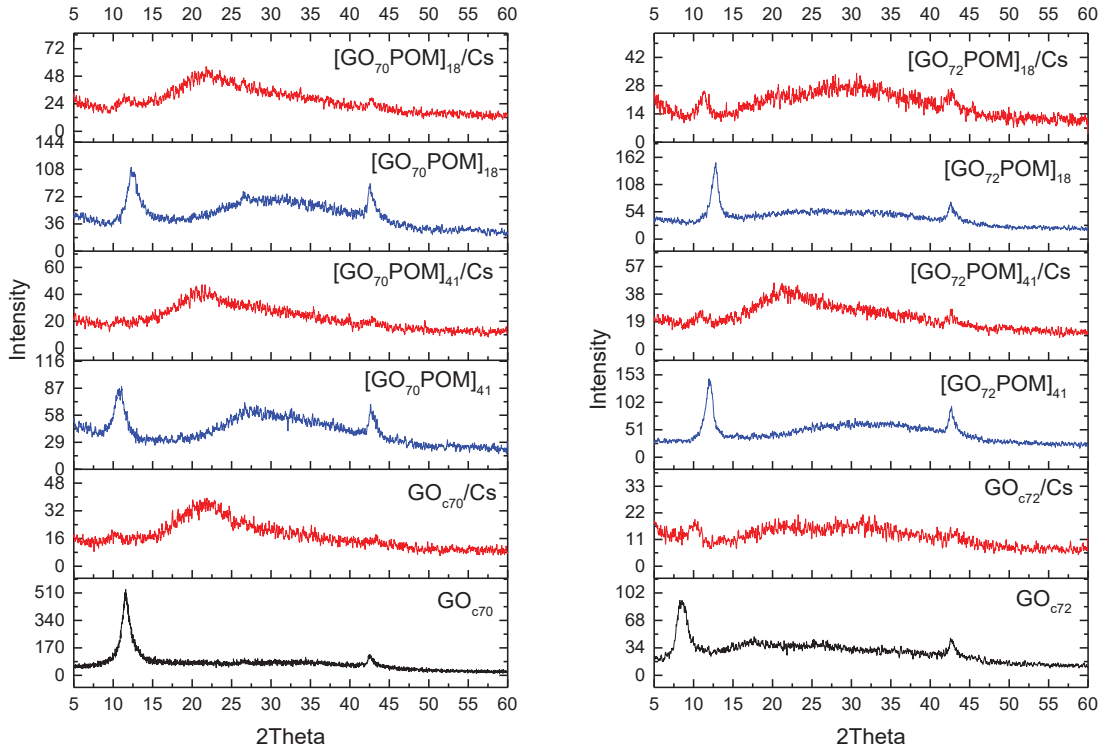

Figure 4. PXRD patterns of GO_{c70}, GO_{c72}, and their GO-POM nanocomposite before and after Cs adsorption.

As discussed above, these data have a good correlation with the information that is observed in Raman spectra. Based on Raman analysis (Figure 5 and S9, S10, S11, S12 (see supporting information)), it was found that the change in spectrum by Cs adsorption was similar for both the GO-only samples and composite samples. It can be seen that the second order peaks have changed after Cs adsorption. In previous studies, it was strengthened that the second order peak indicates the crystallite size has changed. This indicator showed that the spectrum broadens consistently with decreasing the domain size [46]. Therefore during the chemical processing (Cs adsorption), the significant structural change of the carbon framework occurred. In addition, based on the sample experiment using $[GO_{39}POM]_{41}$, there is a slight shift in the D band from 1347 cm^{-1} before Cs adsorption to 1352 cm^{-1} after Cs adsorption. The same shift also occurred in the other samples, $[GO_{70}POM]_{18}$ and $[GO_{70}POM]_{41}$ (Figure S9, see supporting information). It might be caused by the interaction of ether hole defect in GO sheets with Cs cation [47]. Thus, the change that the crystal structure after Cs adsorption has altered by amorphization could be confirmed.

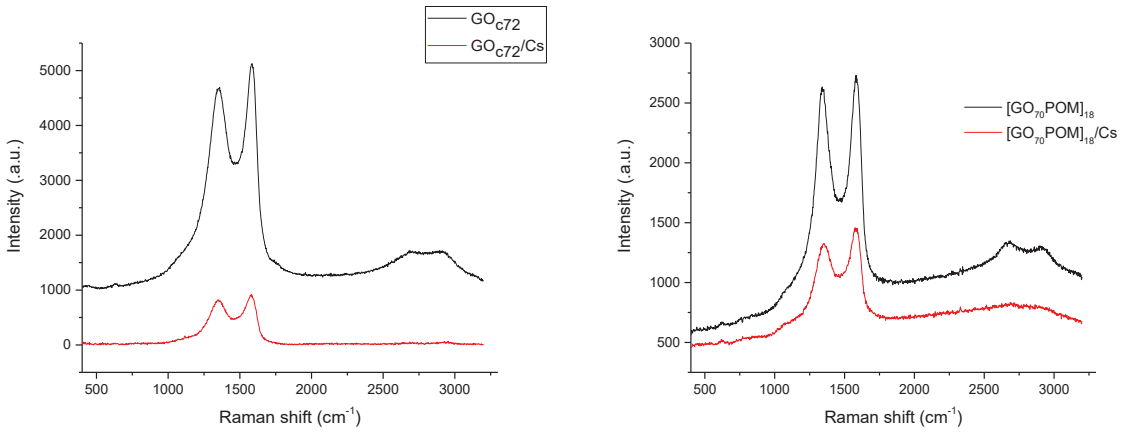

Figure 5. Raman spectra before and after Cs adsorption for (**a**) GO_{c72} (**b**) $[GO_{70}POM]_{18}$.

3.7.2. Adsorption efficiency and adsorption capacity of GO-POM nanocomposite

Table 3. Adsorption capacity, adsorption efficiency, and adsorption condition.

Materials	Composition	Concentration GO:POM	Adsorption Efficiency (%)	Adsorption capacity (mmol/gr)	Stirring Time	Sonification time (minute)
$[GO_{70}POM]_{18}$	(GO_{c70}/POM)	1 : 8	84.0	47.3	24 h	5
$[GO_{70}POM]_{41}$	(GO_{c70}/POM)	4 : 1	62.7	35.3	24 h	5
$[GO_{72}POM]_{18}$	(GO_{c72}/POM)	1 : 8	75.4	42.4	24 h	5
$[GO_{72}POM]_{41}$	(GO_{c72}/POM)	4 : 1	78.7	44.3	24 h	5
$[GO_{39}POM]_{18}$	(GO_{c39}/POM)	1 : 8	72.7	40.9	24 h	5
$[GO_{39}POM]_{41}$	(GO_{c39}/POM)	4 : 1	81.7	45.9	24 h	5
$[GO_{40}POM]_{18}$	(GO_{c40}/POM)	1 : 8	70.7	39.8	24 h	5
$[GO_{40}POM]_{41}$	(GO_{c40}/POM)	4 : 1	73.5	41.3	24 h	5

Table 3 shows the result of Cs adsorption by using GO-POM nanocomposite. The GO-POM nanocomposite (Table 3) increased the Cs adsorption capacity effectively compared to the adsorption capacity of original material (Table 2). The change range is around 6.7% to 42.9%. This result is in consistent with the previous finding that signified the characteristic of surface area showing an important role of POM species with carbon materials [61], [62]. As consequence, the Cs^+ adsorption becomes high. We compared the average increment of Cs adsorption of the composite material between GO having 70-72 wt% C element and GO having 39-40 wt% C element. Because the functional groups of GO provide a binding point for chemical modification [24]. It is seen in Figure 6 that there is not significant difference between GO having 70-72 wt% C element and GO having 39-40 wt% C element.

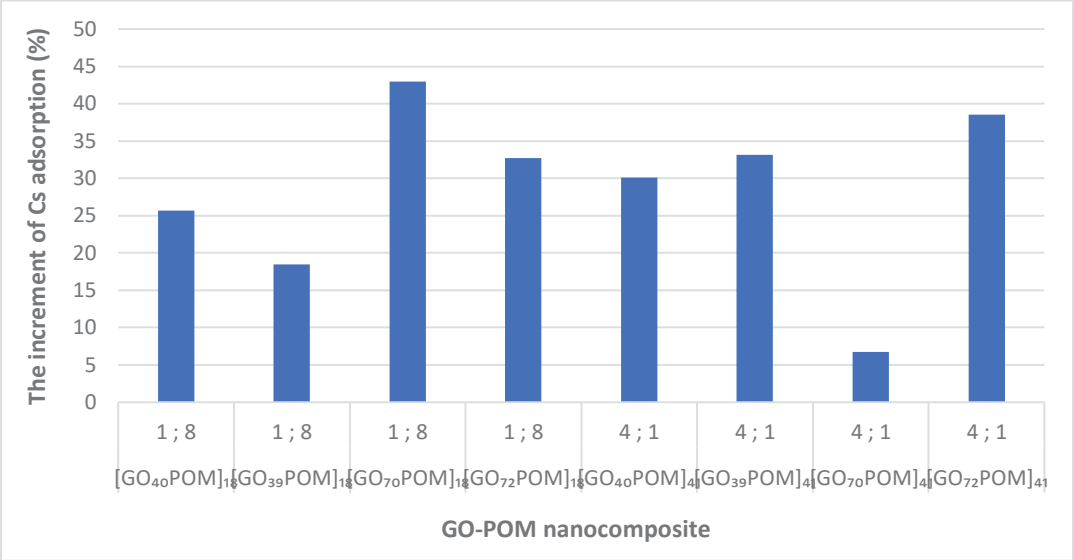

Figure 6. The increment of Cs adsorption capacity (%) calculated by using the ratio before and after forming composite in each GO samples.

We compared the average increment of Cs adsorption of the composite material between concentration ratio 1:8 and concentration ratio 4:1, but we could not find the significant difference. In principle, the adsorption behavior of GO-POM nanocomposite might be influenced by the significant role of GO as electron acceptor and Dawson-type POM as the electron donor that led to enhance the attraction between Cs^+ and the composite [53]. The other phenomena authenticated by other researcher confirmed that the interaction between POMs and GO can provide more mobile protons and flexible pathways [54]. Also, Wang's group reported that the surface charges of GO modified by functional groups (GO-COOH, GO-NH_2, GO-OCH_3) can be used to modulate the charge transport [55]. Therefore, the presence of Dawson-type POM in the GO system enhanced the negative charge of GO part in the composite and provided a good adsorption of Cs^+ ion (Fig S3, see supporting information). The interaction of Cs^+ ion with Dawson-type POM was an ion-pair complex [82]. The anion surface of Dawson-type POM is electron rich and has strong interaction with Cs^+. Therefore, the introduction of Dawson-type POM in our adsorbent system was important to enhance the adsorption of Cs^+ ion. However, further investigation is still needed to find out the mechanism that occurred behind the phenomenon.

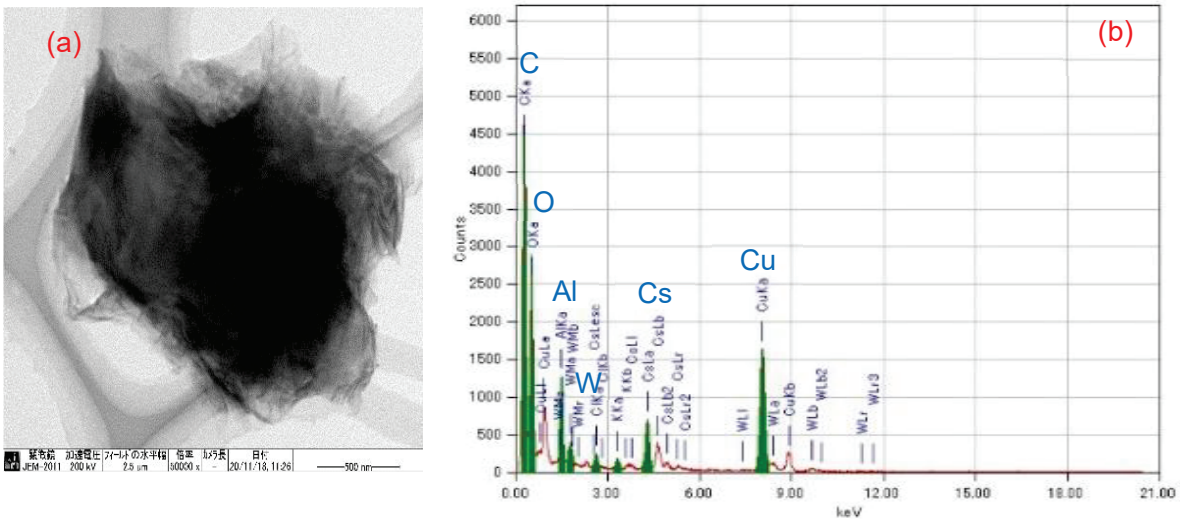

Fig 7. TEM image by using $[GO_{70}POM]_{18}$ (a) Aggregation process after Cs adsorption (b) Elemental analysis of fig 7(a).

It is also reported that the mechanism of cation-GO interaction in the adsorption behaviour should be considered together with aggregation process [49]. In the present study, the Figure 7 (a), (b) exhibited that the aggregation occurred after Cs adsorption by using GO-POM nanocomposite. The results demonstrated that the composite samples immediately coagulate after Cs adsorption except for $[GO_{70}POM]_{41}$ that still forms a stable solution after one hour keeping at ambient temperature (see Figure S15, supporting information). We predicted that a small granule of Cs was formed and crinkled GO sheets coating around (see Figure S18, supporting information). It can be signified that a stronger bond was formed. It might be predicted that there is a different composition of oxidative debris (OD) component among the GO-samples. As a previous study explained, the OD of GO has a significant role in the origin of GO acidity [78]. It is already discussed in the previous section (section 3.7.1 regarding the contribution of GO acidity to the cation exchange capacity). However, further investigation is still needed to prove it and to get a strong evidence. Unfortunately, the elemental analysis of Figure S18 (supporting information) was not conducted. Regarding this phenomenon, it can be assumed that there are two important factors which might contribute to the aggregation behaviour. First, the size of the GO and composite sample. As presented in the Table S12, the size of each sample is diverse. The range of value is around 4.3 nm to 34.78 nm. It was strengthen by the previous study that the size of GO (nano GO, colloid GO, micron GO) can strongly influence the aggregation behaviour [72]. Second, the other factor is the degree of acidity. It is strongly related with the functionalities of GO sample. It was explained in earlier section in this work that there are two types of GO-sample, which has

different C/O composition. The evidence was shown by the previous study that the GO (single or multilayers) coagulates in highly acidic condition because of losing their surface charge [73]. It is also correlated well with other work that identified the effect of cations on aggregation [48]. Moreover, it was strengthened in the previous theoretical analysis that considered an important role of H_2O as dipole molecule involving cation-π interaction. Therefore, the electrostatic interaction would be significantly influenced [50][51]. As calculated in the previous studies, the value of the internuclear distances $d_{ion\text{-}water}$ of Cs^+ is 0.315 nm [52]. Therefore, the interaction of Cs^+ with GO-POM nanocomposite becomes more easy to diffuse through the interlayer distance of GO-POM nanocomposite which has d-spacing around 0.69 nm-0.81 nm and 0.77 nm – 1.02 nm for GO sample (see Fig S11, supporting information).

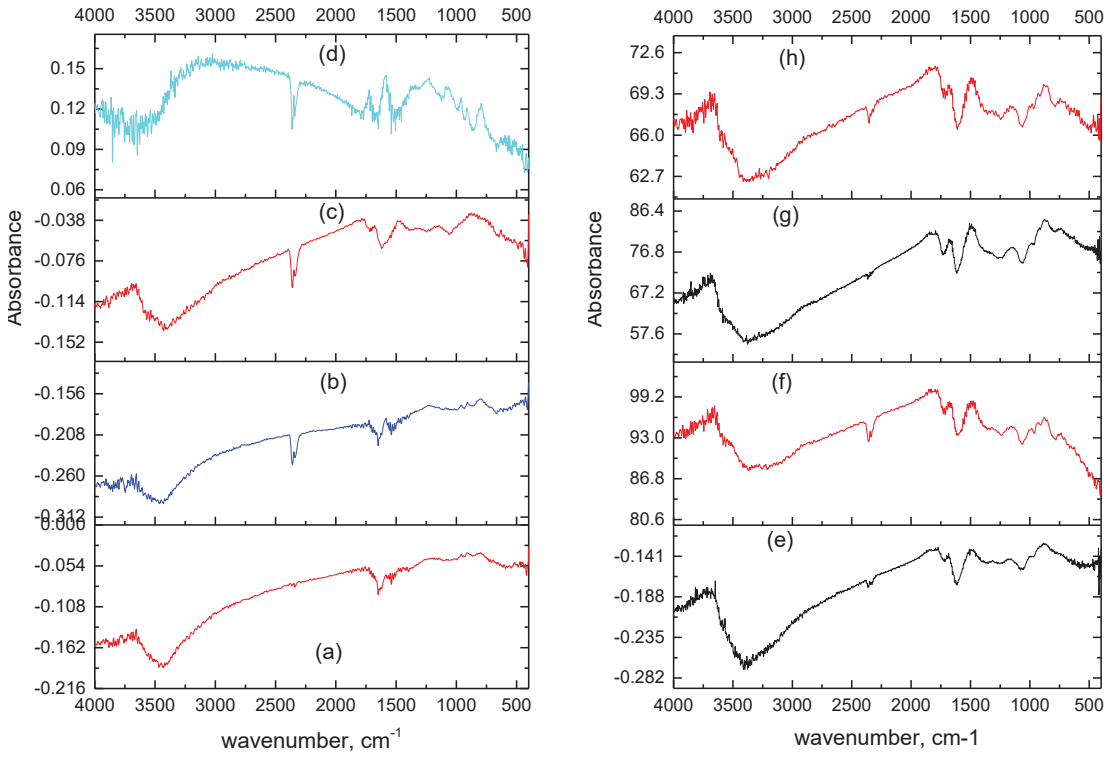

Fig 8. IR spectra for (a)$[GO_{70}POM]_{18}$, (b)$[GO_{70}POM]_{18}$ after Cs adsorption, (c)$[GO_{70}POM]_{41}$, (d)$[GO_{70}POM]_{41}$ after Cs adsorption, (e)$[GO_{40}POM]_{18}$, (f)$[GO_{40}POM]_{18}$ after Cs adsorption, (g) $[GO_{40}POM]_{41}$, (h)$[GO_{40}POM]_{18}$ after Cs adsorption.

By FTIR spectra, a specific changes are marked at 1150 cm^{-1}-1350 cm^{-1} after Cs adsorption in all GO-POM nanocomposite. Especially for composites which consist of ~39

wt% C element, the IR spectrum shows more significant change (see Fig 8 (e)-(h), S7A in supporting information), whereas the composites which consist of 70-72wt% C element the peak shifts are not so significant, thus making analysis are quite difficult (see Fig 8 (a)-(d), S7B in supporting information). A similar tendency also occurred in all GO sample after Cs adsorption (see Fig S6 in supporting information). This result indicates that there is a change in the interlayer chemistry of the sample and influences the defect (hole) formation and functional group formation. It might be caused by the interaction between GO functional group (including carboxyl, phenol, multi-group ether) and the Cs cation [47]. As explained by the other researcher that the pH-driven reversible epoxide formation in GO (epoxy opening/closing reactions) should be considered as an important part of reactivity and properties of GO [77]. The tendency is observed that the interlayer distance after Cs adsorption in all nanocomposite samples were expanded, even though the increment was not so high (see Table S14, supporting information). For example, in composite $[GO_{40}POM]_{18}$, $[GO_{40}POM]_{41}$, $[GO_{39}POM]_{18}$, and $[GO_{39}POM]_{41}$, the interlayer distances were changed from 7.6 A to 8.3 A, 7.6 to 7.8 A, 7.4 A to 8.1 A 7.4 to 7.9 A, respectively. It also happened in composite $[GO_{70}POM]_{18}$, $[GO_{70}POM]_{41}$, $[GO_{72}POM]_{41}$, and $[GO_{39}POM]_{18}$, where the d-spacing was expanded from 7.2 A to 7.9 A, 8.1 A to 8.6 A, 7.3 A to 7.9 A and 6.9 A to 7.7 A, respectively. In addition, the other study confirmed that the CO_2 gas is trapped within the multilayers of GO (marked at 2357 cm^{-1} – 2359 cm^{-1}). Intentionally, they verified that the intercalated water has an essential role for accelerating the reaction by some specific mechanism [83].

Another work also confirmed that the functional group of GO can act as a ligand to replace the water molecule from the metal cations in the first coordination sphere. Previous work verified that the relaxation time by using NMR relaxation method can be considered as an essential variable for identifying the metal complexing mechanism of GO in different charge, size and electron configuration of the metal as a function of pH and GO concentration [37]. It was also confirmed by the other study that the presence of wrinkle-like water tunnels has a strong relation with the water adsorption ability of GO [64].

Table 4. The sp^2/sp^3 carbon cluster on each composite surface.

Material	Composition	Graphitic zone (G%)	Oxidized zone (%)
GO_{c70}	-	69.7	30.3
GO_{c72}	-	75.4	24.6
GO_{c39}	-	74.9	25.1

GO_{c40}	-	74.5	25.5
$[GO_{70}POM]_{18}$	GO_{c70}/POM, 1:8	68.4	31.6
$[GO_{70}POM]_{41}$	GO_{c70}/POM, 4:1	71.4	28.6
$[GO_{72}POM]_{18}$	GO_{c72}/POM, 1:8	67.5	32.5
$[GO_{72}POM]_{41}$	GO_{c72}/POM, 4:1	69.0	30.9
$[GO_{39}POM]_{18}$	GO_{c39}/POM, 1:8	69.0	31.0
$[GO_{39}POM]_{41}$	GO_{c39}/POM, 4:1	69.3	30.7
$[GO_{40}POM]_{18}$	GO_{c40}/POM, 1:8	69.1	30.0
$[GO_{40}POM]_{41}$	GO_{c40}/POM, 4:1	69.5	30.5

Deeper investigation into carbon species in each composite sample was performed. It was shown in the Table 4, where the graphitic zone can be calculated by using the integrated intensity of graphitic (2 ɵ = 26.6) and oxidized peaks (2 ɵ = 8.66 - 15) in the PXRD pattern. The amount of graphitic zone (G%, unoxidized region) was calculated using equation 7, as follows:

$$G\% = \frac{I_{graphite}}{I_{oxidized} + I_{graphite}} \times 100\% \quad (7)$$

Where $I_{graphite}$ and $I_{oxidized}$ are the intensities of graphitic and oxidized diffraction peaks of GO in the PXRD pattern, respectively [60].

As presented in the Table 4, the diversification of sp^2/sp^3 carbon cluster on each sample has been produced. This variance among the samples indicates that there is a difference in the degree of oxidation. However, a peculiar phenomenon was seen in GO_{c70} sample. The data in Table 4 show that the percentage of the oxidized zone of GO_{c70} is higher compared to GO_{c72}, GO_{c39}, and GO_{c40}. The ratio of the oxidized zone is not much different for GO_{c72}, GO_{c39}, and GO_{c40}. The GO_{c70} shows the shorter interlayer distance than GO_{c72}, GO_{c39}, and GO_{c40}. This may cause the peculiarity of GO_{c70}. But, the peculiarity of GO_{c70} is still under study. According to the literature, the ratio of the oxidized zone does not have a linear correlation with oxidation ratio [75]. The unusual characteristic of GO_{c70} also has a direct effect on the composite material produced by using GO_{c70} (discussion is provided at the beginning in section 3.7.2). Further investigation is needed to get more understanding of the dependence of these factors. Recent study revealed that the ratio C/O has a big influence on the physical properties because of the change of the surface speciation [35]. Other investigation also confirmed a strong correlation between the content of Lewis acid sites (via basal plane epoxide) and Bronsted acidic carboxylic group in GO sample with strong acidity and high oxidation degree [36].

Furthermore, the data show that the oxidized zone (sp^2/sp^3 hybrid carbon) of each composite sample was enlarged compared to the corresponding original GO. Only $[GO_{70}POM]_{41}$, which consists of GO_{c70}/POM with concentration ratio 4:1 was decreased.

It is correlated well with the in- plane crystallite size of each composite material that being expanded (see table S14, supporting information). Particularly, GO-POM nanocomposite with concentration ratio 4:1, shows the in-plane crystallite size larger than GO-POM nanocomposite with concentration ratio 1:8. It could be assumed that there is an electron transfer from POM species to GO [56][57]. Other researcher also confirmed that the surface area of GO-POM composite was improved five times due to covalent bond between POM species and GO [34]. In general, the enhancement of adsorption capacity is in line with the increase of sp^2/sp^3 carbon cluster on each composite surface. Based on the result in Figure 6, the lowest value of the percentage increase of Cs adsorption capacity is observed in $[GO_{70}POM]_{41}$. It is only 6.7%. This might be caused by the decreased oxidized zone (sp^2/sp^3 hybrid carbon) after composite was formed (see Table 4). From Table 4, it was shown that the value decreased from 30.3% (GO_{c70}) to 28.6% (GO_{c70}/POM composite). It is also confirmed by PXRD pattern, which shows the same tendency in $[GO_{70}POM]_{41}$, that the diffraction has reduced from 11.57° to 10.99° if compared with GO_{c70} as precursor material. Some researchers have tried to address the complexity of GO especially to produce graphene-based hybrid material in diverse application. For example researcher has attempted to control sp^2/sp^3 hybrid carbon structure in GO by simple ethanol solvothermal method [58]. Furthermore, a similar trend was investigated to enlarge the carbon cluster size by increasing the sonication time [59].

2.4. Conclusions

In this work, the GO-based POM nanocomposite was successfully obtained. The Cs adsorption capacity increased by forming nanocomposite. The result proposed, first, the C/O ratio of GO sample has significantly influenced the characteristic of GO-POM nanocomposite for Cs adsorption performance after forming composite. Specifically, GO sample, which consists of 70-72 wt% C element, is a good precursor material to incorporate Dawson-type POM compared to the GO that has ~39 wt% C element in their atomic composition. Second, the concentration ratio of GO/POM in forming composite material can be considered to maximize the adsorption performance. Additionally, the size and the acidity of the GO also influence the aggregation state. However, it still needs

further investigation to know the size-tunability and the role of acidic properties of GO in different C/O composition for Cs adsorption. The further calculation was performed to quantify the graphitic zone in each sample. The result revealed that the oxidized zone was enhanced after forming composite in all samples except $[GO_{70}POM]_{41}$ that shows a different character. Further scrutiny is needed to open the understanding of the role of oxidative debris (OD) component of GO and the level of hydration of GO for adsorption capacity.

Supporting Information

Supportive SEM imaging, FT-IR spectra, PXRD data, Raman data, Plausible interaction GO with Dawson-type POM, Table of the ratio ID/IG of GO-POM nanocomposite, Table of the crystallite size of GO and composite material.

References

[1] K. Nishihara *et al.*, "Radionuclide release to stagnant water in the Fukushima-1 nuclear power plant1," *J. Nucl. Sci. Technol.*, vol. 52, no. 3, pp. 301–307, 2015.

[2] R. J. M. Konings, T. Wiss, and O. Beneš, "Predicting material release during a nuclear reactor accident," *Nat. Mater.*, vol. 14, no. 3, pp. 247–252, 2015.

[3] S. Uchida and K. Tagami, "Soil-to-plant transfer factors of fallout 137Cs and native 133Cs in various crops collected in Japan," *J. Radioanal. Nucl. Chem.*, vol. 273, no. 1, pp. 205–210, 2007.

[4] K. Shizuma, Y. Fujikawa, M. Kurihara, and Y. Sakurai, "Identification and temporal decrease of 137Cs and 134Cs in groundwater in Minami-Soma City following the accident at the Fukushima Dai-ichi nuclear power plant," *Environ. Pollut.*, vol. 234, pp. 1–8, 2018.

[5] J. Koarashi, M. Atarashi-Andoh, T. Matsunaga, T. Sato, S. Nagao, and H. Nagai, "Factors affecting vertical distribution of Fukushima accident-derived radiocesium in soil under different land-use conditions," *Sci. Total Environ.*, vol. 431, pp. 392–401, 2012.

[6] K. Kamiya *et al.*, "Long-term effects of radiation exposure on health," *Lancet*, vol. 386, no. 9992, pp. 469–478, 2015.

[7] A. Hasegawa *et al.*, "Health effects of radiation and other health problems in the aftermath of nuclear accidents, with an emphasis on Fukushima," *Lancet*, vol. 386, no. 9992, pp. 479–488, 2015.

[8] N. Matsuda, S. Nakashima, "Radioactive cesium in water and soil and its adsorption to rice plant (interim report) (in japanese)," *Radiat. Saf. Manage.*, vol. 13, no. 1, pp. 84–91, 2014.

[9] TEPCO, "The Evaluation Status of Reactor Core Damage at Fukushima Daiichi Nuclear Power Station Units 1 to 3," p. 28, 2011.

[10] T. Yousefi, M. Torab-Mostaedi, M. A. Moosavian, and H. G. Mobtaker, "Potential application of a nanocomposite:HCNFe@polymer for effective removal of Cs (I) from nuclear waste," *Prog. Nucl. Energy*, vol. 85, pp. 631–639, 2015.

[11] S. C. Jang *et al.*, "Synergistically strengthened 3D micro-scavenger cage adsorbent for selective removal of radioactive cesium," *Sci. Rep.*, vol. 6, no. June, pp. 1–12, 2016.

[12] K. Tamura, T. Kogure, Y. Watanabe, C. Nagai, and H. Yamada, "Uptake of cesium and strontium ions by artificially altered phlogopite," *Environ. Sci. Technol.*, vol. 48, no. 10, pp. 5808–5815, 2014.

[13] J. Guerrero-Contreras and F. Caballero-Briones, "Graphene oxide powders with different oxidation degree, prepared by synthesis variations of the Hummers method," *Mater. Chem. Phys.*, vol. 153, no. March, pp. 209–220, 2015.

[14] Z. Liu, T. Rios-Carvajal, M. P. Andersson, M. Ceccato, S. L. S. Stipp, and T.

Hassenkam, “Ion effects on molecular interaction between graphene oxide and organic molecules,” *Environ. Sci. Nano*, vol. 6, no. 7, pp. 2281–2291, 2019.
[15] V. V. Neklyudov, N. R. Khafizov, I. A. Sedov, and A. M. Dimiev, “New insights into the solubility of graphene oxide in water and alcohols,” *Phys. Chem. Chem. Phys.*, vol. 19, no. 26, pp. 17000–17008, 2017.
[16] B. Konkena and S. Vasudevan, “Understanding aqueous dispersibility of graphene oxide and reduced graphene oxide through p K a measurements,” *J. Phys. Chem. Lett.*, vol. 3, no. 7, pp. 867–872, 2012.
[17] C. Ritchie *et al.*, “Reversible redox reactions in an extended polyoxometalate framework solid,” *Angew. Chemie - Int. Ed.*, vol. 47, no. 36, pp. 6881–6884, 2008.
[18] R. Kawahara, S. Uchida, and N. Mizuno, “Redox-induced reversible uptake-release of cations in porous ionic crystals based on polyoxometalate: Cooperative migration of electrons with alkali metal ions,” *Chem. Mater.*, vol. 27, no. 6, pp. 2092–2099, 2015.
[19] S. Uchida, “Frontiers and progress in cation-uptake and exchange chemistry of polyoxometalate-based compounds,” *Chem. Sci.*, vol. 10, no. 33, pp. 7670–7679, 2019.
[20] S. Hitose and S. Uchida, “Rapid Uptake/Release of Cs+ in Isostructural Redox-Active Porous Ionic Crystals with Large-Molecular-Size and Easily Reducible Dawson-Type Polyoxometalates as Building Blocks,” *Inorg. Chem.*, vol. 57, no. 9, pp. 4833–4836, 2018.
[21] H. Li, S. Pang, X. Feng, K. Müllen, and C. Bubeck, “Polyoxometalate assisted photoreduction of graphene oxide and its nanocomposite formation,” *Chem. Commun.*, vol. 46, no. 34, pp. 6243–6245, 2010.
[22] R. D. Gall, C. L. Hill, and J. E. Walker, “Carbon powder and fiber-supported polyoxometalate catalytic materials. Preparation, characterization, and catalytic oxidation of dialkyl sulfides as mustard (HD) analogues,” *Chem. Mater.*, vol. 8, no. 10, pp. 2523–2527, 1996.
[23] S. Eigler and A. Hirsch, “Chemistry with graphene and graphene oxide - Challenges for synthetic chemists,” *Angew. Chemie - Int. Ed.*, vol. 53, no. 30, pp. 7720–7738, 2014.
[24] D. R. Dreyer, S. Park, C. W. Bielawski, and R. S. Ruoff, “The chemistry of graphene oxide,” *Chem. Soc. Rev.*, vol. 39, no. 1, pp. 228–240, 2010.
[25] E. Aliyev, V. Filiz, M. M. Khan, Y. J. Lee, C. Abetz, and V. Abetz, “Structural characterization of graphene oxide: Surface functional groups and fractionated oxidative debris,” *Nanomaterials*, vol. 9, no. 8, 2019.
[26] W. S. Hummers and R. E. Offeman, “Preparation of Graphitic Oxide,” *J. Am. Chem. Soc.*, vol. 80, no. 6, p. 1339, 1958.
[27] P. Ranjan, S. Agrawal, A. Sinha, T. R. Rao, J. Balakrishnan, and A. D. Thakur, “A Low-Cost Non-explosive Synthesis of Graphene Oxide for Scalable Applications,” *Sci. Rep.*, vol. 8, no. 1, pp. 1–13, 2018.

[28] I. M. Mbomekalle, Y. W. Lu, B. Keita, and L. Nadjo, “Simple, high yield and reagent-saving synthesis of pure α-K 6P2W18O62 · 14H2O,” *Inorg. Chem. Commun.*, vol. 7, no. 1, pp. 86–90, 2004.
[29] L. J. Cote, J. Kim, Z. Zhang, C. Sun, and J. Huang, “Tunable assembly of graphene oxide surfactant sheets: Wrinkles, overlaps and impacts on thin film properties,” *Soft Matter*, vol. 6, no. 24, pp. 6096–6101, 2010.
[30] K. Krishnamoorthy, M. Veerapandian, K. Yun, and S. J. Kim, “The chemical and structural analysis of graphene oxide with different degrees of oxidation,” *Carbon N. Y.*, vol. 53, pp. 38–49, 2013.
[31] S. Shukla and S. Saxena, “Spectroscopic investigation of confinement effects on optical properties of graphene oxide,” *Appl. Phys. Lett.*, vol. 98, no. 7, pp. 2010–2012, 2011.
[32] N. I. Kovtyukhova, “Layer-by-layer assembly of ultrathin composite films from micron-sized graphite oxide sheets and polycations,” *Chem. Mater.*, vol. 11, no. 3, pp. 771–778, 1999.
[33] A. B. S. Mohindar S. Seehra, Vishal Narang, Usha K. Geddam, “Correlation between X-ray diffraction and Raman spectra of 16 commercial graphene-based materials and their resulting classification,” *Carbon N Y*, vol. 111, no. 5, pp. 380–384, 2017.
[34] R. Wang, L. Dang, Y. Liu, and W. Jiao, “Preparation, characterization and photocatalytic activity of Dawson type phosphotungstate/graphene oxide composites,” *Adv. Powder Technol.*, vol. 30, no. 7, pp. 1400–1408, 2019.
[35] T. Szabó *et al.*, “Evolution of surface functional groups in a series of progressively oxidized graphite oxides,” *Chem. Mater.*, vol. 18, no. 11, pp. 2740–2749, 2006.
[36] V. D. Ebajo, C. R. L. Santos, G. V. Alea, Y. A. Lin, and C. H. Chen, “Regenerable Acidity of Graphene Oxide in Promoting Multicomponent Organic Synthesis,” *Sci. Rep.*, vol. 9, no. 1, 2019.
[37] R. R. Amirov, J. Shayimova, Z. Nasirova, A. M. Dimiev, “Chemistry of graphene oxide. reactions with transition metal cations,” *Carbon*, 116, 356–365, 2017.
[38] D. C. Marcano *et al.*, "Improved synthesis of graphene oxide," *ACS Nano*, vol. 4, 4806-4814, 2010.
[39] C. Petit and T. J. Bandosz, “Graphite Oxide/Polyoxometalate nanocomposites as adsorbents of ammonia,” *J. Phys. Chem. C*, vol. 113, no. 9, pp. 3800–3809, 2009.
[40] N. Mizuno and M. Misono, “Heterogeneous catalysis,” *Chem. Rev.*, vol. 98, no. 1, pp. 199–217, 1998.
[41] T. Okuhara, T. Nishimura, H. Watanabe, and M. Misono, “Insoluble heteropoly compounds as highly active catalysts for liquid-phase reactions,” *J. Mol. Catal.*, vol. 74, no. 1–3, pp. 247–256, 1992.
[42] R. Sharma, N. Chadha, and P. Saini, “Determination of defect density, crystallite size and number of graphene layers in graphene analogues using X-ray diffraction

and Raman spectroscopy," *Indian J. Pure Appl. Phys.*, vol. 55, no. 9, pp. 625–629, 2017.
[43] M. S. Dresselhaus, A. Jorio, A. G. Souza Filho, and R. Saito, "Defect characterization in graphene and carbon nanotubes using Raman spectroscopy," *Philos. Trans. R. Soc. A Math. Phys. Eng. Sci.*, vol. 368, no. 1932, pp. 5355–5377, 2010.
[44] A. A. K. King *et al.*, "A new raman metric for the characterisation of graphene oxide and its derivatives," *Sci. Rep.*, vol. 6, pp. 1–6, 2016.
[45] C. Y. Su *et al.*, "Highly efficient restoration of graphitic structure in graphene oxide using alcohol vapors," *ACS Nano*, vol. 4, no. 9, pp. 5285–5292, 2010.
[46] R. J. Nemanich and S. A. Solin, "First- and second-order Raman scattering from finite size-crystals of graphite," *Phys. Rev. B*, vol. 20, no. 2, p. 392, 1979.
[47] P. Kaewmee, J. Manyam, P. Opaprakasit, G. T. Truc Le, N. Chanlek, and P. Sreearunothai, "Effective removal of cesium by pristine graphene oxide: Performance, characterizations and mechanisms," *RSC Adv.*, vol. 7, no. 61, pp. 38747–38756, 2017.
[48] T. Xia, Y. Qi, J. Liu, Z. Qi, W. Chen, and M. R. Wiesner, "Cation-inhibited transport of graphene oxide nanomaterials in saturated porous media: The hofmeister effects," *Environ. Sci. Technol.*, vol. 51, no. 2, pp. 828–837, 2017.
[49] K. Yang, B. Chen, X. Zhu, and B. Xing, "Aggregation, Adsorption, and Morphological Transformation of Graphene Oxide in Aqueous Solutions Containing Different Metal Cations," *Environ. Sci. Technol.*, vol. 50, no. 20, pp. 11066–11075, 2016.
[50] J. C. Ma and D. A. Dougherty, "The cation-π interaction," *Chem. Rev.*, vol. 97, no. 5, pp. 1303–1324, 1997.
[51] Y. Xu, J. Shen, W. Zhu, X. Luo, K. Chen, and H. Jiang, "Influence of the water molecule on cation-π interaction: Ab initio second order møller-plesset perturbation theory (MP2) calculations," *J. Phys. Chem. B*, vol. 109, no. 12, pp. 5945–5949, 2005.
[52] Y. Marcus, "Ionic Radii in Aqueous Solutions," *Chem. Rev.*, vol. 88, no. 8, pp. 1475–1498, 1988.
[53] D. Zhou and B. G. Han, "Graphene-based nanoporous materials assembled by mediation of polyoxometalate nanoparticles," *Adv. Funct. Mater.*, vol. 20, no. 16, pp. 2717–2722, 2010.
[54] Y. Liu *et al.*, "Polyoxometalate-Modified Sponge-Like Graphene Oxide Monolith with High Proton-Conducting Performance," *Adv. Funct. Mater.*, vol. 25, no. 28, pp. 4480–4485, 2015.
[55] Q. Tu *et al.*, "Effects of surface charges of graphene oxide on neuronal outgrowth and branching," *Analyst*, vol. 139, no. 1, pp. 105–115, 2013.
[56] K. N. Kudin, B. Ozbas, H. C. Schniepp, R. K. Prud'homme, I. A. Aksay, and R. Car, "Raman spectra of graphite oxide and functionalized graphene sheets," *Nano Lett.*, vol. 8, no. 1, pp. 36–41, 2008.

[57] Y. Kim and S. Shanmugam, "Polyoxometalate-reduced graphene oxide hybrid catalyst: Synthesis, structure, and electrochemical properties," *ACS Appl. Mater. Interfaces*, vol. 5, no. 22, pp. 12197–12204, 2013.

[58] S. Wang *et al.*, "The role of sp2/sp3 hybrid carbon regulation in the nonlinear optical properties of graphene oxide materials," *RSC Adv.*, vol. 7, no. 84, pp. 53643–53652, 2017.

[59] S. Il Ahn, "Changing the sp2 carbon clusters in graphene oxide during exfoliation," *Trans. Electr. Electron. Mater.*, vol. 16, no. 1, pp. 49–52, 2015.

[60] H. Yan *et al.*, "Influence of the surface structure of graphene oxide on the adsorption of aromatic organic compounds from water," *ACS Appl. Mater. Interfaces*, vol. 7, no. 12, pp. 6690–6697, 2015.

[61] M. A. Schwegler, P. Vinke, M. van der Eijk, and H. van Bekkum, "Activated carbon as a support for heteropolyanion catalysts," *Appl. Catal. A, Gen.*, vol. 80, no. 1, pp. 41–57, 1992.

[62] A. Khodadadi Dizaji, H. R. Mortaheb, and B. Mokhtarani, "Preparation of supported catalyst by adsorption of polyoxometalate on graphene oxide/reduced graphene oxide," *Mater. Chem. Phys.*, vol. 199, pp. 424–434, 2017.

[63] I. Sánchez-García, A. Núñez, L. J. Bonales, J. M. Perlado, and J. Cobos, "Study of the adsorption capacity of graphene oxide under gamma radiation in different media," *Radiat. Phys. Chem.*, vol. 165, no. July, p. 108395, 2019.

[64] B. Lian, S. De Luca, Y. You, S. Alwarappan, M. Yoshimura, V. Sahajwalla, S. C. Smith, G. Leslie and R. K. Joshi, "Extraordinary water adsorption characteristics of graphene oxide," *Chem. Sci.*, vol. 9, 5106.

[65] Dimiev, Ayrat.M., Eigler, S., 2017, "Graphene Oxide:Fundamentals and Applications", John Wiley & Son, Ltd, UK.

[66] Ho. Tuan. A., Striolo. A, "Polarizability effects in molecular dynamics simulations of the graphene-water interface," *The Journal of Chem. Phys.*, vol. 138, 054117, 2013.

[67] J. Sala. E. Guardia, J. Marti, "Specific ion effects in aqueous electrolyte solutions confined within graphene sheets at the nanometric scale," *Phys. Chem. Chem. Phys.*, 14, 10799-10808, 2012.

[68] R. R. Nair, H. A. Wu., P. N. Jayaram., I. V. Grigorieva, A. K. Geim, "Unimpeded permeation Of water through helium-leak-tight-graphene –based membranes," *Science*, 335 (6067), 442-444, 2012.

[69] A. Y. Romanchuk, A. S. Slesarev, S. N. Kalmykov, D. V. Kosynkin, J. M. Tour, "Graphene Oxide for effective radionuclide removal," *Phys. Chem. Chem. Phys.*, 15, 2321, 2013.

[70] L. R. Radovic, "Active site in graphene and the mechanism of CO_2 formation in carbon Oxidation," *J. AM. CHEM. SOC.*, 131, 17166-17175, 2009.

[71] G. D. Parfitt, C. H. Rochester, 1983, "Adsorption from solution at the solid/liquid interface," Academic Press, London.

[72] T. Szabo, P. Maroni, I. Szilagyi, "Size-dependent aggregation of graphene oxide," *Carbon*, 160, 145-155, 2020.
[73] A. M. Dimiev, L. B. Alemany, J. M. Tour, "Graphene oxide. Origin of acidity, Its instability in water, and a new dynamic structural model," *ACS Nano*, 7, 576-588, 2013.
[74] T. Szabo, E. Tombacz, E. Illes, I. Dekany, "Enhanced acidity and pH-dependent surface Charge characterization of succively oxidized graphite oxides," *Carbon*, 44, 537-545, 2006.
[75] K. Erickson, R. Erni, Z. Lee, N. Alem, W. Gannet, and A. Zettl, "Determination of the local chemical structure of graphene oxide and reduced graphene oxide," *Adv. Mater.*, 22, 4467-4472, 2010.
[76] D. Bousa, J. Luxa, V. Mazanek, O. Jankovsky, D. Sedmidubsky, K. Klimova, M. Pumera, and Z. Sofer, "Toward graphene chloride: chlorination of graphene and graphene oxide", *RSC Adv.*, 6, 66884, 2016.
[77] T. Taniguchi, S. Kurihara, H. Tateishi, K. Hatakeyama, M. Koinuma, H. Yokoi, M. Hara, H. Ishikawa, and Y. Matsumoto, "pH-driven, reversible epoxy ring opening/closing in graphene oxide", *Carbon*, 84, 560-566, 2015.
[78] J. Zhang, C. Xiong, Y. Li, H. Tang, X. Meng, and W. Zhu, "The critical contribution of oxidation debris on the acidic properties of graphene oxide in an aqueous solution", *Journal of Hazardous Materials*, 402, 123552, 2021.
[79] B. S. Nugroho, M. N. K. Wihadi, F. Grote, S. Eigler, and S. Nakashima, "Potentiality of graphene oxide and polyoxometalate as radionuclides adsorbent to restore the environment after fukushima disaster: A mini review", *Indones. J. Chem.*, 21 (3), 776-786, 2021.
[80]. K. A. Mkhoyan, A. W. Countryman, J. Sylcox, D. A. Stewart, G. Eda, C. Mattevi, S. Miller, M. Chhowalla,"Atomic and electronic structure of graphene oxide", *Nano Letter*, 9 (3), 1058-1063, 2009.
[81] R. Contant and R. Thouvenot, "A Reinvestigation of Isomerism in the Dawson structure: syntheses and ^{183}W NMR Structural Characterization of Three New Polyoxotungstates $[X_2W_{18}O_{62}]^{6-}$ (X = P^v, As^v)", *Inorg.Chim.Acta*, 212, 41-50, 1993.
[82] A. Misra, K. Kozma, C. Streb, M. Nymann, "Beyond Charge Balance: Counter-cation in Polyoxometalate Chemistry", *Angew. Chem. Int. Ed.*, 59, 596-612, 2020.

[83] M. Acik, C. Mattevi, C. Gong, G. Lee, K. Cho, M. Chhowalla, Y. J. Chabal, "The role of intercalated water in multilayered graphene oxide", ACS Nano, 4 (10), 5861-5868, 2010.

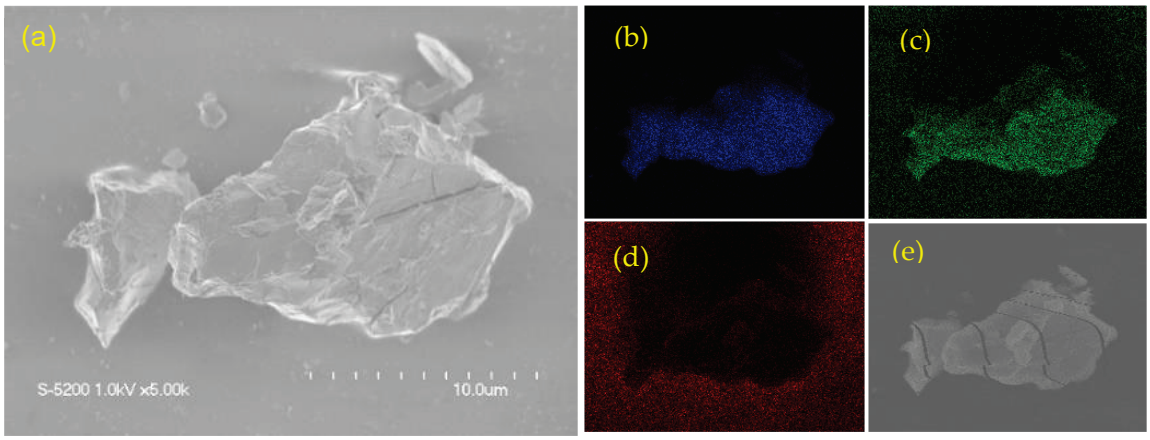

Fig S1. SEM measurement (a)α-$K_6P_2W_{18}O_{62}.14H_2O$ (b)Tungsten element (c)Oxygen element (d)Carbon K- α X-ray element (e)Secondary electron image

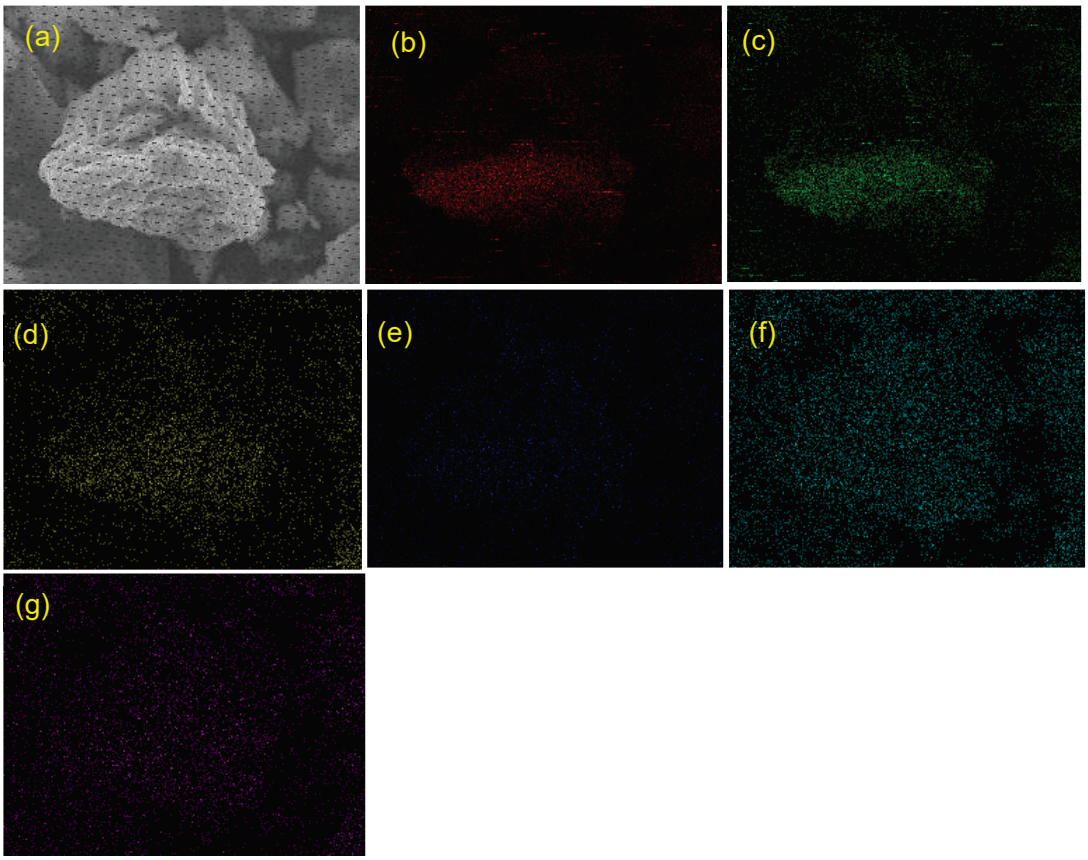

Fig S2. SEM measurement, $[GO_{70}POM]_{41}$ (a)Secondary electron image (b)Carbon K- α X-ray element (c)Oxygen element (d)Tungsten element (e)Aluminum element (f)Cesium element (g)Chloride element

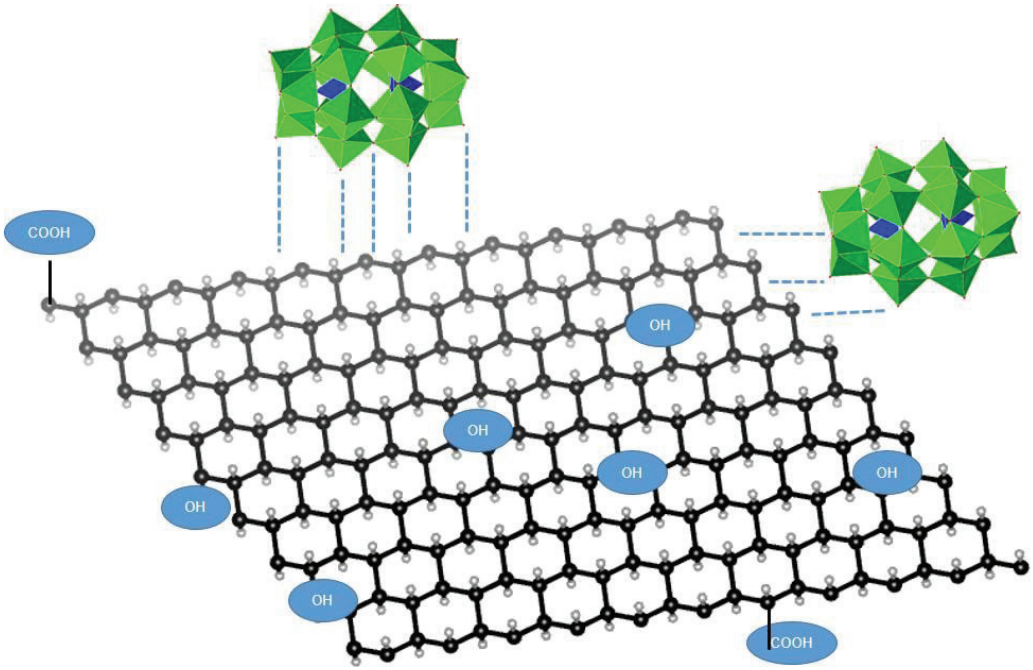

Fig S3. Plausible Interaction between Graphene-Oxide (GO) and Dawson-type Polyoxometalates (POMs). The black and the grey balls corresponds to carbon and hydrogen. The polyhedral model represents to Dawson-type polyoxometalates. The blue dashes indicated of the presence of interaction between GO-POMs.

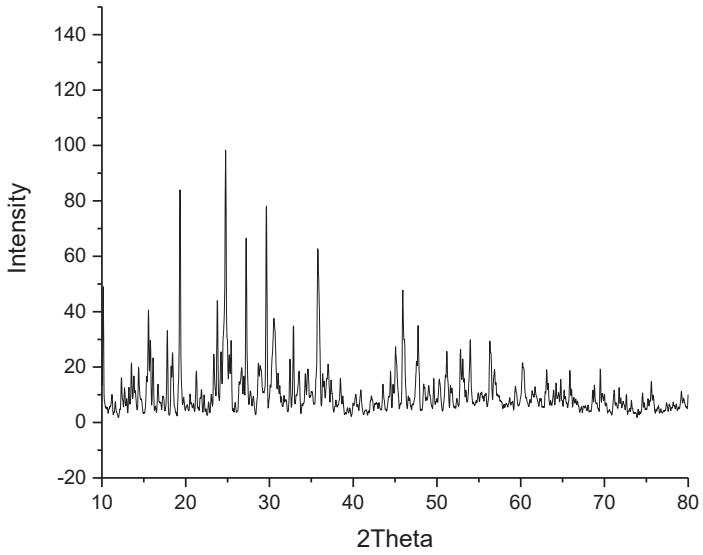

Fig S4. Xrd pattern of α-$K_6P_2W_{18}O_{62}.14H_2O$

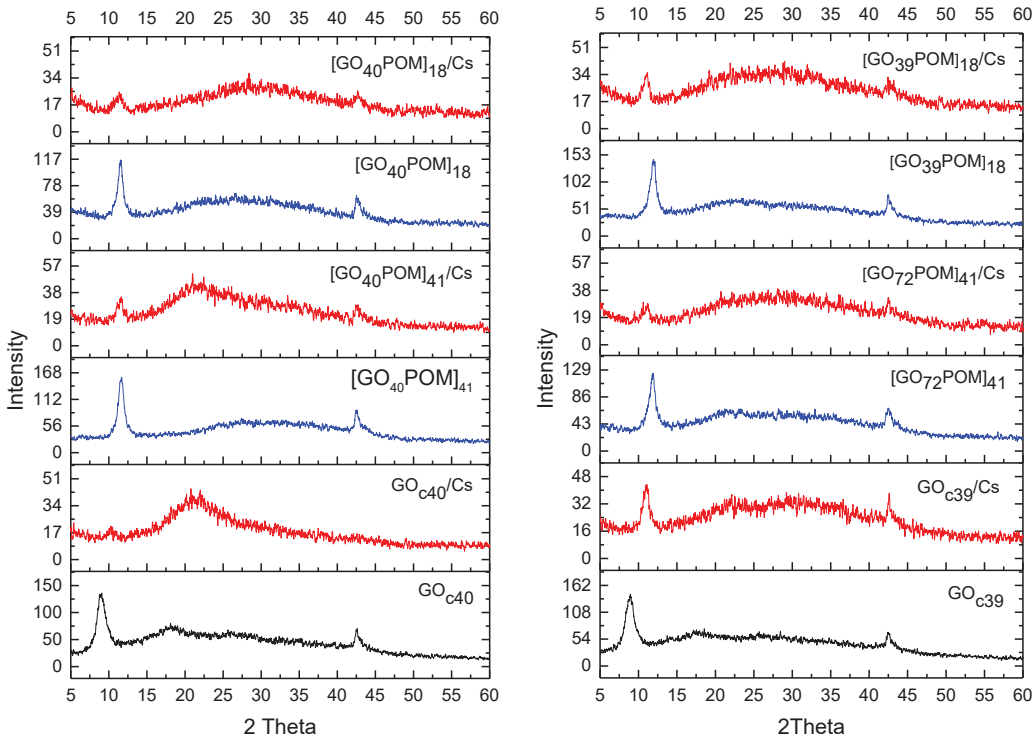

Fig S5. XRD pattern of GO_{c39}, GO_{c40}, GOPOM composite before and after Cs adsorption

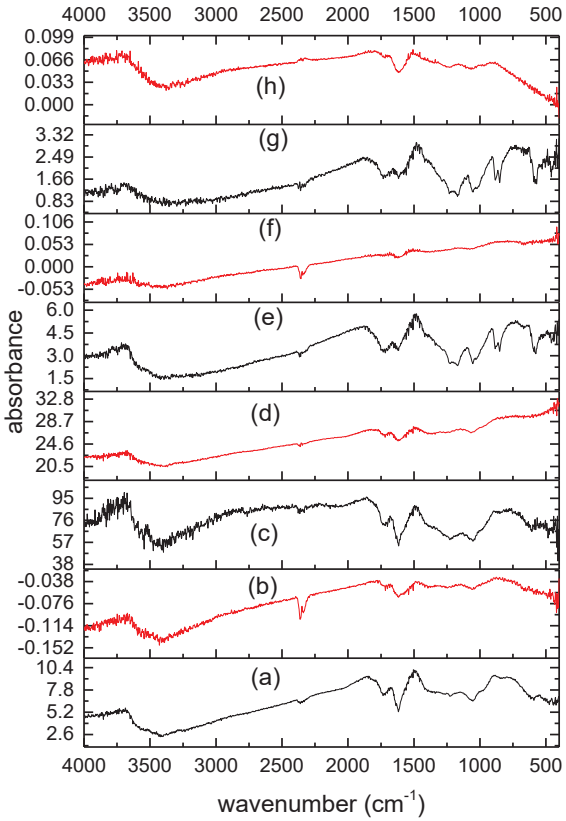

Fig S6. IR spectra for (a)GO_{c70} (b)GO_{c70} after Cs adsorption (c)GO_{c72} (d)GO_{c72} after Cs adsorption (e)GO_{c39} (f)GO_{c39} after Cs adsorption (g)GO_{c40} (h)GO_{c40} after Cs adsorption

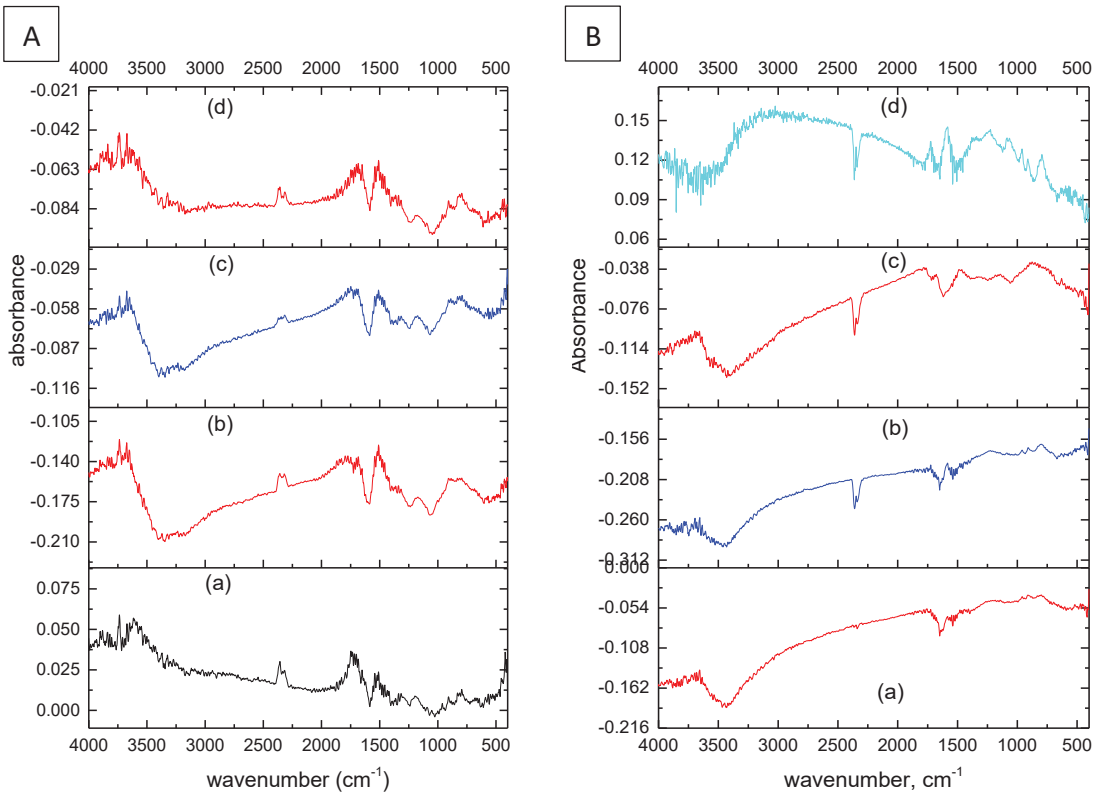

Fig S7A. IR spectra for (a) $[GO_{39}POM]_{18}$ (b) $[GO_{39}POM]_{18}$ after Cs adsorption (c) $[GO_{39}POM]_{41}$ (d) $[GO_{39}POM]_{41}$ after Cs adsorption, S7B. (a)$[GO_{70}POM]_{18}$ (b)$[GO_{70}POM]_{18}$ after Cs adsorption (c)$[GO_{70}POM]_{41}$ (d)$[GO_{70}POM]_{41}$ after Cs adsorption.

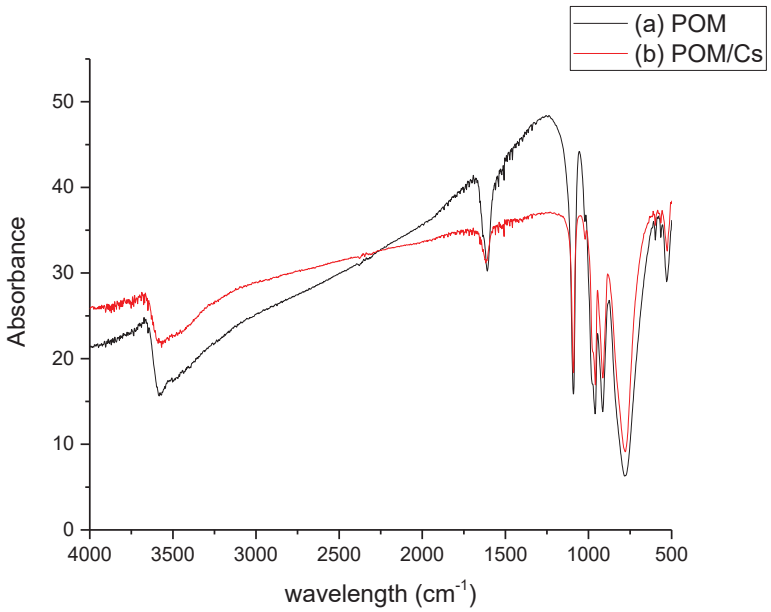

Fig S8. IR spectra for (a)POM (b)POM after Cs adsorption

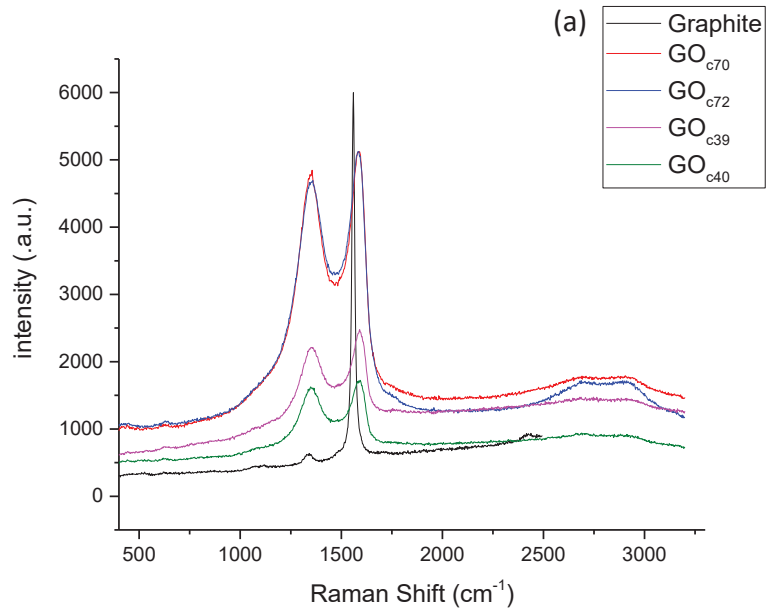

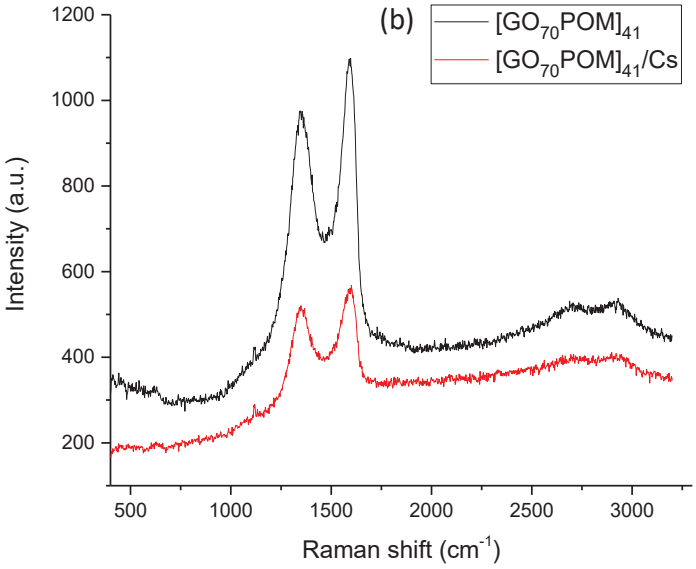

Fig S9. Raman spectra (a)Graphite, GO_{c70}, GO_{c72}, GO_{c39}, GO_{c40}, (b) $[GO_{70}POM]_{41}$ and after Cs adsorption

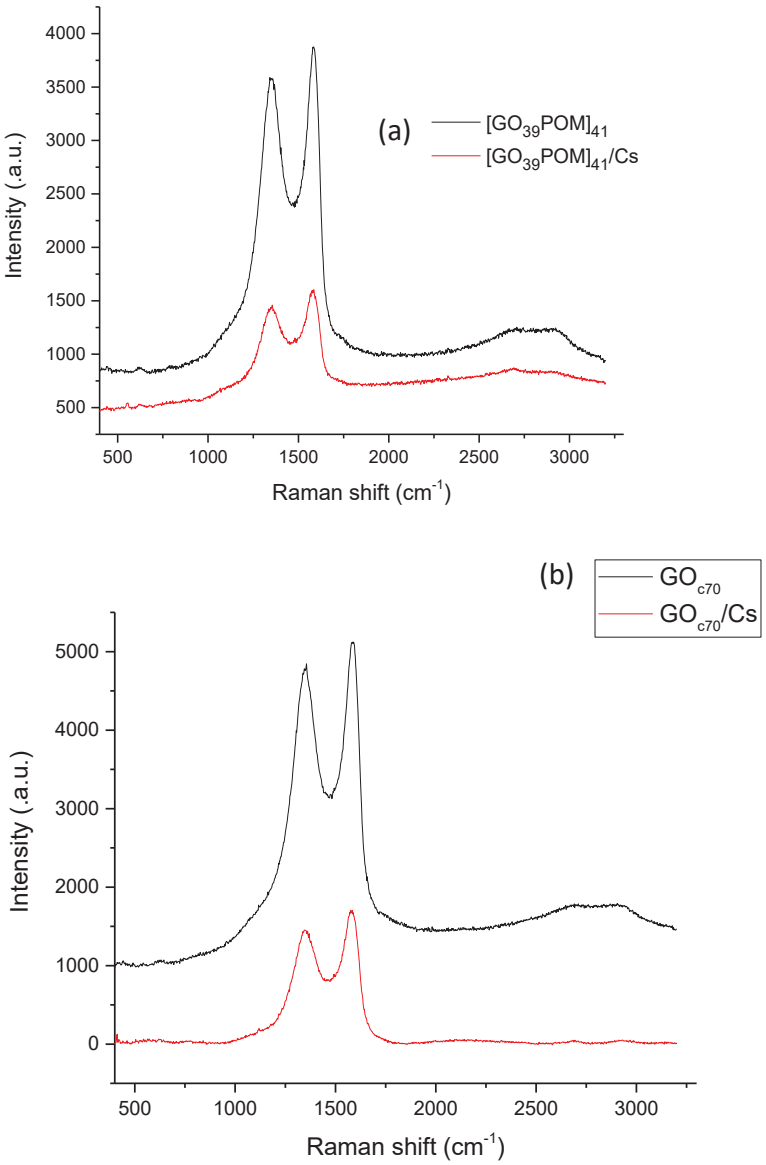

Fig S10. Raman spectra composite (a) $[GO_{39}POM]_{41}$ before and after Cs adsorption (b)GO_{c70} before and after Cs adsorption

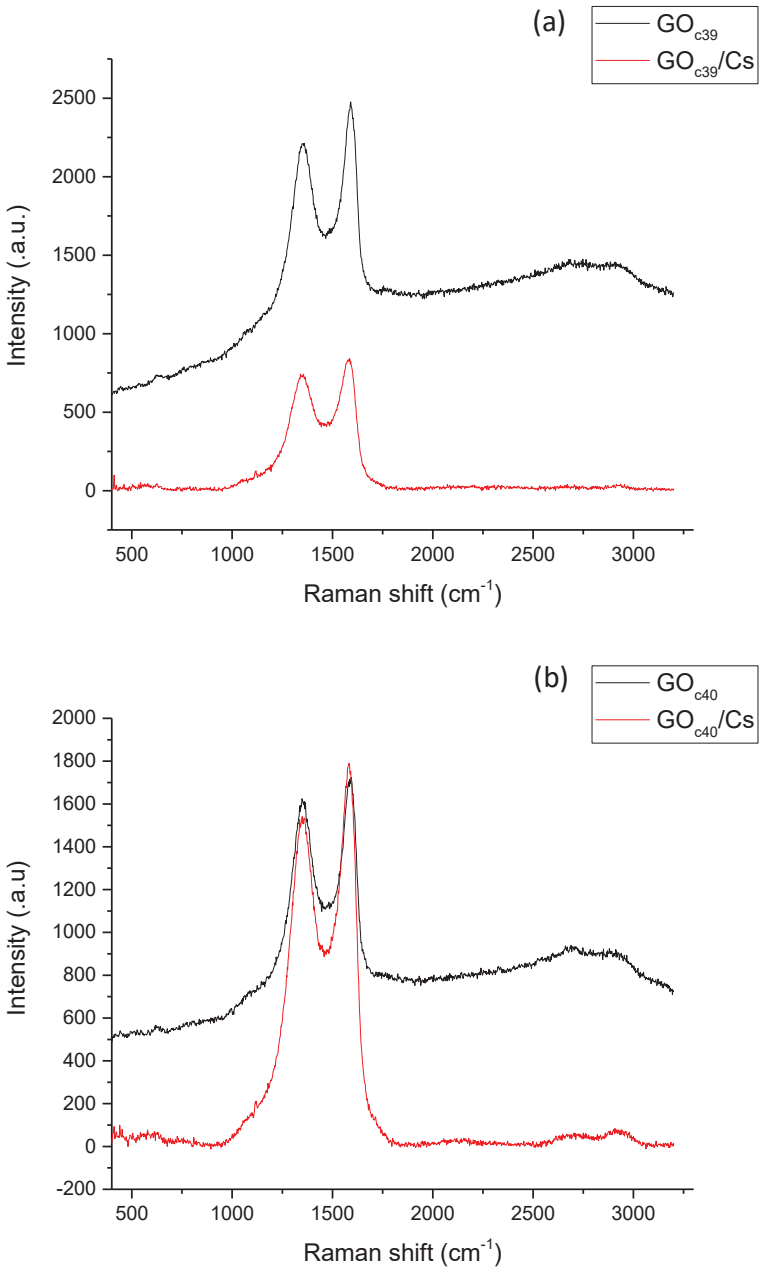

Fig S11. Raman spectra (a)GO_{c39} before and after Cs adsorption (b)GO_{c40} before and after Cs adsorption

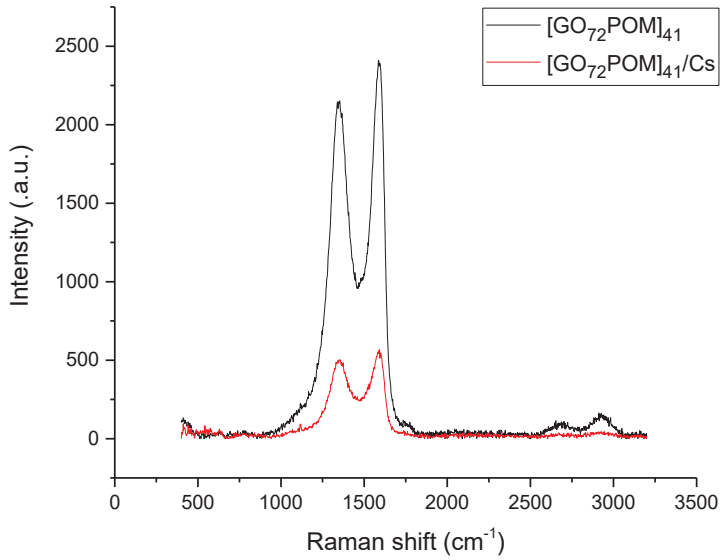

Fig S12. Raman spectra composite $[GO_{72}POM]_{41}$ before and after Cs adsorption

Table S13.The ratio I_D/I_G of Graphene oxide and composite before and after Cs adsorption

No.	Material	D band	G band	Ratio I_D/I_G
1	GO_{c70}	1356	1586	0.93
2	GO_{c72}	1352	1581	0.91
3	GO_{c39}	1352	1590	0.89
4	GO_{c40}	1347	1590	0.88
5	$[GO_{39}POM]_{41}$	1347	1581	0.92
6	$[GO_{39}POM]_{41}/Cs$	1352	1586	0.90
7	$[GO_{70}POM]_{18}$	1347	1586	0.96
8	$[GO_{70}POM]_{18}/Cs$	1352	1577	0.92
9	$[GO_{70}POM]_{41}$	1357	1592	0.88
10	$[GO_{70}POM]_{41}/Cs$	1343	1602	0.93

Table S14. The crystallize size of GO

Sample	Concentration ratio GO:POM	2Φ (°)	FWHM (ß)	Out of plane crystallite size – D (nm)	d (nm)	d (nm) after Cs adsorption	Layer (n)	In plane crystallite size – L (nm)
Graphite	-	26.6	0.28	30.49	0.34	-	90.67	10.27
GO_{c70}	-	11.58	1.93	4.3	0.77	-	6.58	2.59
GO_{c72}	-	8.66	1.69	4.9	1.02	-	5.80	2.53
GO_{c39}	-	8.91	1.57	5.3	0.99	-	6.19	2.56
GO_{c40}	-	9.13	1.47	5.7	0.97	-	6.75	2.61
$[GO_{70}POM]_{18}$	1:8	12.28	1.63	5.12	0.72	0.79	-	2.54
$[GO_{70}POM]_{41}$	4:1	10.99	1.48	5.64	0.81	0.86	-	2.61
$[GO_{72}POM]_{18}$	1:8	12.75	1.10	7.60	0.69	0.77	-	3.04
$[GO_{72}POM]_{41}$	4:1	12.05	1.07	7.80	0.73	0.79	-	3.09
$[GO_{39}POM]_{18}$	1:8	11.92	1.19	7.02	0.74	0.81	-	2.89
$[GO_{39}POM]_{41}$	4:1	11.86	1.07	7.80	0.74	0.79	-	3.09
$[GO_{40}POM]_{18}$	1:8	11.57	0.84	9.94	0.76	0.83	-	3.71
$[GO_{40}POM]_{41}$	4:1	11.57	0.24	34.78	0.76	0.78	-	11.95

*FWHM was calculated by using origin software

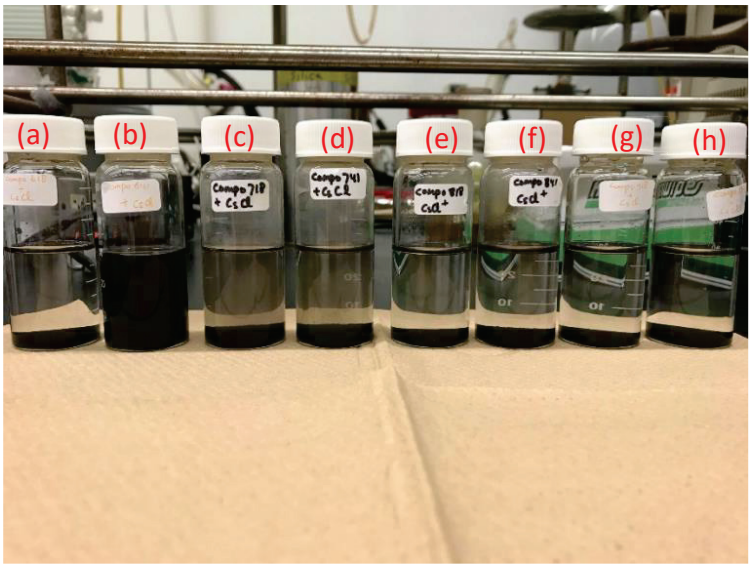

Fig S15. The composite solution after Cs adsorption. Only Composite $[GO_{70}POM]_{41}$ (b) that forms stable solution (black color). Another composite solution shows remains coagulated. The photo was taken after more than one-hour stay at ambient temperature.

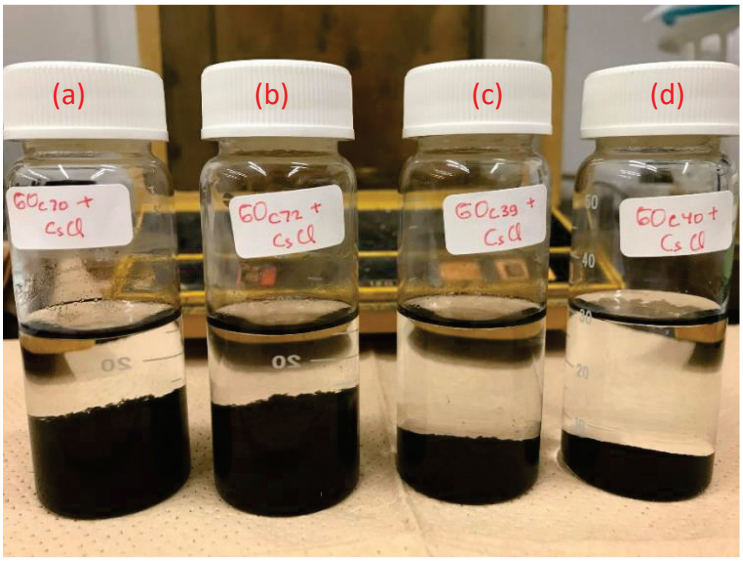

Fig S16. The GO solution after Cs adsorption. All GO solutions shows remains coagulated. (a) GO_{c70} and (b) GO_{c72} shows different coagulated behavior with (c) GO_{c39} and (d) GO_{c40}. The photo was taken after more than one-hour stay at ambient temperature.

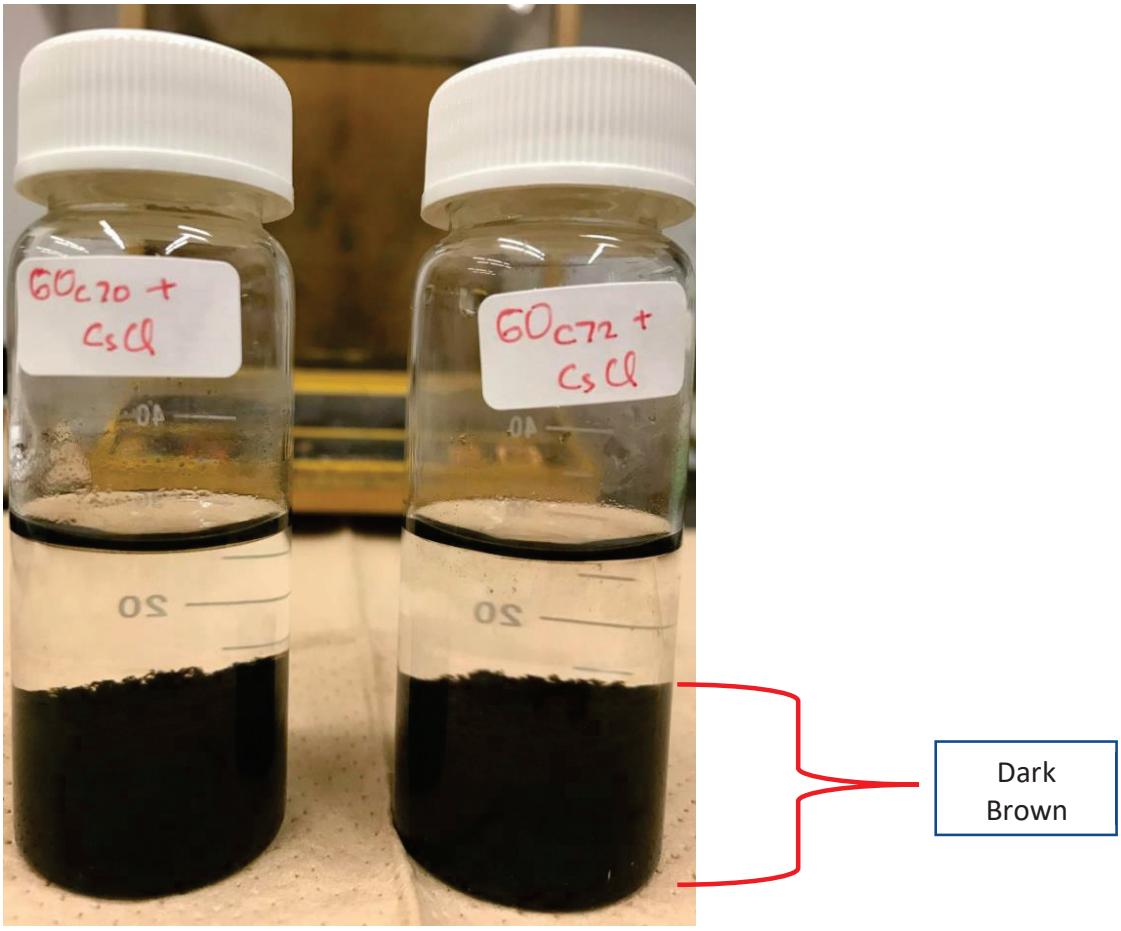

Fig S17. Coagulation process after Cs interaction with (a) GO_{c70} and (b) GO_{c72}. The photo was taken after more than one-hour stay at ambient temperature.

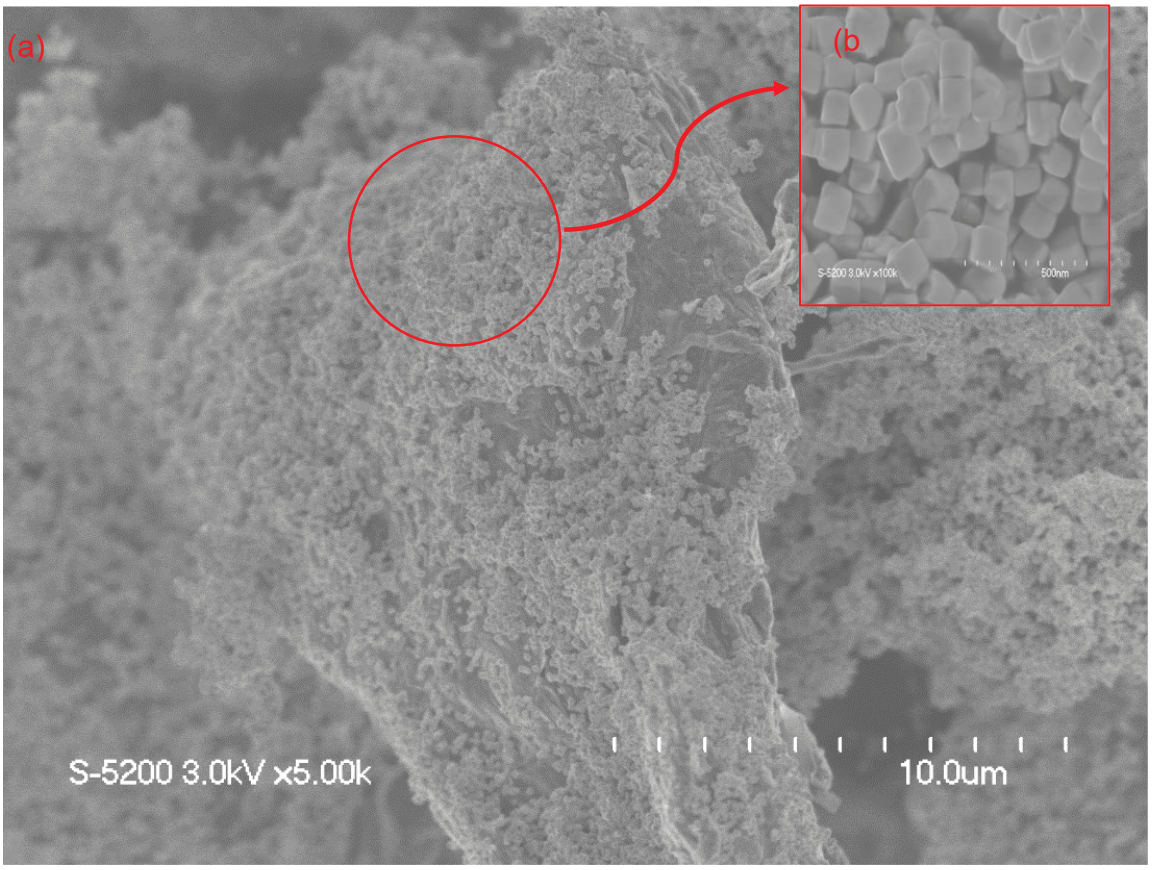

Fig S18. SEM image by using composite (a) $[GO_{70}POM]_{41}$ after Cs adsorption and (b) Cs particle (zoom mode based on figure a).

Chapter III. Improvement of Cs detection performance and formation of CsCl and Cs nanoparticles by tuning graphene oxide quantum dot-based nanocomposite

3.1.Introduction

The Fukushima Dai-ichi Nuclear Power Plant (FDNPP) disaster that occurred in 2011 has attracted the attention of researchers. Specifically, the release of radioactive materials like Cs-137 (with half-life of 30.1 years) has drawn the attention because of the immediate and long-term effects on the environment [1],[2]. Since the radioactive cesium (Cs) has a high solubility in water and a long half-life, it can migrate from one pond to the river, move far away to the paddy field [3], and finally come into the groundwater. As reported in the previous work, the radioactive Cs was detected in the tap water and ground water with different degree of contamination in some area of Fukushima [4]. Consequently, it was restricted to be consumed by all people who stay around the FDNPP area. Therefore, the detection of Cs is of great importance to address the problem of Cs contamination in water.

Currently, several types of methods for Cs detection exist including atomic absorption spectroscopy, electrochemical devices, germanium detector, inductively coupled plasma mass spectroscopy, and fluorescence-based method. Especially the fluorescence-based method, which is infrequently used in Cs detection system, has a potential to become a non-destructive detector with low-cost. In the previous study squaraine dye as a mixed solution (DMSO/Water) exhibited a good response in Cs detection. This compound can work effectively and selectively by quenching the fluorescence intensity after Cs detection. According to this method, the blue fluorescence of the compound solution turned OFF after the Cs addition[5]. In the other work, T. Mori *et al.* have successfully designed a new supramolecular material (cesium green, $C_{32}H_{33}NO_8$) as Cs sensor expecting intermolecular fluorescence approaches (fluorescence resonance energy transfer (FRET) or exciplex mechanism) [6]. The study of energy transfer has been reported experimentally for different kinds of nanomaterials (quantum dots, nanoparticles) that act as energy donors or acceptors [7],[8]. Another researcher also demonstrated that the Cs can be detected using green fluorescence by cesium green (in methanolic solution) for the freeze-dried stem of plants that have already been treated with cesium carbonate[9]. However, the cesium green molecule has several limitations in

Cs detection application, since it can work effectively only in solid-state, without water, and in basic condition. Therefore, several technical problems should be addressed to make it more useful and easily to be used in order to identify Cs in contaminated water.

In recent years, graphene oxide (GO) and graphene oxide quantum dots (GOQDs) are widely studied in several applications such as metal adsorbent (Cs^{+}, Eu^{3+}, Sr^{2+})[10],[11], and designed as fluorescence probes by considering their quantum confinement and the edge effect [12],[13]. In addition, the GO and GOQDs have almost similar properties because they have various oxygen functional groups. The functional group can act as a binding point to synthesize a new nanocomposite to improve their properties [14],[15]. Another important thing is that the photoluminescence (PL) of GOQDs was independent of pH. It means that the emission wavelength does not shift in different pH condition (only change in the PL intensity) [16]. Further investigation also revealed that the PL of GO has shown a reversible response to ionic strength and pH [17],[18]. The previous work confirmed that the different number of layers of GO (single and a few layers) showed different optical responses in various organic solvent [19]. More currently, Yao *et al.* have employed graphene quantum dot-based fluorescence sensing as a dual detector of copper ion (Cu^{2+}) and tiopronin (MPG). They proposed a novel fluorescence turn OFF for the Cu^{2+} detection and turn ON for the tiopronin (MPG) detection [20].

Therefore, to facilitate the development of a Cs detection system, it is highly desirable to create a new nanocomposite using functionalized graphene oxide quantum dots (GOQDs) with cesium green molecule. The main purpose of the present study is to produce a new nanocomposite that has the ability to recognize Cs in water with different pH conditions (acidic and basic condition) by considering the turn ON/OFF response.

3.2.Experimental Section

3.2.1. Reagents and materials

Graphite, cesium green ($C_{32}H_{33}NO_8$), potassium permanganate ($KMnO_4$), hydrogen peroxide (H_2O_2), sulfuric acid (H_2SO_4), sodium nitrate ($NaNO_3$), sodium hydroxide (NaOH), cesium chloride (CsCl), hydrochloric acid (HCl), and potassium hydroxide (KOH) were analytical grade and were used without any further purification.

3.2.2. Synthesis of GO and GOQDs

Graphene oxide (GO) samples were prepared using modified Hummer`s method with graphite and the oxidizing agent, $KMnO_4$ (1:4, mass ratio) [21]. In this synthesis protocol, pre-cooling procedure and one minute stop-one minute go was implemented when adding the $KMnO_4$ according to our work [10]. The GOQDs were synthesized by using

as-prepared few-layers GO. In a typical synthesis, the ratio of GO and NaOH was 1:1 (mass ratio). First, dispersed the starting material GO (0.19 g) into distilled water followed by sonification for 5 minutes. Then, added NaOH (0.19 g) and stirred for 5 minutes at ambient temperature. Second, the solution was refluxed at 80 ^{o}C for two hours. After finished the reflux process, kept the solution at room temperature for a while. Then, came to the final step, centrifuged the solution for two times (4000 rpm for 10 minutes and 9500 g-force (relative centrifuge force) for 50 minutes). The brown solution was obtained as GOQDs solution. There is no further treatment for as-obtained GOQDs solution (Fig. 2e).

3.2.3. Synthesis of GOQD-based nanocomposite

The nanocomposite was generated by combining GOQDs solution as precursor material with cesium green (CG) solution. In this study, the nanocomposite was produced in two different concentration ratios of GOQDs:Cesium green (concentration ratio 5:1 and 8:1). In order to obtain the nanocomposite with a concentration ratio of 5:1, first, prepare 25 mL GOQDs solution (distilled water) and prepare the cesium green solution by dissolving 1 mg cesium green in 5 mL THF solvent. After that, mixed the GOQDs solution with cesium green solution followed by stirring for 30 minutes. A similar treatment was performed for the nanocomposite with a concentration ratio of 8:1. In order to distinguish both nanocomposites, the term composite-51 and composite-81 were applied. Each index number attached to the composite name is corresponded to the concentration ratio of GOQDs:cesium green molecule.

3.2.4. Photoluminescence detection of cesium

The Cs detection was performed at room temperature. There are two different concentrations of cesium chloride (CsCl) solution. The CsCl solution was made by adding 0.6 g CsCl in 30 mL distilled water. Based on that, the concentration of the CsCl solution was 0.12 mmol/L. Then, prepared the second CsCl solution to get a concentration of 0.06 mmol/L. The next step was that the different amounts of CsCl solution (changing volume from 200 ⍰L-800 ⍰L) were added into the nanocomposite solution. The photoluminescence spectra were measured and recorded under excitation slit 10 nm, emission slit 10 nm, PMT voltage 400 V, and excitation wavelength 330 nm. Finally, plotted the data as a standard curve graph (the PL intensity unit is cps as measured from the instrument).

3.2.5. Instrumentation and Characterization

Atomic force microscopy (AFM) was conducted by Asylum, MFP-3D origin (Oxford, UK). Ultraviolet-visible spectroscopy (UV-Vis) measurements were carried out using

JASCO V-650 spectrophotometer (Japan). Photoluminescence spectroscopy measurement was performed by Fluorescence spectrophotometer F-7000, Hitachi (Fukuoka, Japan). Transmission electron microscopy (ultra-high resolution transmission electron microscope) was performed using JEM-2010 (Tokyo, Japan). Zeta potential measurements were performed using Zeta potential and particle size analyser ELSZ-series 2000 (Otsuka, Japan). Elemental analysis was carried out using Perkin Elmer CHNS/O 2400II (USA).

3.3. Results and Discussion

3.3.1. Characterization of GO and GOQDs

The transmission electron microscopy (TEM) (Fig. 1a and 1b) and atomic force microscopy (AFM) (Fig. 1c and 1d) were performed to characterize the morphology and structure of GO as precursor material and GOQDs after reflux process. It is observed that the GO sample is wrinkles and overlap (Fig. 1a). For the ratio of graphite to potassium permanganate ($KMnO_4$) as oxidizing agent, 1:4, the graphite was successfully exfoliated. The elemental analysis of the GO sample was carried out to confirm the C, H, N, and O element as displayed in the Table. 1. In addition, the as obtained GO was employed as a precursor to fabricate GOQDs. As shown in Fig. 1b, the GOQDs image was produced. The NaOH reflux process has detached well the flake of oxidation debris (OD) from GO sample. These pieces (several nm) fell down on the GO layer. These are GO quantum dots (GOQDs). The GOQDs have a heterogeneous particle size distribution as is shown in TEM imaging (Fig. 1b). As proposed by previous experimental work, these small particles are adsorbed on the surface of graphene-like sheets [22]. And these small particles can be separated from GO by base treatment. Rourke at al. used the terminology for this small particle as `oxidation debris` [23].

Table 1. Elemental analysis of GO sample

Sample	C%	H%	N%	O%	C/O
GO	43.82	2.97	0.18	52.4	0.84

Furthermore, to confirm the thickness of the GO and GOQDs sample, the AFM imaging was conducted. Fig. 1c exhibited the height of GO is about 2-3 nm. It is also convinced that the GO material consists of a few layers. In addition, there are two types of dots for as-obtained GOQDs. The aggregating dots (aggregates) and small dots were confirmed with an average thickness of about 2 nm and 1.5 nm, respectively (Fig. 1d, S1a, see

supporting information). This value (for small dots) is close to the value corresponding to the thickness of OD as previously obtained by AFM (0.5-1.5 nm) [24] and SNR or specular neutron reflectivity (1 nm) [25]. It is suggested that the aggregates are composed of many single GOQDs gathered as disc pile up (H-type aggregation) (Fig. S1b, see supporting information) rather than head to tail arrangement (J-type aggregation). Another group has reported that there is a unique emission of graphene quantum dots induced by self-assembled aggregation [26].

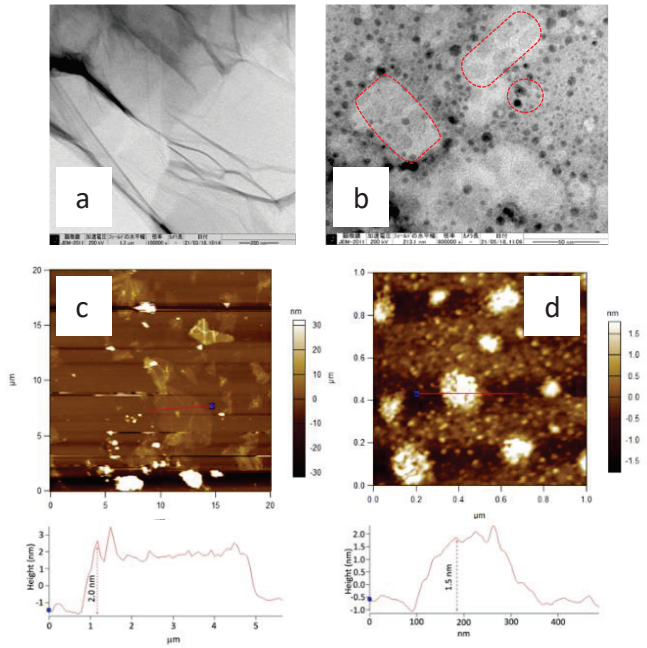

Fig.1. TEM imaging of (a) GO, scale bars: 200 nm, (b) GOQDs, scale bars: 50 nm. (c) AFM image of GO, and (d) GOQDs deposited on freshly cleaved silicon substrate.

3.3.2 Optical properties of GOQDs and their nanocomposite

The optical properties of GOQDs were characterized. UV-Vis absorption spectra (Fig. 2a) show a broad absorption from 800 to 200nm and have one peak at 205nm and two shoulders at 270nm and 330nm for GOQDs. The photoluminescence (PL) spectra (Fig. 2b) show that the different PL peak intensity appeared before (Fig. 2d) and after centrifugation process (Fig. 2e). This method also has been considered by another researcher to achieve the tunable optical properties [27]. In particular, the centrifugation method demonstrated an effective way to decrease the size of functionalized graphene oxide (GO). This is in good accordance with the characterization data shown in an early section (Fig. 1b). The TEM image emphasized a different size of GOQDs. Moreover, in the Fig. S5a (see supporting information), the larger particle has been isolated. It showed

the presence of large sheets, almost similar in size with the as-produced GO (Fig. 1a). As a result, it is expected that as-produced GOQDs have an intrinsic PL intensity. The other experimental studies were reported to identify the disintegration of GO during the base treatment [22]. In their work, the concentration ratio of GO to NaOH, 1:1, was used to treat with heating for 1-5 hours. The results showed that the prolonged base treatment leads to disintegration of the flake of GO into smaller pieces. This work also confirmed that insignificant deoxygenation would proceed if base treatment was conducted without heating. On the contrary, heating without base treatment does not bring in detectable deoxygenation. It is consistent with our result that confirmed the deoxygenation after base treatment with reflux process. As is shown in Fig. S5b (see supporting information), the elemental analysis obtained by TEM shows that the oxygen content decreased significantly.

The photoluminescence (PL) spectra of GOQDs, cesium green (CG) and their nanocomposite in THF solvent were shown in Fig. 2 and Fig. 3. The PL spectra of GOQDs are significantly different between acidic and basic conditions. As is reported by a previous study the GOQDs are strongly sensitive to the deprotonation and protonation

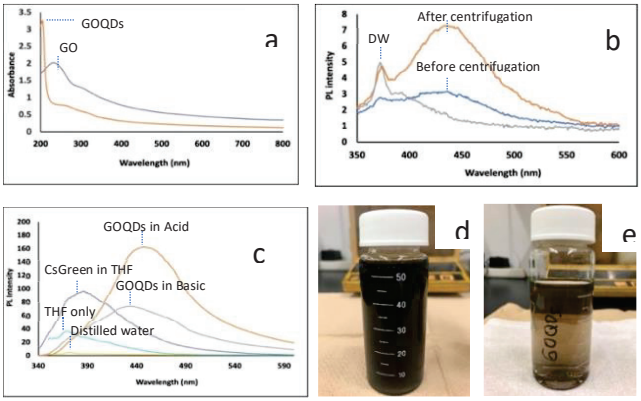

Fig.2. UV-Vis absorbance of (a) GO, GOQDs. Photoluminescence emission spectra of (b) GOQDs before and after centrifugation process, (c) GOQDs in acidic and basic condition, Cesium green in THF. (d) GO solution after reflux process (before centrifugation). (e) GOQDs solution after centrifugation.

process [28]. It is suggested that the different concentration in OH^- and H^+ influences the change of electronic transition of π-π^* and n-π^* in GOQDs. It is also amplified by Taniguchi et al. that the proposed concept of the reversible epoxy formation leads to pH-dependent on/off PL of GO [18]. They found that the enhancing and quenching PL of GO can be induced by increasing/decreasing the epoxy concentration and will be influenced by the

presence of charge transfer exciton (CTE). In the present study, the PL intensity of GOQDs in acidic condition increased compared to that in basic condition. The present result may be explained by pH-dependent change of functional group. The peak also red-shifted from 435nm to 454nm by changing from basic to acidic condition (Fig. 2c).

On the other hand, as shown in Fig. 3, after the nanocomposite was formed, the PL intensity drastically increased in basic condition (pH 11.01) for both nanocomposites (composite-51 and composite-81), while the PL intensity was slightly quenched in acidic condition. In this case, the PL of the nanocomposite exhibited an opposite response for acidic and basic conditions compared with the original sample. For original sample, the GOQDs exhibited enhancing PL intensity in acidic condition and quenching PL intensity in basic condition. Whilst for the nanocomposites, the decreased PL intensity was observed in acidic condition and the increased PL intensity was observed in basic condition. In the other work the GO showed the reversible response upon acidic and basic condition [27]. Fig. 3b shows that the spectrum of the nanocomposite is almost the

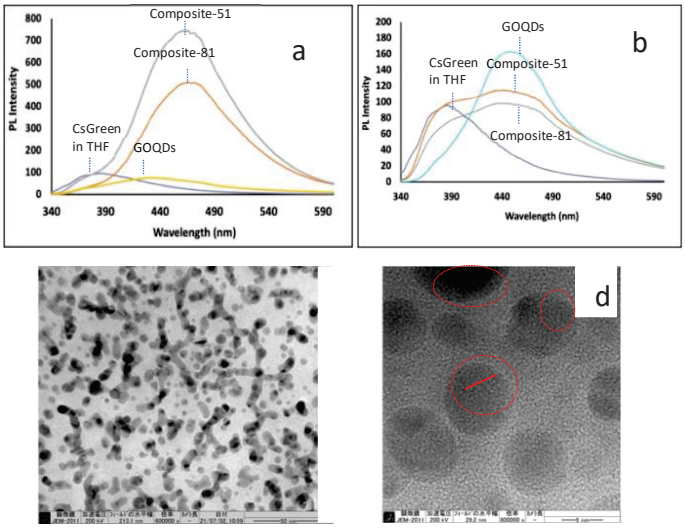

Fig.3. Photoluminescence emission spectra of (a)composite-51, composite-81 in basic condition, (b) composite-51, composite-81 in acidic condition. (c) TEM image of GOQDs-based nanocomposite (composite-81). Scale bars: 50 nm. (d) High-resolution TEM image of individual nanodot (composite-81) labelled by red circle with inset of the Fast Fourier Transform (FFT) from the selected region. Scale bars: 5 nm.

superposition of the GOQDs and CG in acidic condition, suggesting the physical mixture of GOQDs and CG in acidic condition. On the other hand, the PL intensity of the nanocomposite was significantly enhanced under basic condition (Fig. 3a). In basic condition the chemical bond was suggested between GOQDs and CG. This enhancement in basic condition is in accordance with PL of conventional carbon nanodots with edge-

located COH/COOH/C=O groups [30]. In the present experiment, the pH condition was changed from basic condition to acidic condition. Then we also investigated the PL intensity of the nanocomposite from acidic condition to basic condition. As a result, the peak moved back to the original position and the intensity significantly increased (Fig. S13, see supporting information).

As is already reported, the GOQDs-PEG (Polyethylene glycol) interaction exhibited a typical excitation wavelength dependence of the photoluminescence [31], [32]. Fig. 3c, and Figs. S3, S4 (see supporting information) show the TEM image of the present composite. It can be seen that the nanodots are combined. Figure 3d shows high-resolution TEM image of an individual nanodot (composite-81). This indicates high crystallinity (localized in lattice fringes labelled by red circle) of GOQDs after forming a composite. It is also suggested that the cesium green (CG) molecule functionalization of GOQDs does not cause significant damage to the graphene π system.

3.3.3. Cs detection performance

3.3.3.1. Cs detection in acidic condition

The PL response of the nanocomposite to the Cs cation was tested by mixing a nanocomposite solution with an aqueous solution of CsCl. In this experiment, the Cs treatment was carried out in two different pH conditions (acidic and basic condition) of the nanocomposite by adding two concentrations of CsCl (0.12 mmol/L and 0.06 mmol/L). Then, the CsCl addition was conducted in the volume range 200 ◎L-800 ◎L.

The results show that the addition of 0.12 mmol/L cesium chloride (200◎L-800◎L) in acidic condition led to increase the PL intensity gradually (turn ON) by employing composite-51 (Fig. 4a). For composite-81, using similar method with the case of composite-51, the PL intensity was decreased (turn OFF) at the first time of Cs addition (200◎L), and then the PL intensity increased (turn ON) gradually after adding another 200◎L CsCl solution (Fig. 4b). The turn ON PL phenomenon also occurred in composite-81 by reducing the concentration of CsCl (0.06 mmol/L) (Fig. 4c). This might be explained by the fact of composite-81 having much GOQDs part compared with the composite-51. At first GOQDs part reacts with CsCl, leading to the decrease in PL intensity (Fig. 4b) as is observed in GOQDs (Fig. 4d). After that, turn ON occurs as is the case of composite-51.

We also considered that another factor such as structural defect (holes) effect might contribute to the PL phenomenon. The presence of holes in nm-size was investigated in HRTEM studies of GO [33]. Another researcher also considered these tiny vacancy defect

as a part of the oxidized domains [34]. As is explained previously, during the base-treatment the functional groups have been reduced (deoxygenation) from π surface and disintegration of the flake of GO occurred. In this situation, it can be predicted that numerous additional defects were formed. In the present study the evidence of the structural change was shown through the Zeta potential value change (from -19.67 mV for GO to -34.63 mV for GOQDs). As a result, these defects can serve as a trap or binding point since the functional groups (especially the carbonyls) likely exist along the edges of the holes [35]. Subsequently, a TEM measurement was performed to consider the adsorption behaviour of Cs by nanocomposite. The information obtained from the TEM image (Fig. 5a) confirmed the small black spots. It is considered as Cs cluster on the nanocomposite layer by using its eds (Fig. 5b). This might be related to the GO acidity. Our previous work presented that the different C/O ratio of GO (different in degree of oxidation) has significant aspect in producing the diversification of sp^2/sp^3 carbon cluster of GO and influenced the Cs adsorption performance [10]. Another study also authenticated that the oxidation debris (OD) has an important role in GO acidity [36]. The study also proved that the amount of acid site density of OD is almost 3 times higher than that of GO. As we considered in the early section of the present study GOQDs are termed as the small size of OD produced by reflux process (with base treatment). A chemical

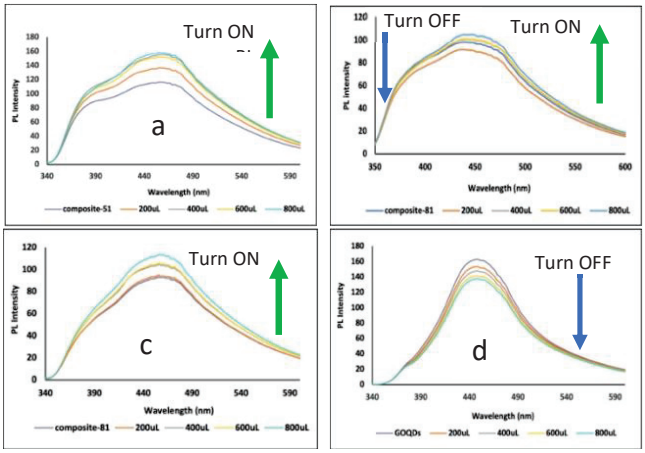

Fig.4. Photoluminescence emission spectra of (a) composite-51 before and after Cs treatment for 0.12 mmol/L (in acidic condition), (b, c) composite-81 before and after Cs treatment for 0.12 mmol/L and 0.06 mmol/L (in acidic condition), (d) GOQDs after and before Cs treatment for 0.12 mmol/L (in acidic condition). A colour line (graphic) in each figure indicate the PL response signal by the additional amount of CsCl solution, with volume range 200 µL (orange), 400 µL (gray), 600 µL (yellow), and 800 µL (blue).

analysis by TEM (Fig. 5d) revealed that Cs rich structure is the main constituent along with other species (C, O, Na, Cl). However, it might include the undesired impurities (Si,

Na, K, S) as revealed in Fig. 5 (b). Si and K might come from the re-used laboratory glassware as a source. In addition, the remaining Na is originated from a part of NaOH addition during the base-treatment. Specifically, we assumed that the formation of Cs cluster is produced as a part of the moiré fringe pattern formation (Fig. 5c) mechanism. It was verified as a consequence of the decomposition process of the adatoms nanoparticle under electron beam irradiation [37]. Nakashima`s group also reported the CsCl and Cs rich particle formation depending on the substrate concentration and the solvent [38]. Further discussion is presented based on several phenomena in the section 3.3.4 regarding the Cs metal formation on GOQDs and nanocomposite layer.

However, as is shown in Fig. 4d, there is no PL enhancement (turn OFF) after 0.12 mmol/L CsCl solution addition by employing original GOQDs solution, and also quenching occurred in basic condition (Fig. 6a). This is due to the interaction between GOQDs and Cs^{+}. Some researchers have proved that the fluorescence-quenching phenomenon occurred after addition of metal and nanoparticles like Fe^{3+} ions in GO solution and unbonded gold nanoparticles (NPs) to graphene quantum dots [39], [40]. Typically, GO and GOQDs can act as both an attractive fluorophores and remarkable

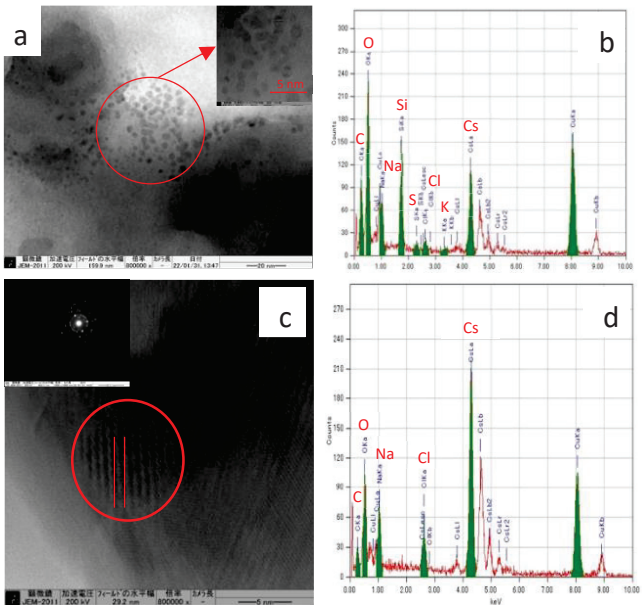

Fig.5. (a) TEM image of composite-81 after Cs treatment (in acidic condition), small black spots are identified with inset of HRTEM from the selected area. Scale bars: 20 nm. (b) Elemental analysis of figure a. (c) HRTEM image of composite-51 after Cs treatment (in acid condition) with inset of the Fast Fourier Transform (FFT) from the selected region. Scale bars: 5 nm. (d) Elemental analysis of figure c.

quencher [41]. As enhancing agent, the fluorophores can serve the tunable PL emission and in contrary, as quencher, the GO and GOQDs revealed an effective quenching efficiency through either electron transfer or fluorescence resonance energy transfer (FRET) mechanism.

It can be thought that the surface charge has a significant role in the PL of GOQDs when interacted with Cs cation. As is already shown, Zeta potential was -34.63 mV for GOQDs and -19.67 mV for GO in the present study. The surface of GOQDs is more negative than that of GO. In addition, since the GOQDs still have an oxygen functional group, it can be assumed that the interaction between Cs cation and -COOH has induced PL quenching in the detection system. Another possibility is the -OH on the surface area can coordinate to Cs cation. Previous study has proposed the concept of dynamic structural model of GO responsible for binding metal ions [42]. Particularly, the dynamic structural model is well supported by the conversion process from vicinal diols (formed by opening the epoxides) to enols as the structural transformation of the functional groups led to enols being acidic. The other researcher has revealed the reversible epoxy formation [18]. More current work also strongly suggested a possibility that the other functional groups (not only carboxyl) have played a significant role for binding to metal ions [43]. The as-formed enols as the product resulted from reorganization of GO structure might serve as a chelating agent for the metal cations.

3.3.3.2. Cs detection in basic condition

The significant PL quenching was observed in the Cs detection performance in basic condition. As shown in Fig. 6, the PL intensity of all samples decreased gradually after Cs treatment with different concentration, 0.12 mmol/L and 0.06 mmol/L (200㎕L-800㎕L Cs addition). This quenching phenomenon was clearly different from Cs treatment in acidic condition that shows enhancing phenomenon. It can be seen in the Fig. 6 (b), (c), (d) that no change at 380nm and large change at 470nm. Unlike in acidic condition, the carboxylic acid groups are present as $–COO^-$ and the surface of GOQDs plane is negatively charged in basic condition. It is also well known that many metal ions can act as a PL quencher in several ways such as the effect of complexation, fluorescence resonance energy transfer, or charge transfer. The previous work emphasized that the quenching reaction can be considered as a longer or shorter distance effect between donor and acceptor molecules [44], [45]. Furthermore, another study confirmed that in strong basic condition, GO has a greater interaction for binding metal, which is provoked by a surface modification of GO structure [46].

In the present study, the modification of GO structure was induced by a chemical reaction through the base-treatment followed by the reflux process. And as-obtained pH value of GOQDs solution was 11.60. As was suggested by A. M. Dimiev et al. the base-treatment of aqueous GO solution led to hydrolysis of organic sulfates and trigger the reaction and cause a C-C bond cleavage with formation of ketone at the new edge. Then, the ketones further transform into carboxylates [22]. The other observation additionally convinced that the negatively charged GO as a ligand can replace water molecule from the first coordination sphere of metal [34]. Therefore, the oxygen functional group of GOQDs dominantly plays a significant role (activated) for Cs detection as its natural environment even after forming the nanocomposite. The TEM image (Fig. S6 (a, c), see supporting information) was taken and the interaction between Cs cation and nanocomposite shows a similar tendency with the previous section (in acidic condition), and the CsCl and Cs clusters were observed.

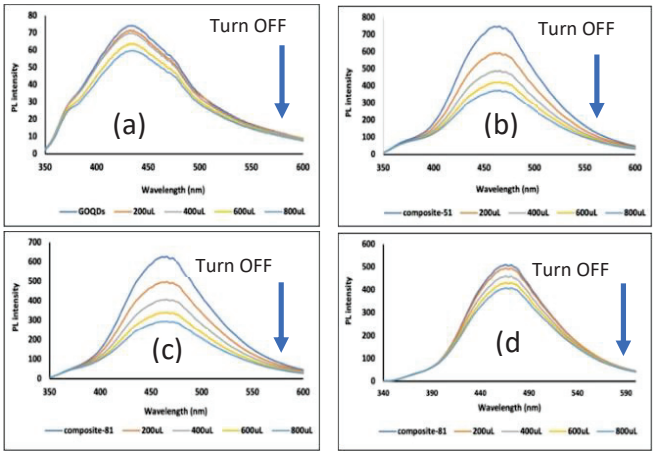

Fig.6. PL emission spectra of (a) GOQDs before and after Cs treatment for 0.12 mmol/L (in basic condition), (b) PL emission spectra of composite-51 before and after Cs treatment for 0.12 mmol/L (in basic condition), (c, d) PL emission spectra of composite-81 before and after Cs treatment for 0.12 mmol/L and 0.06 mmol/L, respectively (in basic condition). A colour line (graphic) in each figure indicate the PL response signal by the additional amount of CsCl solution, with volume range 200 μL (orange), 400 μL (gray), 600 μL (yellow), and 800 μL (blue).

3.3.3.3. The detection behaviour of Sr^{2+}, K^{+}

For comparison, the effect of the other cation addition was investigated. Under similar conditions to the Cs^{+} treatment, the Sr^{2+} and K^{+} treatment was performed in acidic and basic conditions by using a composites solution. In acidic condition, as exhibited in Fig. 7 (a, b), the addition of KCl solution (from 200uL-800uL) shows a decrease in PL intensity (turn OFF). However, in the case of Sr^{2+} treatment, the PL intensity increased (turn ON) for the first 200uL $SrCl_2$ addition both in composite-51 and composite-81, and then, the

PL intensity decreased (turn OFF) gradually after adding another 200uL $SrCl_2$ solution (Fig. 8 (a, b)).

Moreover, under basic conditions, the presence of K^+ and Sr^{2+} in the composite solutions exhibited a similar quenching phenomenon (Fig. 7 (c, d) and Fig. 8 (c, d)).

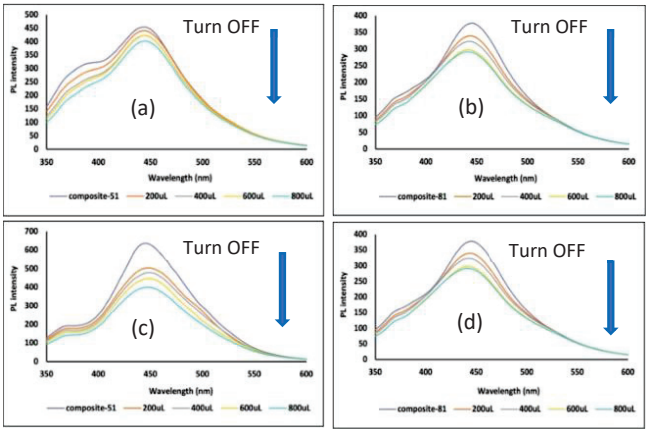

Fig.7. PL emission spectra of (a) composite-51 before and after K^+ treatment for 0.12 mmol/L (in acidic condition), (b) composite-81 before and after K^+ treatment for 0.12 mmol/L (in acid condition), (c) composite-51 before and after K^+ treatment for 0.12 mmol/L (in basic condition), (d) composite-81 before and after K^+ treatment for 0.12 mmol/L (in basic condition). A colour line (graphic) in each figure indicate the PL response signal by the additional amount of KCl solution, with volume range 200 µL (orange), 400 µL (gray), 600 µL (yellow), and 800 µL (blue).

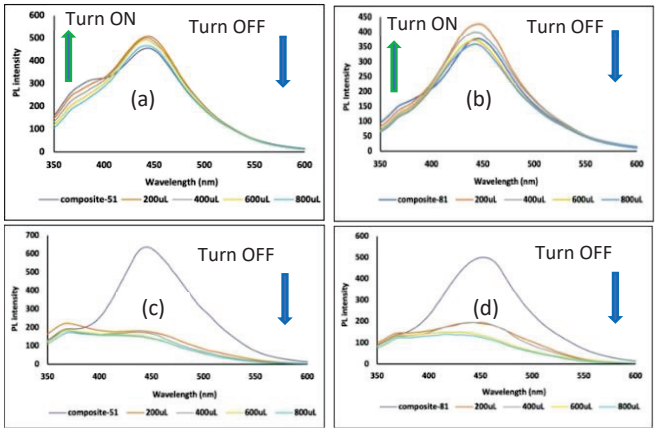

Fig.8. PL emission spectra of (a) composite-51 before and after Sr^{2+} treatment for 0.12 mmol/L (in acidic condition), (b) composite-81 before and after Sr^{2+} treatment for 0.12 mmol/L (in acidic condition), (c) composite-51 before and after Sr^{2+} treatment for 0.12 mmol/L (in basic condition), (d) composite-81 before and after Sr^{2+} treatment for 0.12 mmol/L (in basic condition). A colour line (graphic) in each figure indicate the PL response signal by the additional amount of $SrCl_2$ solution, with volume range 200 µL (orange), 400 µL (gray), 600 µL (yellow), and 800 µL (blue).

Especially for Sr^{2+} treatment, the quenching phenomenon occurred drastically in the first 200uL $SrCl_2$ addition. It might be caused by the Sr^{2+} having a higher 2+ charge to form coordination compounds. The precipitation was directly observed after the Sr^{2+} addition, which is the cause of drastic decrease in PL. These observations suggested that the nanocomposite in this experiment has a different selectivity and sensitivity to the target metal ions (Cs^+, Sr^{2+}, K^+). This feature is an important factor for the detection system. As is expected, the nanocomposite is more sensitive to the Cs^+ by enhancing the PL intensity (turn ON) in acidic conditions compared to other metal cation (Sr^{2+}, K^+). The result also indicated that the nanocomposite can be used as a promising Sr detection candidate, and future investigation is required.

The interaction among GOQDs, cesium green molecule, and some different metal cations indicated a different PL response signal as displayed in the table S1, see supporting information. The input-output detection mechanism was constructed to identify the PL response signal in different pH conditions as applied in the previous work [20]. Here, the different metal cations and cesium green molecule are used as input factor, and the presence of the input factor is represented by `1` and `0` for the absence of the input factor. In addition, as output factor, `1` represents the turn ON PL, and `0` represents the turn OFF PL. In acidic condition, the result shows that, when the input factor is (0, 0), (1, 1) both for Cs^+ and Sr^{2+} treatment, the PL response signal turns ON, therefore the output is `1`. This tendency was confirmed by using composite-51 and composite-81. On the other hand, the output is `0` for K^+ treatment by applying (1, 1) as input factor. A similar phenomenon was observed in the basic condition, i.e., the output is `1` when the input factor (0, 1) was applied but was not found in the acidic condition both for composite-51 and composite-81. Furthermore, the quenching phenomenon appeared in all input factor (0, 0), (1, 1) in basic condition. Therefore, these results concluded that the presence of different metal cations will activate a different PL response signal. It is also influenced by the pH condition and the addition of cesium green molecule in the system.

3.3.3.4. Cs metal formation on GOQDs and nanocomposite layer

An unexpected phenomenon was observed during the TEM measurement. By using a composite sample, the movement of particle or rearrangement of structure was observed in composite-51 (acidic condition), refer to supporting information, Video S15.1. It can be attributed to crystal movement between locations or rotation around axis during the electron beam exposure [37]. The effect of electron beam was considered as a possible

reason for the mobility of the particle during the scanning process [47]. Thus, a moiré fringe pattern under electron beam exposure was formed (red line (Fig. 5c). As theoretically proved, the moiré fringe pattern was formed when crystalline surfaces with a lattice mismatch or a rotational misorientation are vertically stacked [48]. It also corresponded to the crystalline conductive area of small sp^2 domains [49]. In the present study, the lattice size of composite-51 after Cs treatment is 0.39 nm, and the lattice size of GOQDs after Cs treatment is 0.31 nm (This corresponds to (200) of Cs metal.) (Fig. S7, see supporting information). It has a larger lattice-size compared with the as obtained-nanocomposite before Cs treatment (Fig. 3d) and original GO sample, 0.21 nm (Fig. S8, see supporting information). This value (for GO sample) is aligned with previously observed value [50].

Moreover, this phenomenon might be influenced by the role of cesium green (CG) molecule that led to enhance the properties of the nanocomposite. It is correlated well with other phenomena that have been proved by using aromatic molecules (which are non-covalently bound to 2D material), which affected the electronic properties of the 2D materials significantly [51]. This also confirmed that the moiré superlattices have arisen in bilayer graphene. It was strengthened by other researchers that the PL of GO was attributed to the electronic energy transition [52], and theoretically proposed by speculating the effect of the different oxidation levels of GO [53]. Their calculation analysis also showed that hydroxyl and epoxy groups have a responsibility for the change of hybridization of sp^2 to sp^3. In the present study, a similar behaviour (the adatoms movement) was observed in Figure S6 (a), (b), for composite-81 after Cs treatment (in basic condition) by the HRTEM image (refer to supporting information, Video S15.2, S15.3). It is also amplified by other researchers who theoretically suggested that the formation of CsI (cluster shape) was assigned based on the number of atom or ion [54]. For example, a four-ion cluster and a six-ion cluster of CsI were supposed to have a square planar structure and to form planar hexagon sequentially. It is consistent with our result (Fig. 5 (c), S7 see supporting information) as discussed in the previous section, which predicted the interaction between CsCl and the nanocomposite layer generates a moiré fringe pattern under electron beam irradiation. It can be explained that two or more crystals are overlapping with slightly different orientation.

To understand the present phenomenon, the mechanism of the moiré fringe pattern formation should be considered together with

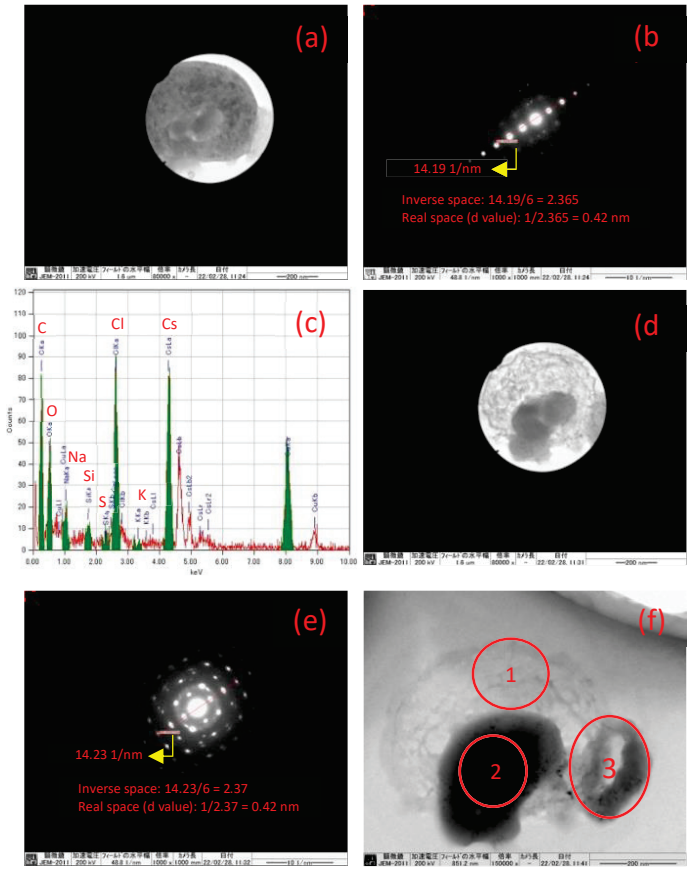

Fig.9. TEM image of GOQDs after Cs treatment in basic condition (a) soon after TEM measurement was conducted. Scale bars: 200 nm. (b) Fast Fourier Transform (FFT) to figure a. (c) Elemental analysis of figure a. (d) After electron beam irradiation was applied for the second time. Scale bars: 200 nm. (e) Fast Fourier Transform (FFT) to figure d. (f) Specific spot area of the observed sample of figure d. Scale bars: 200 nm.

the formation of two-dimensional nanocrystal on the substrate layer, as is observed in the previous work [37]. Therefore, another phenomenon is worth mentioning. Through the electron microscopy characterization by using GOQDs sample after Cs treatment (in acidic and basic condition), the crystal structure transformation was observed. The results demonstrated the different phenomenon between acidic and basic conditions. In acidic condition, as shown in Fig. S9 (see supporting information), the crystal structure has changed from single crystals to amorphous form (Fig. S10, see supporting information). The FFT of Figure S9 (c) is provided in Figure S9 (d), where (110) reflections of CsCl are observed at 0.29 nm. In Fig. S9 (b), the elemental analysis revealed that the Cs and Cl are strongly detected. On the other hand, Cl content decreased (Fig. S10(b)), but still remained after electron beam exposure. Furthermore, in basic condition, the crystal

transformation was also recorded by TEM. As shown in Fig. 9, the sample was further identified. Soon after TEM measurement the observed crystal formation was recorded (Fig. 9(b)). Continuously, the prolonged electron beam irradiation was applied to confirm the stability of the sample. In contrast to the Fig. 9(a), the TEM image exhibited a different morphology (Fig. 9(d)) and different crystal formation (Fig. 9(e)). Following these observations, we evaluated the FFT of Fig. 9 (b) and Fig. 9 (e), where (100) reflection of CsCl at 0.42 nm has similarity for both crystal formations. The observed sample was distinguished in three different investigated areas (Fig. 9 (f)). It was found that there are three different types of crystal formation as depicted in Fig. S11 (a, c, e). These findings suggest that the characterization of the nature of the active sites of the graphene layers has an essential aspect to promote different reactions [55]. Also, it is well known theoretically that the active site is not uniformly found over the surface area. Other literature obviously investigated that the catalytic activity of GO is affected by the acid and base addition [56]. We predicted that several impurities (chemical contaminations) are determined by the chemical analysis (Fig. S11 (b, d, f)). Interestingly, if compared with basic condition, the Cl content was significantly decreased in acidic condition.

Our speculation is that the crystal formation phenomenon might be established on the substrate layers of GOQDs in three continuous steps. The first step is the decomposition of CsCl nanoparticles under prolonged electron beam exposure (see supporting information, Video S15.4). From this process, the Cs rich cluster (or residual Cs and Cl adatoms) is formed. The second step is the rearrangement process of residual Cs and Cl atoms to form a two-dimensional nanocrystal (Fig. 9 (b, e)). The motion of adatoms (adsorbed Cs and Cl atoms) is a reasonable explanation. The consequence of the electron beam effect (200 kV) causes the bond breakage of the nanocomposite layer. This phenomenon was clearly observed (the layer was broken then moved around/rotated) in GOQDs sample after Cs treatment (in basic condition), refer to supporting information, Video S15.5. This makes the movement of atom on the basal plane be easily accelerated, even though the restoration of the graphitic layer is possible due to the remaining functionalities [35]. This is also found in the present work (refer to supporting information, Fig. S12, Video S15.6). The interaction of electron beam with the GOQDs surface after Cs treatment in acidic condition led to the GOQDs layer being reorganized. The third step is that the interaction between a two-dimensional nanocrystal and the graphitic layer produces the moiré fringe pattern formation (see supporting information, Fig. S7 (a, b)). Therefore, the unveiling moiré fringe pattern

formation has an important role to understand the electronic properties of graphene [57]. Thus, it can significantly influence the PL phenomena (turn ON response) after Cs treatment in acidic condition.

Additionally, the present experiments also indicated the formation of Cs metal (cluster). It should be noted, however, that more effort is still necessary to get strong evidence and also to open the understanding of the role of oxygen functional group and the various defects that act as an active site of the GOQDs for Cs metal formation.

Moreover, since the GOQDs and nanocomposite still include Na originated from NaOH addition during the reflux process (see Fig. S3 (A3), S4 (A3), supporting information), the presence of Na cation can be considered as a part of the process of two dimensional Cs nanocrystal formation via charge transfer between Na atom and aromatic rings of the graphene layer [58]. However, in the present work, the overall mechanism process is complex, and it is influenced by many conditions such as the composition of the nanocomposite, the pH, the concentration of CsCl, and the solvent. Therefore, this result suggests that the observed cluster was formed because of the migration effect of the adatoms on nanocomposite layer (specifically trapped to defect site in the graphene lattice) and transformation of the local adsorption environment induced by electron beam exposure.

Conclusions

The nanocomposite was effectively fabricated by functionalized GOQDs and cesium green molecule in mixed solution (Distilled water/THF). Until now, no study has investigated the development of the application of cesium green (CG) molecule for Cs detection in aqueous solution. In the present study we showed that as-produced nanocomposite can be essentially used to recognize the presence of Cs cation in the aqueous solution both in acidic condition and basic condition with turn ON/OFF photoluminescence (PL) response. There are several important keys that solved in the present paper. (1) The unique properties of GOQDs (pH dependent) have a dual role as an enhancer and quencher in composite in the presence of Cs cation. In acidic condition, the PL behaviour shows turn ON the PL after detecting the Cs cation. On the contrary, the turn OFF PL occurred in basic condition. (2) Cesium green molecule can be used as Cs cation detection material not only in solid state (as previous works reported) but also in aqueous mixed solution. (3) Cesium green molecule can work effectively in basic and acidic condition. (4) The co-solvent application in the nanocomposite system might have

a contribution to the Cs detection process. (5) The nanocomposites are more sensitive as Cs detection (turn ON) compared to other metal like Sr and K in acid condition. (6) The Cs cluster was formed under electron beam irradiation as consequence of adatom mobility on the substrate layer. In this phenomenon, the pH condition of the nanocomposite system has an important key in the PL response in mixed solvent. In particular, for the sensitivity and the accuracy of the nanocomposite system further investigation is needed, since GO structure as precursor material has different local arrangement of functional group from one batch to the other. Also, it is expected that this work as an initial stage of GOQDs-cesium green molecule research offers a new chemical pathway and widely increases the application in environmental protection with more deep investigation.

References

[1] T. J. Yasunari, A. Stohl, R. S. Hayano, J. F. Burkhart, S. Eckhardt, and T. Yasunari, "Cesium-137 deposition and contamination of Japanese soils due to the Fukushima nuclear accident," *Proc. Natl. Acad. Sci. U. S. A.*, vol. 108, no. 49, pp. 19530–19534, 2011, doi: 10.1073/pnas.1112058108.

[2] T. Basuki, S. Miyashita, M. Tsujimoto, and S. Nakashima, "Deposition density of 134Cs and 137Cs and particle size distribution of soil and sediment profile in Hibara Lake area, Fukushima: an investigation of 134Cs and 137Cs indirect deposition into lake from surrounding area," *J. Radioanal. Nucl. Chem.*, vol. 316, no. 3, pp. 1039–1046, 2018, doi: 10.1007/s10967-018-5809-1.

[3] M. TSUJIMOTO, S. MIYASHITA, H. T. NGUYEN, and S. NAKASHIMA, "Monthly Change in Radioactivity Concentration of ^{137}Cs, ^{134}Cs, and ^{40}K of Paddy Soil and Rice Plants in Fukushima Prefecture," *Radiat. Saf. Manag.*, vol. 19, no. 0, pp. 10–22, 2020, doi: 10.12950/rsm.181219.

[4] K. Shizuma, Y. Fujikawa, M. Kurihara, and Y. Sakurai, "Identification and temporal decrease of 137Cs and 134Cs in groundwater in Minami-Soma City following the accident at the Fukushima Dai-ichi nuclear power plant," *Environ. Pollut.*, vol. 234, pp. 1–8, 2018, doi: 10.1016/j.envpol.2017.11.018.

[5] B. Radaram, T. Mako, and M. Levine, "Sensitive and selective detection of cesium via fluorescence quenching," *Dalt. Trans.*, vol. 42, no. 46, pp. 16276–16278, 2013, doi: 10.1039/c3dt52215f.

[6] T. Mori *et al.*, "Micrometer-level naked-eye detection of caesium particulates in the solid state," *Sci. Technol. Adv. Mater.*, vol. 14, no. 1, 2013, doi: 10.1088/1468-6996/14/1/015002.

[7] M. Achermann, M. A. Petruska, S. Kos, D. L. Smith, D. D. Koleske, and V. I. Klimov, "Energy-transfer pumping of semiconductor nanocrystals using an epitaxial quantum well," *Nature*, vol. 429, no. 6992, pp. 642–646, 2004, doi: 10.1038/nature02571.

[8] C. Sönnichsen, B. M. Reinhard, J. Liphardt, and A. P. Alivisatos, "A molecular ruler based on plasmon coupling of single gold and silver nanoparticles," *Nat. Biotechnol.*, vol. 23, no. 6, pp. 741–745, 2005, doi: 10.1038/nbt1100.

[9] M. Akamatsu *et al.*, "Intracellular imaging of cesium distribution in Arabidopsis using cesium green," *ACS Appl. Mater. Interfaces*, vol. 6, no. 11, pp. 8208–8211, 2014, doi: 10.1021/am5009453.

[10] B. S. Nugroho *et al.*, "Exploration of the Cs Trapping Phenomenon by Combining Graphene Oxide with K6P2W18O62 As nanocomposite," *Materials (Basel).*, vol. 14, no. 19, p. 5577, 2021, doi: 10.3390/ma14195577.

[11] B. S. Nugroho, M. N. K. Wihadi, F. Grote, S. Eigler, and S. Nakashima, "Potentiality of graphene oxide and polyoxometalate as radionuclides adsorbent to restore the

environment after fukushima disaster: A mini review," *Indones. J. Chem.*, vol. 21, no. 3, pp. 776–786, 2021, doi: 10.22146/ijc.60493.
[12] N. Fuyuno *et al.*, "Drastic Change in Photoluminescence Properties of Graphene Quantum Dots by Chromatographic Separation," *Adv. Opt. Mater.*, vol. 2, no. 10, pp. 983–989, 2014, doi: 10.1002/adom.201400200.
[13] D. Kozawa *et al.*, "Excitonic photoluminescence from nanodisc states in graphene oxides," *J. Phys. Chem. Lett.*, vol. 5, no. 10, pp. 1754–1759, 2014, doi: 10.1021/jz500516u.
[14] L. Gao, L. Ju, and H. Cui, "Chemiluminescent and fluorescent dual-signal graphene quantum dots and their application in pesticide sensing arrays," *J. Mater. Chem. C*, vol. 5, no. 31, pp. 7753–7758, 2017, doi: 10.1039/c7tc01658a.
[15] X. Fang *et al.*, "Graphene quantum dot incorporated perovskite films: Passivating grain boundaries and facilitating electron extraction," *Phys. Chem. Chem. Phys.*, vol. 19, no. 8, pp. 6057–6063, 2017, doi: 10.1039/c6cp06953c.
[16] ahmadzia sherzad, hakimeh zare, zahra shahedi, F. Ostovari, Y. Fazaeli, and Z. Pourghobadi, "Effect of pH on Optical Properties of Graphene Oxide Quantum Dots," *Int. J. Opt. Photonics*, vol. 14, no. 2, pp. 135–142, 2020, doi: 10.52547/ijop.14.2.135.
[17] J. L. Chen and X. P. Yan, "Ionic strength and pH reversible response of visible and near-infrared fluorescence of graphene oxide nanosheets for monitoring the extracellular pH," *Chem. Commun.*, vol. 47, no. 11, pp. 3135–3137, 2011, doi: 10.1039/c0cc03999c.
[18] T. Taniguchi *et al.*, "PH-driven, reversible epoxy ring opening/closing in graphene oxide," *Carbon N. Y.*, vol. 84, no. 1, pp. 560–566, 2015, doi: 10.1016/j.carbon.2014.12.054.
[19] Y. Dong *et al.*, "One-step and high yield simultaneous preparation of single- and multi-layer graphene quantum dots from CX-72 carbon black," *J. Mater. Chem.*, vol. 22, no. 18, pp. 8764–8766, 2012, doi: 10.1039/c2jm30658a.
[20] J. Yao and L. Wang, "switching : mechanism and molecular logic gate," 2021, doi: 10.1039/d1nj01908b.
[21] W. S. Hummers and R. E. Offeman, "Preparation of Graphitic Oxide," *J. Am. Chem. Soc.*, vol. 80, no. 6, p. 1339, 1958, doi: 10.1021/ja01539a017.
[22] A. M. Dimiev and T. A. Polson, "Contesting the two-component structural model of graphene oxide and reexamining the chemistry of graphene oxide in basic media," *Carbon N. Y.*, vol. 93, pp. 544–554, 2015, doi: 10.1016/j.carbon.2015.05.058.
[23] J. P. Rourke *et al.*, "The real graphene oxide revealed: Stripping the oxidative debris from the graphene-like sheets," *Angew. Chemie - Int. Ed.*, vol. 50, no. 14, pp. 3173–3177, 2011, doi: 10.1002/anie.201007520.
[24] X. Chen and B. Chen, "Direct Observation, Molecular Structure, and Location of Oxidation Debris on Graphene Oxide Nanosheets," *Environ. Sci. Technol.*, vol. 50,

no. 16, pp. 8568–8577, 2016, doi: 10.1021/acs.est.6b01020.
[25] D. López-DÍaz, M. D. Merchán, M. M. Velázquez, and A. Maestro, "Understanding the Role of Oxidative Debris on the Structure of Graphene Oxide Films at the Air-Water Interface: A Neutron Reflectivity Study," *ACS Appl. Mater. Interfaces*, vol. 12, no. 22, pp. 25453–25463, 2020, doi: 10.1021/acsami.0c05649.
[26] S. Chen, J. W. Liu, M. L. Chen, X. W. Chen, and J. H. Wang, "Unusual emission transformation of graphene quantum dots induced by self-assembled aggregation," *Chem. Commun.*, vol. 48, no. 61, pp. 7637–7639, 2012, doi: 10.1039/c2cc32984k.
[27] J. Wei and J. Qiu, "Tunable optical properties of graphene quantum dots by centrifugation," *ASME Int. Mech. Eng. Congr. Expo. Proc.*, vol. 15, no. November 2013, 2013, doi: 10.1115/IMECE2013-64756.
[28] D. Pan, J. Zhang, Z. Li, and M. Wu, "Hydrothermal route for cutting graphene sheets into blue-luminescent graphene quantum dots," *Adv. Mater.*, vol. 22, no. 6, pp. 734–738, 2010, doi: 10.1002/adma.200902825.
[29] S. Kochmann, T. Hirsch, and O. S. Wolfbeis, "The pH dependence of the total fluorescence of graphite oxide," *J. Fluoresc.*, vol. 22, no. 3, pp. 849–855, 2012, doi: 10.1007/s10895-011-1019-8.
[30] D. Pan, J. Zhang, Z. Li, C. Wu, X. Yan, and M. Wu, "Observation of pH-, solvent-, spin-, and excitation-dependent blue photoluminescence from carbon nanoparticles," *Chem. Commun.*, vol. 46, no. 21, pp. 3681–3683, 2010, doi: 10.1039/c000114g.
[31] Z. Wang *et al.*, "Synthesis of strongly green-photoluminescent graphene quantum dots for drug carrier," *Colloids Surfaces B Biointerfaces*, vol. 112, pp. 192–196, 2013, doi: 10.1016/j.colsurfb.2013.07.025.
[32] Y. Lou *et al.*, "Cane Molasses Graphene Quantum Dots Passivated by PEG Functionalization for Detection of Metal Ions," *ACS Omega*, vol. 5, no. 12, pp. 6763–6772, 2020, doi: 10.1021/acsomega.0c00098.
[33] F. Grote, C. Gruber, F. Börrnert, U. Kaiser, and S. Eigler, "Thermal Disproportionation of Oxo-Functionalized Graphene," *Angew. Chemie - Int. Ed.*, vol. 56, no. 31, pp. 9222–9225, 2017, doi: 10.1002/anie.201704419.
[34] R. R. Amirov, J. Shayimova, Z. Nasirova, A. Solodov, and A. M. Dimiev, "Analysis of competitive binding of several metal cations by graphene oxide reveals the quantity and spatial distribution of carboxyl groups on its surface," *Phys. Chem. Chem. Phys.*, vol. 20, no. 4, pp. 2320–2329, 2018, doi: 10.1039/c7cp07055a.
[35] K. Erickson, R. Erni, Z. Lee, N. Alem, W. Gannett, and A. Zettl, "Determination of the local chemical structure of graphene oxide and reduced graphene oxide," *Adv. Mater.*, vol. 22, no. 40, pp. 4467–4472, 2010, doi: 10.1002/adma.201000732.
[36] J. Zhang, C. Xiong, Y. Li, H. Tang, X. Meng, and W. Zhu, "The critical contribution of oxidation debris on the acidic properties of graphene oxide in an aqueous solution," *J. Hazard. Mater.*, vol. 402, no. July 2020, p. 123552, 2021, doi:

10.1016/j.jhazmat.2020.123552.
[37] N. Vats *et al.*, "Substrate-Selective Morphology of Cesium Iodide Clusters on Graphene," *ACS Nano*, vol. 14, no. 4, pp. 4626–4635, 2020, doi: 10.1021/acsnano.9b10053.
[38] T. Basuki and S. Nakashima, "Cs Adsorption and CsCl Particle Formation Facilitated by Amino Talc-like Clay in Aqueous Solutions at Room Temperature," *ACS Omega*, vol. 6, no. 40, pp. 26026–26034, 2021, doi: 10.1021/acsomega.1c02975.
[39] T. K. Mandal, Y. Hou, Z. Y. Gao, H. Ning, W. S. Yang, and M. Y. Gao, "Graphene oxide-based sensor for ultrasensitive visual detection of fluoride," *Adv. Sci.*, vol. 3, no. 12, pp. 1–6, 2016, doi: 10.1002/advs.201600217.
[40] Y. Liu, W. Q. Loh, A. Ananthanarayanan, C. Yang, P. Chen, and C. Xu, "Fluorescence quenching between unbonded graphene quantum dots and gold nanoparticles upon simple mixing," *RSC Adv.*, vol. 4, no. 67, pp. 35673–35677, 2014, doi: 10.1039/c4ra06408a.
[41] P. Zheng and N. Wu, "Fluorescence and Sensing Applications of Graphene Oxide and Graphene Quantum Dots: A Review," *Chem. - An Asian J.*, vol. 12, no. 18, pp. 2343–2353, 2017, doi: 10.1002/asia.201700814.
[42] A. M. Dimiev, L. B. Alemany, and J. M. Tour, "Graphene oxide. Origin of acidity, its instability in water, and a new dynamic structural model," *ACS Nano*, vol. 7, no. 1, pp. 576–588, 2013, doi: 10.1021/nn3047378.
[43] J. Shayimova, R. R. Amirov, A. Iakunkov, A. Talyzin, and A. M. Dimiev, "Carboxyl groups do not play the major role in binding metal cations by graphene oxide," *Phys. Chem. Chem. Phys.*, vol. 23, no. 32, pp. 17430–17439, 2021, doi: 10.1039/d1cp01734a.
[44] H. Dong, W. Gao, F. Yan, H. Ji, and H. Ju, "Fluorescence resonance energy transfer between quantum dots and graphene oxide for sensing biomolecules," *Anal. Chem.*, vol. 82, no. 13, pp. 5511–5517, 2010, doi: 10.1021/ac100852z.
[45] R. S. Swathi and K. L. Sebastian, "Long range resonance energy transfer from a dye molecule to graphene has (distance)-4 dependence," *J. Chem. Phys.*, vol. 130, no. 8, 2009, doi: 10.1063/1.3077292.
[46] V. S. Talanov, G. G. Talanova, and K. B. Yatsimiskii, "New sulfur-containing derivatives of graphite oxide for use in fixing silver(I) ions," *Icassp*, vol. 21, no. 3, pp. 295–316, 1997.
[47] T. P. Hardcastle *et al.*, "Mobile metal adatoms on single layer, bilayer, and trilayer graphene: An ab initio DFT study with van der Waals corrections correlated with electron microscopy data," *Phys. Rev. B - Condens. Matter Mater. Phys.*, vol. 87, no. 19, pp. 1–16, 2013, doi: 10.1103/PhysRevB.87.195430.
[48] Z. Zou, "Unveiling the Formation of Graphene Moiré Patterns on Fourfold-Symmetric Supports: Geometrical Insight," *J. Phys. Chem. C*, vol. 125, no. 41, pp. 22705–22712, 2021, doi: 10.1021/acs.jpcc.1c03991.

[49] C. T. Chien *et al.*, "Tunable photoluminescence from graphene oxide," *Angew. Chemie - Int. Ed.*, vol. 51, no. 27, pp. 6662–6666, 2012, doi: 10.1002/anie.201200474.
[50] T. Tsugawa, K. Hatakeyama, J. Matsuda, M. Koinuma, and S. Ida, "Synthesis of oxygen functional group-controlled monolayer graphene oxide," *Bull. Chem. Soc. Jpn.*, vol. 94, no. 9, pp. 2195–2201, 2021, doi: 10.1246/bcsj.20210169.
[51] C. R. Dean *et al.*, "Hofstadter's butterfly and the fractal quantum Hall effect in moiré superlattices," *Nature*, vol. 497, no. 7451, pp. 598–602, 2013, doi: 10.1038/nature12186.
[52] S. Zhu *et al.*, "Strongly green-photoluminescent graphene quantum dots for bioimaging applications," *Chem. Commun.*, vol. 47, no. 24, pp. 6858–6860, 2011, doi: 10.1039/c1cc11122a.
[53] C. V. Gomez *et al.*, "Structural and Electronic Properties of Graphene Oxide for Different Degree of Oxidation," *Mater. Today Proc.*, vol. 3, no. 3, pp. 796–802, 2016, doi: 10.1016/j.matpr.2016.02.011.
[54] J. Diefenbach and T. P. Martin, "Model calculations for alkali halide clusters," *J. Chem. Phys.*, vol. 83, no. 9, pp. 4585–4590, 1985, doi: 10.1063/1.449029.
[55] S. Navalon, A. Dhakshinamoorthy, M. Alvaro, M. Antonietti, and H. García, "Active sites on graphene-based materials as metal-free catalysts," *Chem. Soc. Rev.*, vol. 46, no. 15, pp. 4501–4529, 2017, doi: 10.1039/c7cs00156h.
[56] A. Dhakshinamoorthy, M. Alvaro, M. Puche, V. Fornes, and H. Garcia, "Graphene Oxide as Catalyst for the Acetalization of Aldehydes at Room Temperature," *ChemCatChem*, vol. 4, no. 12, pp. 2026–2030, 2012, doi: 10.1002/cctc.201200461.
[57] P. H. Jacobse *et al.*, "Electronic components embedded in a single graphene nanoribbon," *Nat. Commun.*, vol. 8, no. 1, pp. 1–7, 2017, doi: 10.1038/s41467-017-00195-2.
[58] G. Shi *et al.*, "Two-dimensional Na-Cl crystals of unconventional stoichiometries on graphene surface from dilute solution at ambient conditions," *Nat. Chem.*, vol. 10, no. 7, pp. 776–779, 2018, doi: 10.1038/s41557-018-0061-4.

Supporting Information

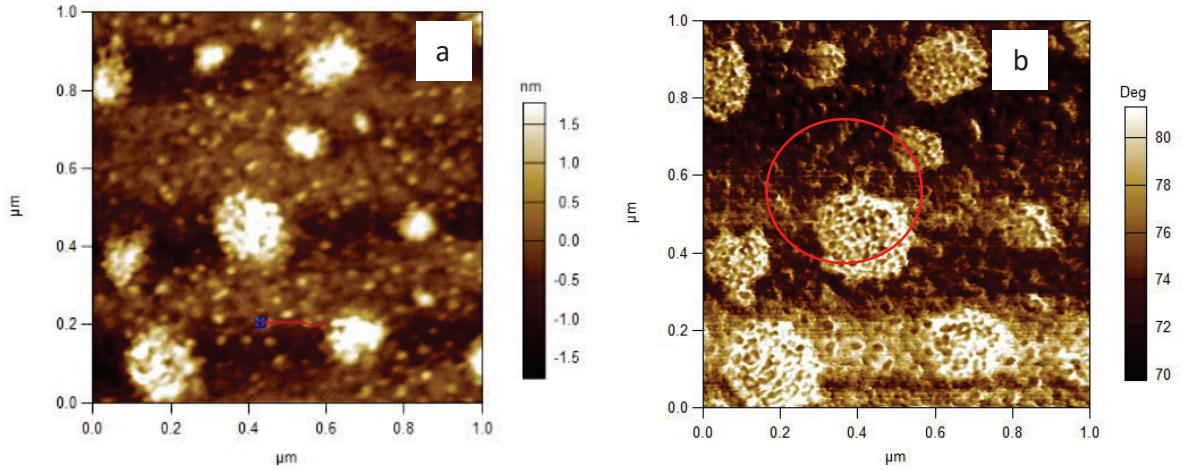

Fig S1. AFM image of GOQDs (a) Small dots (red line) and (b) Aggregating dots (red circle).

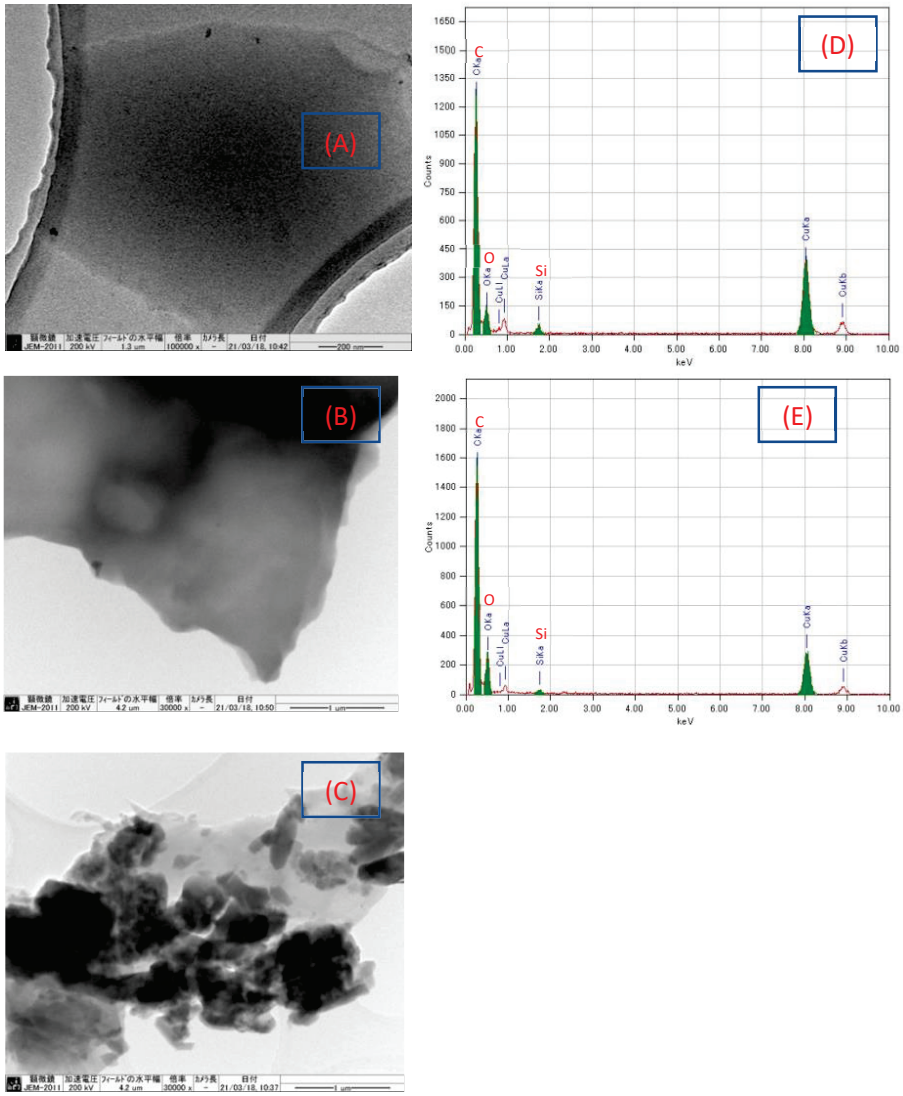

Fig S2. TEM measurement of Cesium Green in different scale. (A) Cesium green in 200 nm scale, (B) Cesium green in 1 µm scale, (C) Cesium green in 1 µm scale (in another point of view). (D) Elemental analysis of figure A. (D) Elemental analysis of figure B.

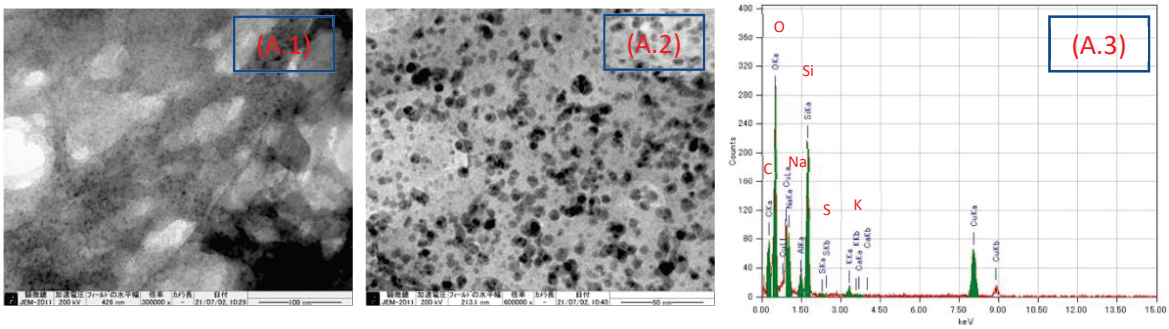

Fig S3. TEM measurement of GOQDs-based composite (ratio 5:1), (A.1) in 100 nm scale, (A.2) in 50 nm scale, (A.3) Elemental analysis of figure A.1.

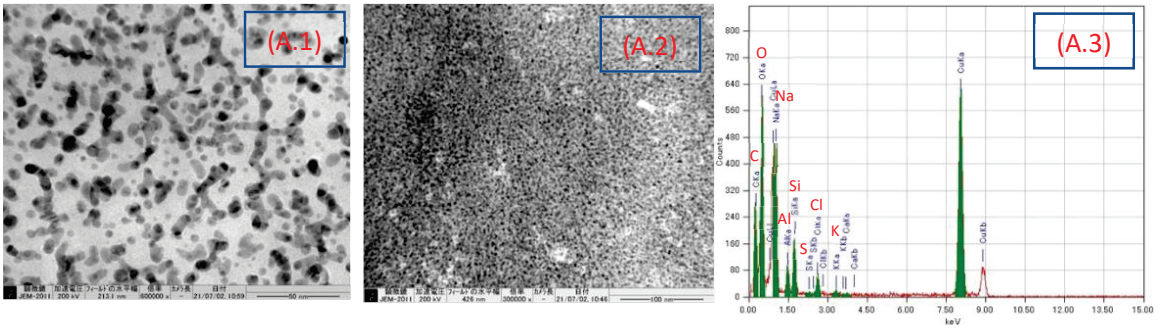

Fig S4. TEM measurement of GOQDs-based composite (ratio 8:1), (A.1) in 50 nm scale, (A.2) in 100 nm scale, (A.3) Elemental analysis of figure A.2.

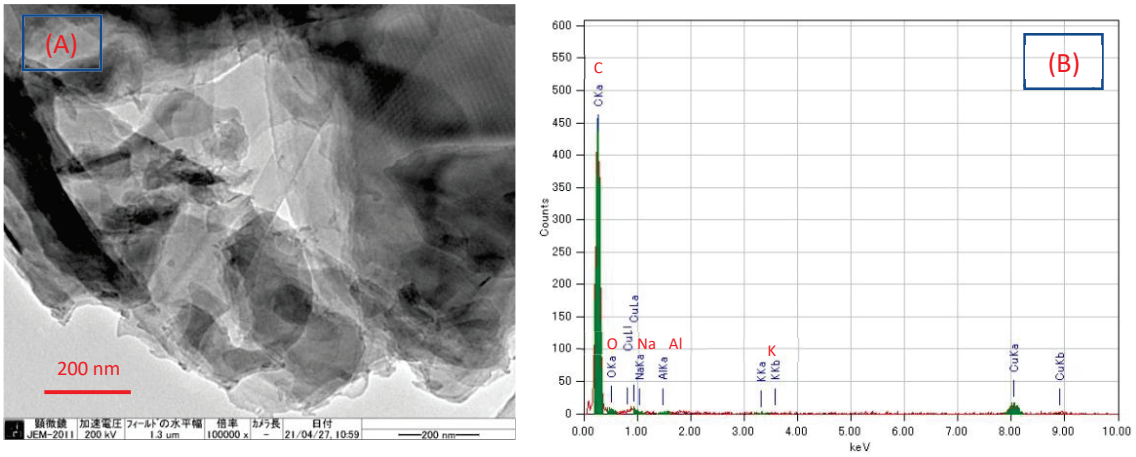

Fig. S5. TEM image of (A) isolated fragment (Larger particle of GO) after base treatment with reflux process followed by double centrifugation process and (B) Elemental analysis of figure A.

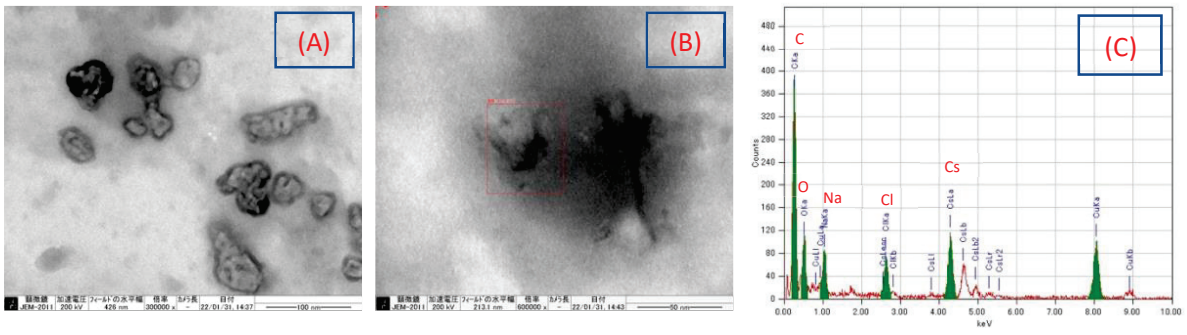

Fig. S6. TEM image of (A) composite-81 after Cs treatment (in basic condition), Cs cluster are identified, (B) moving adatoms, (C) Elemental analysis of figure B.

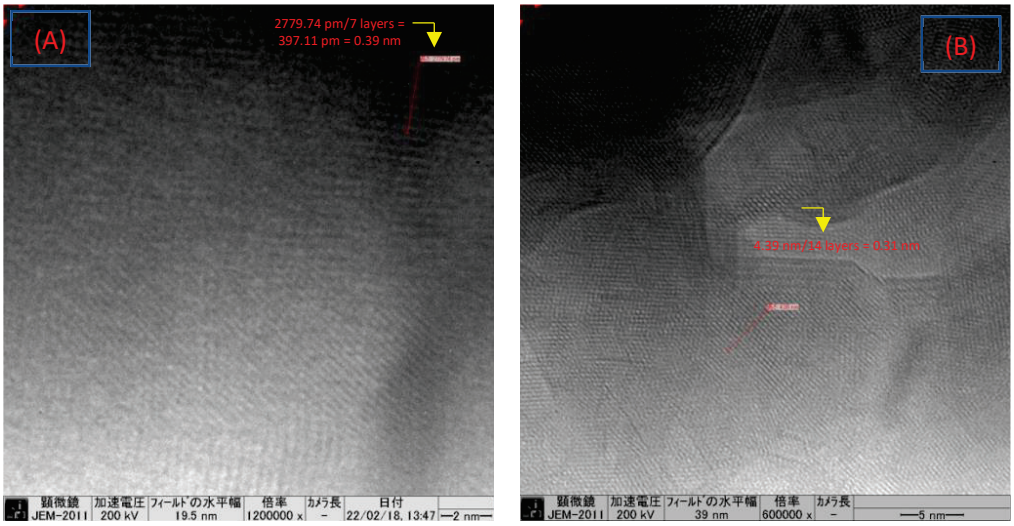

Fig. S7. TEM image of moiré fringe pattern (A) Composite-51 after Cs treatment (in acid condition) under prolonged electron beam irradiation, the lattice size is 0.39 nm and (B) GOQDs after Cs treatment (in basic condition) under prolonged electron beam irradiation, the lattice size is 0.31 nm.

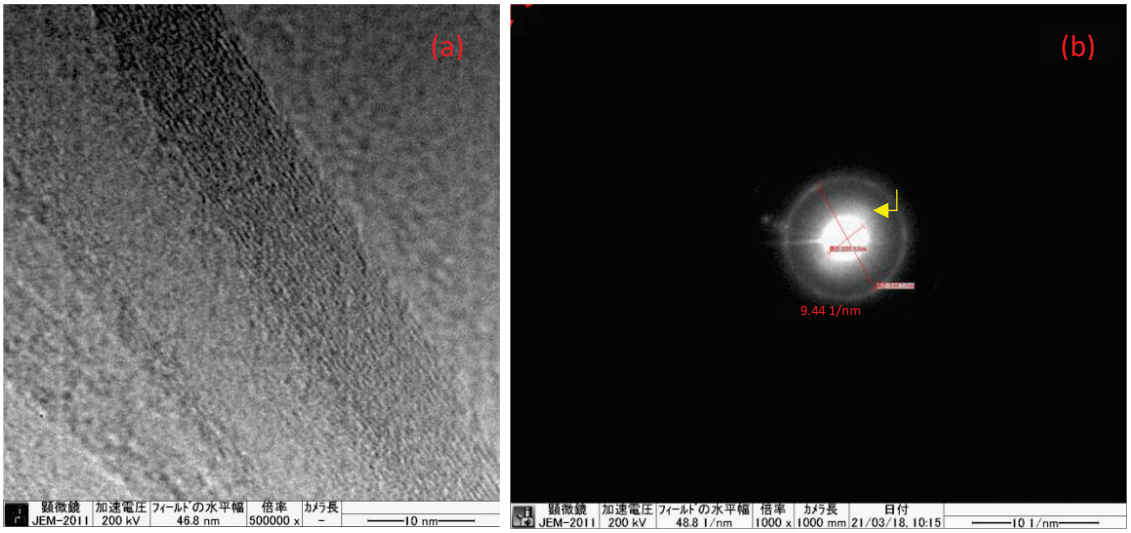

Fig. S8. (a) HRTEM image of GO. Scale bars: 10 nm. (b) Fast Fourier Transform (FFT) from the selected region of GO sample.

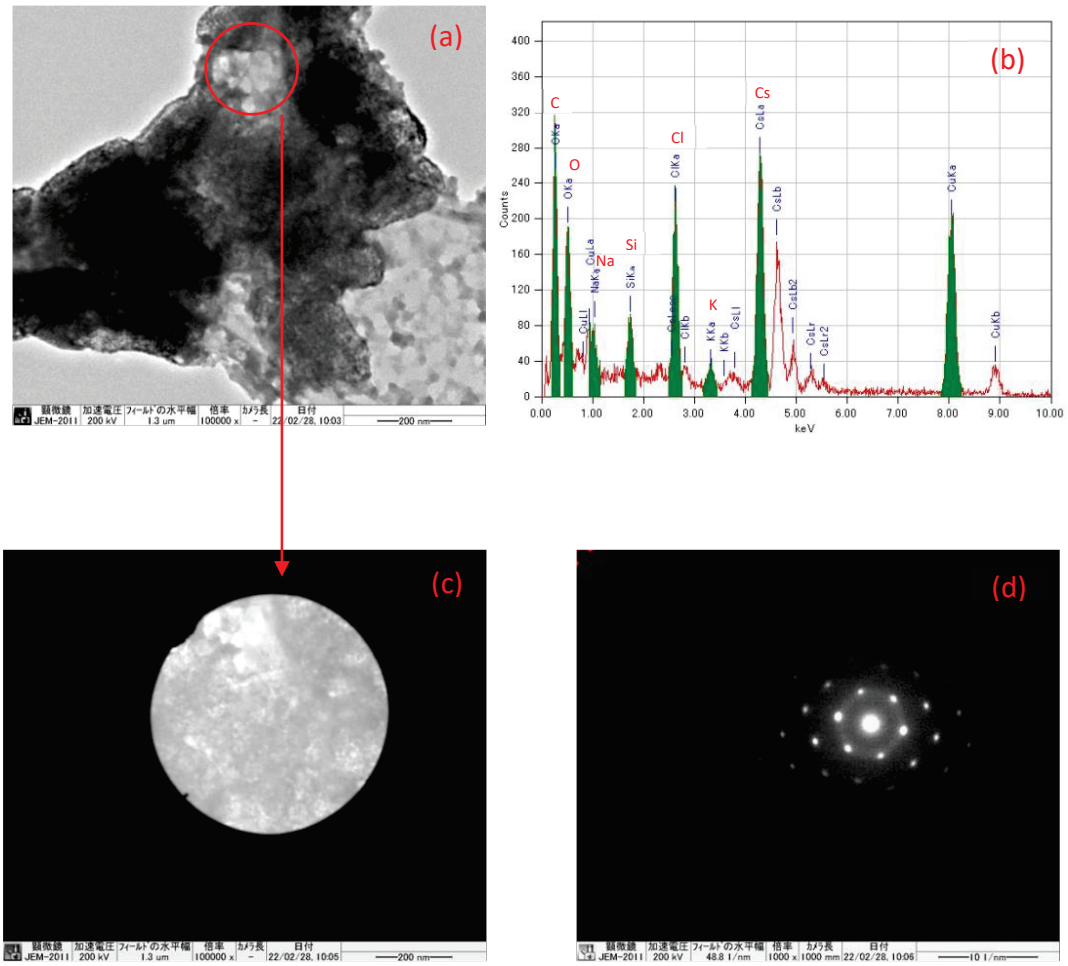

Fig. S9. TEM image of GOQDs after Cs treatment (in acidic condition), (a) under electron beam irradiation (soon after TEM measurement was carried out), (b) Elemental analysis of figure a, (c) Investigated area of figure a, (d) Fast Fourier Transform (FFT) corresponding to figure c.

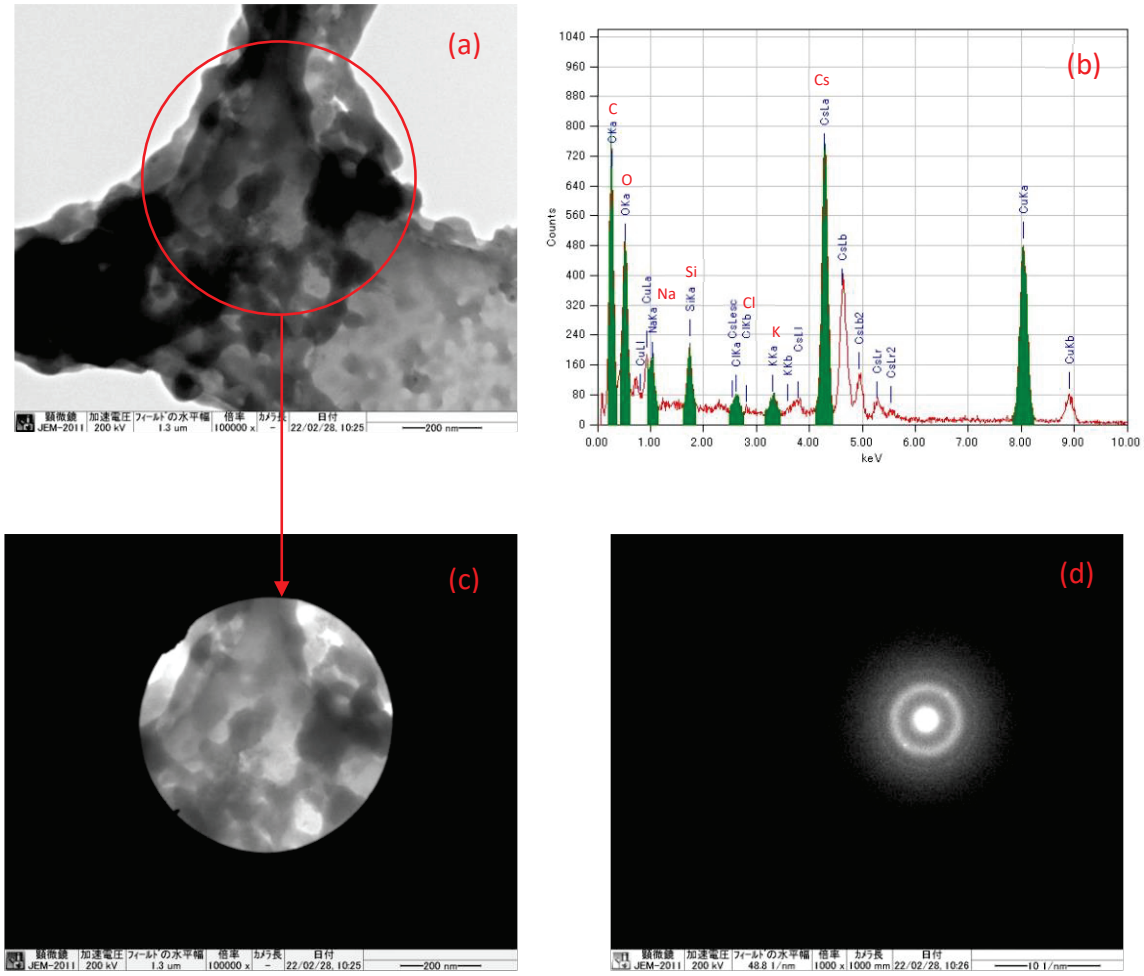

Fig. S10. TEM image of GOQDs after Cs treatment (in acidic condition), (a) after prolonged electron beam irradiation was applied, the graphitic layer being reorganized, (b) Elemental analysis of figure a, (c) Investigated area of figure a, (d) Fast Fourier Transform (FFT) corresponding to figure c.

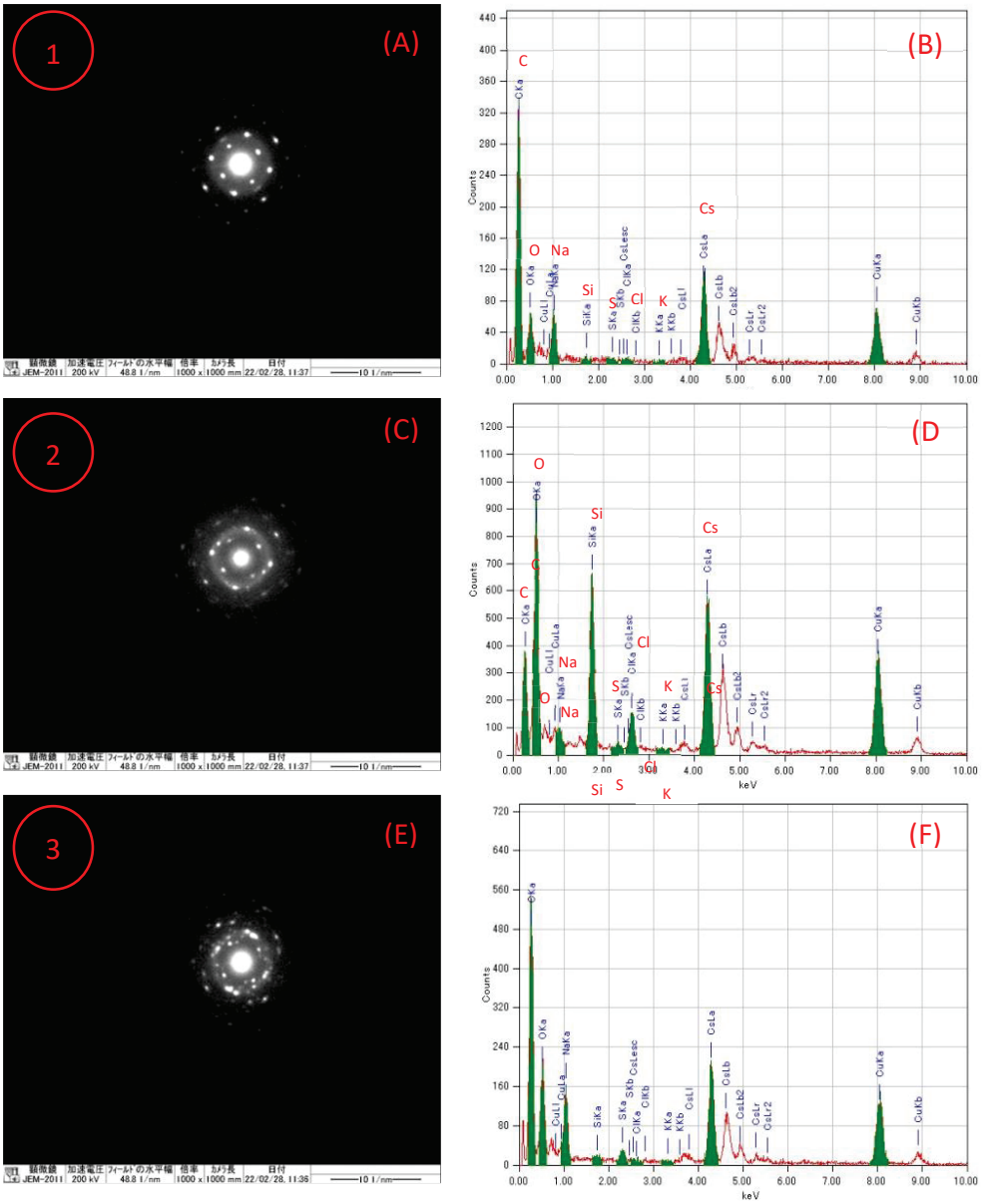

Fig. S11. TEM image of GOQDs after Cs treatment (in basic condition), under electron beam irradiation (soon after electron beam irradiation was applied for the second time, (A) Fast Fourier Transform (FFT) corresponding to figure 9f, (B) Elemental analysis of figure a, (C) Fast Fourier Transform (FFT) corresponding to figure 9f, (D) Elemental analysis of figure c, (E) Fast Fourier Transform (FFT) corresponding to figure 9f, (F) Elemental analysis of figure e.

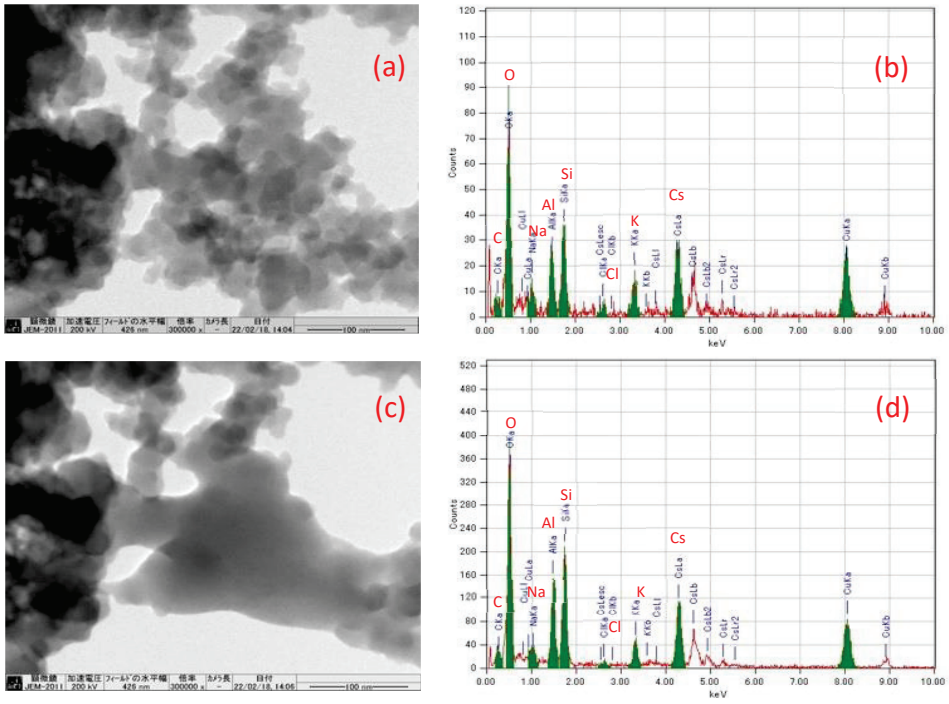

Fig.S12. TEM image of GOQDs after Cs treatment (in acidic condition) under prolonged electron beam irradiation, (a) before recombination process, (b) Elemental analysis of figure a, (c) after recombination process, (d) Elemental analysis of figure c.

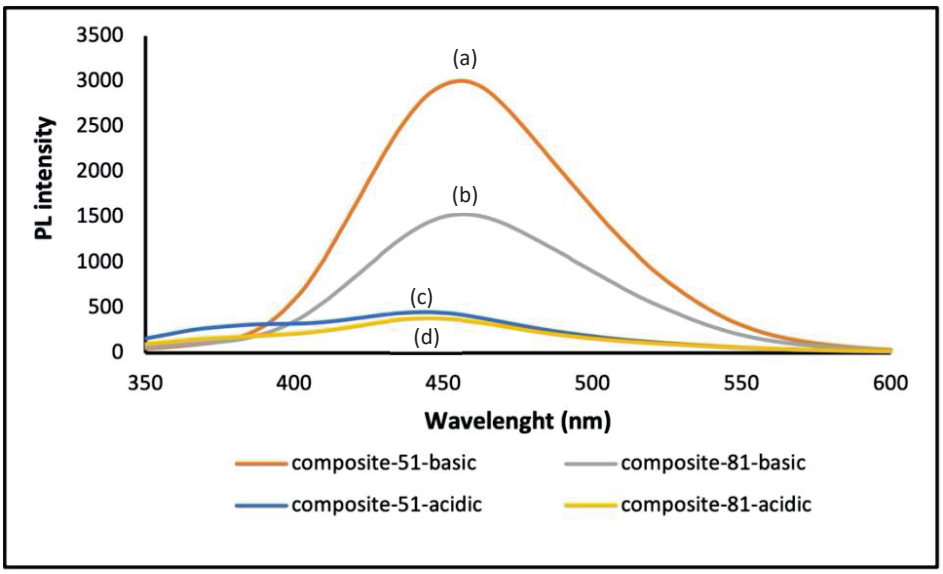

Fig. S13. Photoluminescence emission spectra of (a) composite-51 (basic condition), (b) composite-81 (basic condition), (c) composite-51 (acidic condition), (d) composite-81 (acidic condition). The pH condition was changed from acidic condition to basic condition.

Table S1. The input-output detection mechanism

Precursor material	pH condition	Input				Output
		Metal			Cesium green molecule (5:1 ratio)	
		CsCl	$SrCl_2$	KCl		
	Acidic	0	0	0	0	1
		0	0	0	1	0
		1	0	0	1	1
		0	1	0	1	1
		0	0	1	1	0
GOQDs solution	Basic	0	0	0	0	0
		0	0	0	1	1
		1	0	0	1	0
		0	1	0	1	0
		0	0	1	1	0

Precursor material	pH condition	Input				Output
		Metal			Cesium green molecule (8:1 ratio)	
		CsCl	$SrCl_2$	KCl		
	Acidic	0	0	0	0	1
		0	0	0	1	0
		1	0	0	1	1
		0	1	0	1	1
		0	0	1	1	0
GOQDs solution	Basic	0	0	0	0	0
		0	0	0	1	1
		1	0	0	1	0
		0	1	0	1	0
		0	0	1	1	0

SI-videos

S15.1 The movement of particle or rearrangement of structure in composite-51

S15.2, S15.3 The movement of particle or rearrangement of structure in composite-81

S15.4 The decomposition of CsCl nanoparticles under prolonged electron beam exposure

S15.5 The bond breakage of the GOQDs layers (moving or rotating phenomenon of the layer)

S15.6 Recombination of the GOQDs layers

Chapter IV. General Conclusions

The Fukushima accident of 2011 has led to numerous environmental problems. Radionuclides have become one of the significant concerns of many researchers. Therefore, it is important to design a new nanocomposite that can potentially use to address the issue of radionuclides contamination. This thesis explored the tremendous property of graphene oxide (GO), their derivatives (graphene oxide quantum dots (GOQDs)), and its composites. Specifically, by considering the dynamic nature of the surface area of GO, it can be used as an entry point to design the structure and the function system. In addition, through a better understanding of the specific characteristic and the structural diversity of GO (having different C/O ratio), the optimization of GO properties can potentially generate a new advance nanocomposite. Some methods (covalent bonding, functionalization) and radionuclides removal concepts (ion-trapping, coagulation, electrostatic interaction, and H^+-exchange) offers a bridge among GO, GOQDs and other potential materials. Based on that, chemical modifications open up the idea or tailoring the GO, GOQDs with another compound. In this study, Dawson-type POM (polyoxometalates) and cesium green molecule ($C_{32}H_{33}NO_8$) were identified. Based on that, two types of nanocomposites were produced. First, GO-POM nanocomposite as Cs removal. Second, graphene oxide quantum dot-based nanocomposite (functionalized by cesium green molecule) as Cs detection.

Moreover, in this thesis, GO and GOQDs as precursor material was synthesis by modified Hummer`s method. Further measurement was conducted to evaluate the crystallite morphology and some properties of the sample. Raman spectroscopy, transmission electron microscopy (TEM), scanning electron microscopy (SEM), atomic force microscopy (AFM), UV-Vis spectroscopy, Photoluminescence spectroscopy, PXRD, FTIR, Zeta potential were measured to obtained some evidences by spectroscopic and microscopic data.

As a result, GO-POM nanocomposite increased the Cs adsorption capacity effectively compared to the adsorption capacity of the original material. The change range is around 6.7% to 42.9%. An effective increment value of Cs adsorption can be attributed to several reasons, such as the characteristic of surface area (showing an important role of POM species with GO surface), as well as the functional group of GO provide a binding

point for chemical modification. However, the increment value of Cs adsorption by comparing concentrations 1:8 and 4:1 in the composite material, there is not much significant difference. In addition, it also found that the aggregation process was observed in the adsorption behaviour (the mechanism of cation-GO interaction). The results demonstrated that the composite samples immediately coagulate after Cs adsorption except for $[GO_{70}POM]_{41}$, which still forms a stable solution after one hour keeping at ambient temperature. The unusual behaviour of $[GO_{70}POM]_{41}$ might be predicted that there is a different composition of oxidative debris (OD) component among the GO samples. As is well known that the OD of GO has a significant role in the origin of GO acidity. Further investigation was evaluated by identified the interaction GO samples with Cs cation. Immediately less than one minute after the stirring process, A brown milky coagulation was formed. The same behavior was observed between GO_{c72} and Cs, however, there was a difference for GO_{c39}, the brown milky coagulation was formed in a small quantity, and the milky coagulation was not formed for GO_{c40}. The difference might be related to the variance in C/O ratio between GO_{c70}, GO_{c72}, and GO_{c39}, GO_{c40}. As evident, TEM measurement shows that there are many Cs clusters in the surface of $GO_{c70.}$ The black spots also can be seen in the $[GO_{40}POM]_{41}$, which consists of GO_{c40}/POM. However, the black spots are not uniformly found all over the surface area. Regarding this phenomenon, it can be assumed that there are two important factors that might contribute to the aggregation behavior. First, the size of the GO and composite sample matter. As resulted, the size of each sample is diverse. The range of values is around 4.3 to 34.78 nm. Second, the other factor is the degree of acidity. It is strongly related with the functionalities of the GO sample. It was explained in an earlier section in this work that there are two types of GO samples, which have different C/O compositions.

Furthermore, since GO material consisted of oxidative debris (OD) component (covalently attached to the oxygen functional groups), in this thesis, we had produced graphene oxide quantum dot (GOQDs) by separating the OD from the graphene-like sheet with using base (NaOH) treatment and heating process. Continuously, GOQDs functionalized by cesium green ($C_{32}H_{33}NO_8$) molecule. As a result, the nanocomposite was effectively fabricated by functionalized GOQDs and cesium green molecule in mixed solution (distilled water/THF). In this study, as-produced nanocomposite can be essentially used to recognize the presence of Cs cation in the aqueous solution both in acidic condition and basic condition with turn ON/OFF photoluminescence (PL) response. There are several phenomena observed in this experiment. First, the unique properties of

GOQDs (pH dependent) have a dual role as an enhancer and quencher in composite in the presence of Cs cation. In acidic condition, the PL behaviour shows turn ON the PL after detecting the Cs cation. On the contrary, the turn OFF PL occurred in basic condition. Second, the nanocomposites are more sensitive as Cs detection (turn ON) compared to other metal like Sr and K in acid condition. Third, the Cs cluster was formed under electron beam irradiation as consequence of adatom mobility on the substrate layer. In this phenomenon, the pH condition of the nanocomposite system has an important key in the PL response in mixed solvent. It should be noted, however, that more effort is still necessary to get strong evidence and also to open the understanding of the role of oxygen functional group and the various defects that act as an active site of the GOQDs for Cs metal formation. Therefore, based on this phenomenon, it suggests that the observed cluster was formed because of the migration effect of the adatoms on nanocomposite layer (specifically trapped to defect site in the graphene lattice) and transformation of the local adsorption environment induced by electron beam exposure.

Throughout this study it has been found that GO, GOQDs, and their composite has some remarkable features that are highly Cs adsorbent and Cs detection. More specifically, it shown below:

- The GO-based POM nanocomposite was successfully obtained. The Cs adsorption capacity increased by forming a nanocomposite. The result proposed, that C/O ratio of the GO sample and the concentration ration of GO/POM has significantly influenced the characteristic of the GO-POM nanocomposite for the Cs adsorption performance after forming the composite.
- A new nanocomposite was developed using functionalized graphene oxide quantum dots (GOQDs) with cesium green molecules for the first time. The results demonstrated that the unique properties of GOQDs (pH dependent) have a dual role as an enhancer and quencher in composite in the presence of Cs cation. In acidic condition, the PL behaviour shows turn ON the PL after detecting the Cs cation. On the contrary, the turn OFF PL occurred in basic condition. Additionally, the present experiments also indicated the formation of Cs metal (cluster).
- The overall mechanism process is complex, and it is influenced by many conditions such as the composition of the nanocomposite, the pH, the concentration of CsCl, and the solvent.

However, since GO structure as precursor material has different local arrangement of functional group from one batch to another batch, the accuracy and the sensitivity of

the nanocomposite system further investigation is needed. Further scrutiny is also needed to open understanding of the role of degree of the oxidative debris (OD component) in each GO sample for adsorption capacity and detection system.